Economic Geology, v. 100, pp. 1097–1133

Evolution of a Submarine Magmatic-Hydrothermal System: Brothers Volcano, Southern Kermadec Arc, New Zealand

C. E. J. de Ronde,[†]

Institute of Geological and Nuclear Sciences, P.O. Box 31-312, Lower Hutt, New Zealand

M. D. Hannington,

Department of Earth Sciences, University of Ottawa, Ottawa, Canada K1N 6N5

P. Stoffers,

Institute of Geosciences, Christian-Albrechts University of Kiel, Olshausenstrasse 40, 24118 Kiel, Germany

I. C. Wright,

National Institute of Water and Atmospheric Research, P.O. Box 14-901, Wellington, New Zealand

R. G. Ditchburn, A. G. Reyes,

Institute of Geological and Nuclear Sciences, P.O. Box 31-312, Lower Hutt, New Zealand

E. T. Baker,

Pacific Marine Environmental Laboratory, National Oceanic and Atmospheric Administration, 7600 Sand Point Way, NE Bldg. 3, Seattle, Washington 98115-6349

G. J. Massoth,

Institute of Geological and Nuclear Sciences, P.O. Box 31-312, Lower Hutt, New Zealand

J. E. Lupton,

Pacific Marine Environmental Laboratory, National Oceanic and Atmospheric Administration, 2115 S.E. OSU Drive, Newport, OR 97365-5258

S. L. Walker,

Pacific Marine Environmental Laboratory, National Oceanic and Atmospheric Administration, 7600 Sand Point Way NE, Bldg. 3, Seattle, Washington 98115-6349

R. R. Greene,

Pacific Marine Environmental Laboratory, National Oceanic and Atmospheric Administration, 2115 S.E. OSU Drive, Newport, OR 97365-5258

C. W. R. Soong,

Institute of Geological and Nuclear Sciences, P.O. Box 31-312, Lower Hutt, New Zealand

J. Ishibashi,

Faculty of Science, Kyushu University, Japan

G. T. Lebon,

Pacific Marine Environmental Laboratory, National Oceanic and Atmospheric Administration, 7600 Sand Point Way NE, Bldg. 3, Seattle, Washington 98115-6349

[†] Corresponding author: e-mail, Cornel.deRonde@gns.cri.nz

C. J. Bray,

F. Gordon Smith Fluid Inclusion Laboratory, Department of Geology, University of Toronto, Toronto, Canada M5S 3B1

and J. A. Resing

Pacific Marine Environmental Laboratory, National Oceanic and Atmospheric Administration, 7600 Sand Point Way NE, Bldg. 3, Seattle, Washington 98115-6349

Abstract

Brothers volcano, which is part of the active Kermadec arc, northeast of New Zealand, forms an elongate edifice 13 km long by 8 km across that strikes northwest-southeast. The volcano has a caldera with a basal diameter of ~3 km and a floor at 1,850 m below sea level, surrounded by 290- to 530-m-high walls. A volcanic cone of dacite rises 350 m from the caldera floor and partially coalesces with the southern caldera wall.

Three hydrothermal sites have been located: on the northwest caldera wall, on the southeast caldera wall, and on the dacite cone. Multiple hydrothermal plumes rise ~750 m through the water column upward from the caldera floor, originating from the northwest caldera walls and atop the cone, itself host to three separate vent fields (summit, upper flank, northeast flank). In 1999, the cone site had plumes with relatively high concentrations of gas with a ΔpH of –0.27 relative to seawater (proxy for CO_2 + S gases), dissolved H_2S up to 4,250 n*M*, high concentrations of particulate Cu (up to 3.4 n*M*), total dissolvable Fe (up to 4,720 n*M*), total dissolvable Mn (up to 260 n*M*) and Fe/Mn values of 4.4 to 18.2. By 2002, plumes from the summit vent field had much lower particulate Cu (0.3 n*M*), total dissolvable Fe (175 n*M*), and Fe/Mn values of 0.8 but similar ΔpH (–0.22) and higher H_2S (7,000 n*M*). The 1999 plume results are consistent with a magmatic fluid component with the concentration of Fe suggesting direct exsolution of a liquid brine, whereas the much lower concentrations of metals but higher overall gas contents in the 2002 plumes likely reflect subsea-floor phase separation. Plumes above the northwest caldera site are chemically distinct, and their compositions have not changed over the same 3-year interval. They have less CO_2 (ΔpH of –0.09), no detectable H_2S, total dissolved Fe of 955 n*M*, total dissolved Mn of 150 n*M*, and Fe/Mn of 6.4. An overall increase in $^3He/^4He$ values in the plumes from R/R_A = 6.1 in 1999 to 7.2 in 2002 is further consistent with a magmatic pulse perturbing the system.

The northwest caldera site is host to at least two large areas (~600 m by at least 50 m) of chimneys and subcropping massive sulfide. One deposit is partially buried by sediment near the caldera rim at ~1,450 m, whereas the other crops out along narrow, fault-bounded ledges between ~1,600 and 1,650 m. Camera tows imaged active 1- to 2-m-high black smoker chimneys in the deeper zone together with numerous 1- to 5-m-high inactive spires, abundant sulfide talus, partially buried massive sulfides, and hydrothermally altered volcanic rocks. $^{210}Pb/^{226}Ra$ dating of one chimney gives an age of 27 ± 6 years; $^{226}Ra/Ba$ dating of other mineralization indicates ages up to 1,200 years. Formation temperatures derived from $\Delta^{34}S_{sulfate\text{-}sulfide}$ mineral pairs are 245° to 295° for the northwest caldera site, 225° to 260°C for the southeast caldera and ~260° to 305°C for the cone. Fluid inclusion gas data suggest subsea-floor phase separation occurred at the northwest caldera site.

Alteration minerals identified include silicates, silica polymorphs, sulfates, sulfides, Fe and Mn oxide and/or oxyhydroxides, and native sulfur, which are consistent with precipitation at a range of temperatures from fluids of different compositions. An advanced argillic assemblage of illite + amorphous silica + natroalunite + pyrite + native S at the cone site, the occurrence of chalcocite + covellite + bornite + iss + chalcopyrite + pyrite in sulfide samples from the southeast caldera site, and veins of enargite in a rhyodacitic sample from the northwest caldera site are indicative of high-sulfidation conditions similar to those of subaerial magmatic-hydrothermal systems.

The northwest caldera vent site is a long-lived hydrothermal system that is today dominated by evolved seawater but has had episodic injections of magmatic fluid. The southeast caldera site represents the main upflow of a relatively well established magmatic-hydrothermal system on the sea floor where sulfide-rich chimneys are extant. The cone site is a nascent magmatic-hydrothermal system where crack zones localize upwelling acidic waters. Each of these different vent sites represents diverse parts of an evolving hydrothermal system, any one of which may be typical of submarine volcanic arcs.

Introduction

Volcanic arcs are the surface expression of magmatic systems that result from the subduction of mostly oceanic lithosphere at convergent plate boundaries. Arcs with a submarine component include intraoceanic arcs and island arcs that span almost 22,000 km on Earth's surface, with the vast majority located in the Pacific region (de Ronde et al., 2003a). Subduction zones, where lithosphere is recycled deep into the Earth, delineate sites of fluid transfer into the convecting mantle and zones of chemical heterogeneities. Fractions of the subducted flux of sediments and volatiles are returned to the Earth's surface at these plate boundaries. The study of submarine hydrothermal systems along volcanic arcs thus provides insight into the types of fluid generated in subduction zone-related hydrothermal systems.

The ~2,500-km-long Kermadec-Tonga arc northeast of New Zealand is one of the longest continuos intraoceanic arcs in the world (Fig. 1a). At least 94 volcanoes along the arc are submarine, most (87%) within the Kermadec sector (de Ronde et al., 2003a). Volcanic rocks along the Kermadec arc range from basalt to rhyodacite. Trace element and isotopic data indicate significant magma source heterogeneity both along and across the arc resulting from variable subduction of

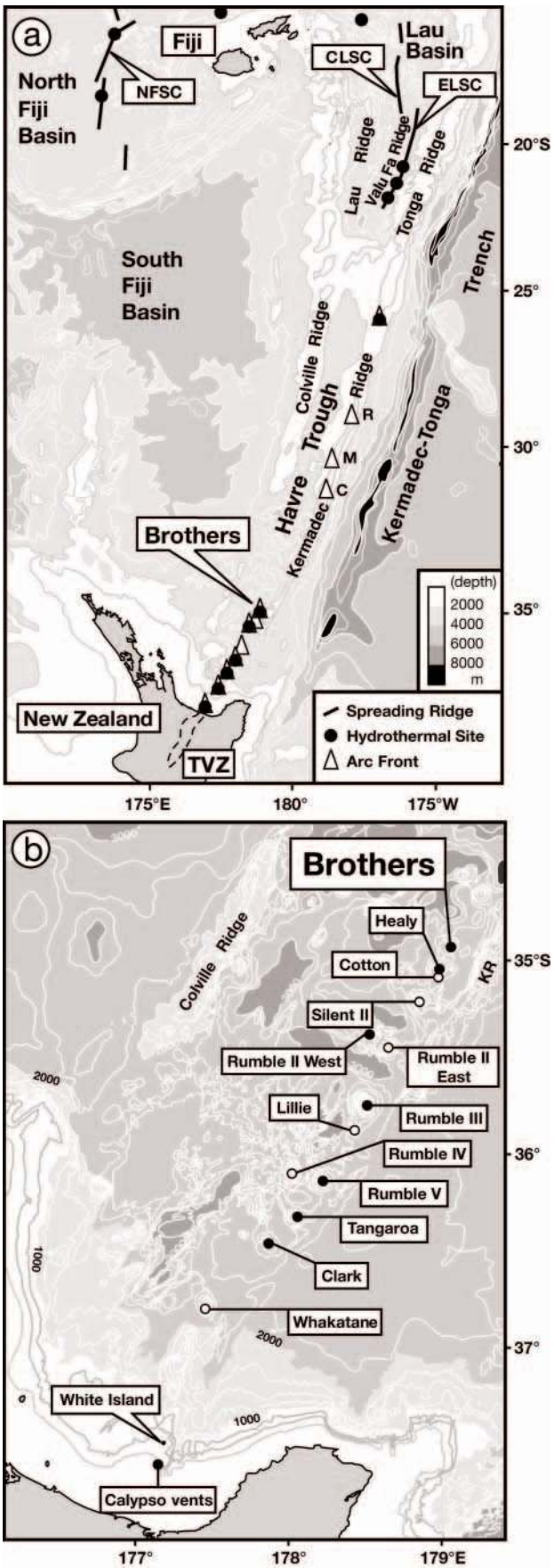

continent-derived sediments, pelagic sediments and oceanic crust, and/or interaction with continental crust (e.g., Gamble and Wright, 1995; Gamble et al., 1996; Haase et al., 2002).

The Kermadec-Tonga arc hosts numerous submarine and subaerial hydrothermal systems. In total, ~2,530 km of the Kermadec-Tonga arc (including the entire 1,220-km Kermadec sector), with ~70 major volcanoes, has been surveyed for hydrothermal emissions (de Ronde et al., 2004). In February 1996, the first sulfide samples from the southern Kermadec arc were dredged from the Brothers and Rumble II West caldera volcanoes (R/V *Tangaroa* cruise TAN96/03, Fig. 1a; Wright et al., 1998; de Ronde et al., 2003b). In September 1998, low-temperature, diffuse venting was discovered at the Monowai, Rumble III, and Clark volcanoes, and high-temperature, black smoker venting was found within the Brothers caldera (R/V *Sonne* cruise SO-135: Stoffers et al., 1999a). The NZAPLUME cruise of March 1999 surveyed 13 volcanoes of the southern Kermadec arc and documented hydrothermal emissions above seven of them (de Ronde et al., 2001; Baker et al., 2003; Massoth et al., 2003). In July 2001, additional mineralized and hydrothermally altered samples were dredged from Brothers volcano (R/V *Tangaroa* cruise TAN01/07). The NZAPLUME II cruise of May 2002 confirmed that venting was still occurring at all the known hydrothermal sites and that eight active vent sites occurred in the middle part of the arc, between Brothers volcano and Macauley Island (de Ronde et al., 2002; Fig. 1a). In March 2003, the TELVE cruise discovered an additional 10 active vent sites along the southern part of the Tofua (Tongan) section of the arc (Massoth et al., 2004). In September-October 2004 NZAPLUME III surveyed the northernmost part of the Kermadec arc, and in November 2004, the NoToVE cruise surveyed the northern part of the Tofua arc.

Subaerial arc volcanoes discharge large volumes of magmatic volatiles (e.g., Hedenquist et al., 1993; Giggenbach, 1996; Giggenbach et al., 2003; Rapien et al., 2003). Similar systems also occur along the Kermadec arc, including the offshore extensions of the Taupo Volcanic Zone. White Island and Raoul Island are host to active magmatic-hydrothermal systems (Giggenbach, 1992) and acidic hot springs and fumaroles discharge magmatic gases on Curtis Island (Smith et al., 1988). In this paper, we document the evolution of an

FIG. 1. a. Tectonic setting of the Kermadec-Tonga arc. The Australian and Pacific plates occur west and east of the Tonga-Kermadec trench, respectively. Rates of extension and age of initial opening of the southern Havre trough are estimated to be 15 to 20 mm yr^{-1} and 5 Ma, respectively (Wright et al., 1996). Flanking the Havre trough, the remnant Colville Ridge and active Kermadec arc margins form longitudinally continuous ridges. Volcanoes of the Tonga-Kermadec arc front occur within a 40-km-wide zone that extends for ~2,500 km and includes >90 volcanoes (Worthington, 1999). Depth contours are in kilometers (shading every 1 km). Abbreviations: C = Curtis Island; CLSC = Central Lau spreading center; ELSC = Eastern Lau spreading center; M = Macauley Island; NFSC = North Fiji spreading center; R = Raoul Island, TVZ = Taupo volcanic zone. b. Location of southern Kermadec arc volcanoes from Brothers (34.86°S, 179.06°E) in the northeast to Whakatane (36.83°S, 177.47 °E) in the southwest that were surveyed during the 1999 NZAPLUME cruise (de Ronde et al., 2001). Submarine hydrothermal activity is known to occur at seven of these arc front volcanoes, some with multiple vent sites. Black dots = active vent site; white dots = inactive site or insufficient evidence to confirm if active; KR = Kermadec Ridge.

analogous magmatic-hydrothermal system on a submarine volcano of the southern Kermadec arc. Brothers volcano provides an opportunity to determine the style and composition of hydrothermal discharge at a submarine arc volcano and to characterize the source of hydrothermal fluids in the formation of associated polymetallic massive sulfide deposits. This work represents a more comprehensive follow-up study to reconnaissance plume mapping surveys and observations made from a few samples recovered by earlier dredging (Wright et al., 1998; de Ronde et al., 2001, 2003b).

Brothers Volcano Host-Rock Geology

Brothers volcano was partially mapped in 1994 by a reconnaissance side-scan survey of the Colville and Kermadec ridges (Wright, 1997). In 1998, the volcano was mapped with HYDROSWEEP multibeam echosounding by the R/V *Sonne* (Stoffers et al., 1999a) and then remapped during the 2002 R/V *Tangaroa* TAN02/05 cruise using a SIMRAD EM300 system (Fig. 2a).

Volcano morphology

Brothers volcano is one of 13 major volcanic edifices, and one of three caldera volcanoes, that form the active Kermadec volcanic arc front between 37° and 34° 50′ S (Wright, 1997; Wright and Gamble 1999). Within this arc segment, volcanoes typically have a range of rock compositions (basalt to rhyodacite). The summits of these volcanoes occur at water depths between 1,200 and 220 m (below sea level). Brothers volcano (Fig. 2) is part of a ~35-km-long and 15-m-wide, predominantly silicic volcanic complex that includes the rhyodacitic Healy caldera to the south (Fig. 1b), which together are elevated above the >2,500-deep Havre tough back-arc basin to the west. This complex is dissected by basement fractures and associated dike-controlled ridges that are 1 to 1.5 km wide and rise 400 to 500 m above the sea loor. These structures strike predominantly 055° to 065° (Fig. 2b), although a conjugate set of faults is observed subparellel to the elongated Brothers edifice and caldera. These orientations are consistent with Havre tough rifting (e.g., Wright et al. 1996; Deltiel et al., 2002; Ruellen et al., 2003) and indicate first-order extensional tectonic control on Brothers volcano.

The base of Brothers volcano rises from a depth of ~2,200 m to a continuous caldera rim at 1,540 m, although locally the northwestern rim shoals to 1,320 m (Fig. 2b). The caldera floor has a basal diameter of 3 to 3.5 km, averages 1,850 m deep, and is surrounded by 290-to 530-m-high walls. An elongate northeast-southwest, 1.5- to 2-km-wide and 350-m-high, post-collapse cone occurs within the caldera, with two smaller

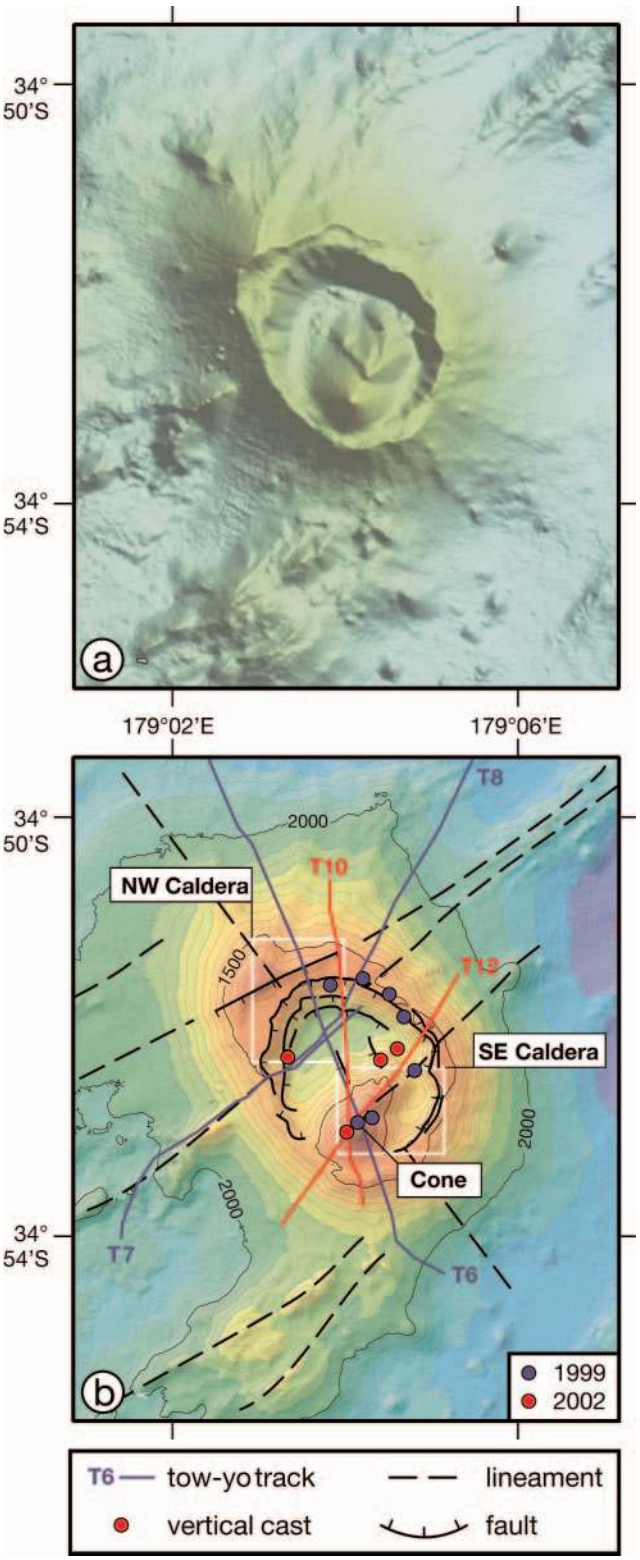

FIG. 2. a. Terrain model of Brothers caldera volcano based on gridded EM300 multibeam echosounding data at a cell size of 25 m (sunlight from the N). The post-collapse volcanic cone, with subsidiary satellite cone(s), can be seen toward the southern margin and center of the caldera, respectively. b. Color bathymetry of Brothers volcano. Highlighted are the alignment of fractures, faults (including ring faults), and volcanic structures parallel to the inferred regional basement fabric. The locations of active hydrothermal vent fields at the northwest caldera and cone sites are controlled by the intersection of the caldera wall and cone with basement fracture lineaments. Also shown are the conductivity-temperature-depth-optical (CTDO) "tow-yo" tracks and vertical cast stations. A tow-yo is a sawtooth path made through the water column as the cable winch continuously pays in and out while the ship travels steadily at speeds of ~2.5 to 3.5 km^{-1} (see Fig. 4). A vertical cast is where the ship remains stationary over a site and the CTDO package is lowered to within 20 m of the sea floor. Boxes outlined in white encompass the northwest caldera, southeast caldera, and cone sites, respectively (see Fig. 7 for details).

satellite cones on its northeast flank. The cone in part coalesces with the southern caldera wall and shoals to 1,220 m.

Intracaldera structure

The intracaldera structure and locations of the hydrothermal systems are considered to be controlled by intersecting basement structures (Fig. 2b). Intersection of the major caldera ring faults and basement ridge lineaments form an apparent rhombic arrangement of the northwest caldera wall. The northwest caldera vent site is situated at the intersection of two major conjugate basement structures with a basement fracture striking 055° in this region controlling the location of maximum caldera collapse (Fig. 2b). Here, progressive collapse of the caldera rim footwall has occurred, with the deeper and innermost ring faults being progressively more active. Similarly, the orientation of the postcollapse cone and its associated vent sites (elongate along a trend of 045°) reflect basement structure, with dissecting faults striking 145° (Fig. 2b).

Host-rock geology

In 1996, rocks were collected in 23 dredges, recovering lavas and coarse volcaniclastic sediments within the caldera, and on the flanks of the edifice (Wright and Gamble, 1999; Fig. 3a, b). The sea floor was also mapped during 17 camera tows. In 1998, rocks were collected in 11 additional dredges and in three TV-controlled grabs. Video and still camera tows (11 individual tracks) were then done over the northwest caldera, southeast caldera, and cone sites (Stoffers et al., 1999a).

Host-rock lavas comprise porphyritic glassy dacite lavas (62.2–65.3 wt % SiO_2) with plagioclase and clinopyroxene as the major phenocryst phases (Gamble and Wright, 1995; Haase et al., 2002). The dacites are vesicular (typically <30% vesicles) with dry densities of 1.8 to 2.3 gm cm^{-3} (Wright and Gamble, 1999; Fig. 3c). Relatively low vesicularity suggests effusive emplacement of the sampled rocks rather than pyroclastic eruption, although the presence of the caldera in association with a silicic cone is more consistent with an overall evolution of the volcano involving pyroclastic eruption and magma chamber collapse.

Petrographic analysis shows that samples recovered from Brothers are dominated by volcanic rocks, including dacite and rhyodacite with relatively minor andesite, ignimbrite and breccia, lapilli sands with abundant fresh glass fragments, and fragments of sulfide-rich chimneys. The primary minerals found in the volcanic rocks include glass, plagioclase, pyroxenes, titanomagnetite, apatite, and rare zircon.

Brothers Hydrothermal System

Hydrothermal plumes

Extensive hydrothermal plume surveys of Brothers volcano were made during all three NZAPLUME cruises in 1999, 2002, and 2004. Multiple hydrothermal plumes extend from the bottom of the caldera upward to a minimum depth of 1,100 m (or ~750 m through the water column) and originate from two dominant sites; one on the northwest caldera wall and the other atop the cone. The presence of these multiple, thick plumes, combined with their distribution, suggests that Brothers is host to the most vigorous and extensive hydrothermal system of those surveyed along the Kermadec arc (de Ronde et al., 2001; Baker et al., 2003). Discharge from the northwest caldera vents originates at ≤1,650 m with the plumes rising to heights mainly below the caldera rim at 1,540 m. Some of the plumes appear to be flushed out of the caldera, probably as a response to tidal effects (Baker et al., 2003; Fig. 4a).

Venting associated with the cone was, in 1999, largely concentrated at the summit with a noticeable plume at 1,195 m although secondary discharge was noted on the upper flank, with a plume at 1,225 to 1,245 m and another at 1,365 m associated with a satellite cone on the northeast flank (Fig. 4a). In 2002, the summit plume was still prevalent although the northeast flank plume was more volumetrically extensive, suggesting an increase in discharge at this site (Fig. 4b, c). The most intense plumes, in terms of particle density (as measured by light scattering), occur between depths of 1,150 and 1,200 m (Baker et al., 2003; Fig. 4).

Additional information on the distribution of particulates within the plumes was obtained using miniature autonomous plume recorders, or MAPRs (Baker and Milburn, 1997), attached to TV grab and video sleds during the 1998 R/V *Sonne* cruise, providing more specific data on the location of the active vents. Three dominant areas of venting were found at the northwest caldera site around 1,650 m (Fig. 5), although active chimneys were not seen in the camera tows through the plume at the easternmost site. There was also no evidence for vigorous venting near the caldera rim. The intensity and distribution of the plumes over the cone site were largely unchanged since 1998 (Fig. 5). A plume survey down the northeast flank of the cone in 2002 suggested intense discharge at the summit of the satellite cone, which the earlier MAPR surveys did not traverse (Figs. 4, 5). There is no evidence for active venting at the southeast caldera site (Fig. 2a).

Chemical analysis of water samples collected from within the plumes shows that the vent sites at the northwest caldera and cone are distinct. In 1999, the areally extensive plume over the summit of the cone (Fig. 4a) contained relatively high concentrations of dissolved gas with a shift of –0.27 pH units relative to background seawater (proxy for CO_2 + S gases; Resing et al., 1999, 2004; Massoth et al., 2003) and H_2S concentrations up to 4,250 n*M*. The concentration of total dissolvable Fe (refers to dissolved Fe plus particulate Fe-bearing phases that are soluble in weak acid) was 4,720 n*M* and total dissolvable Mn was up to 260 n*M*, with Fe/Mn values between 4.4 and 18.2. However, in 2002, plumes from the same summit vent field had noticeably lower total dissolvable Fe (175 n*M*) and Fe/Mn values (0.8), similar total dissolvable Mn (220 n*M*), and a smaller shift in pH (–0.22) but higher H_2S (7,000 n*M*), suggesting large fluctuations for this vent site (Table 1). Total particulate S in the summit plume noticeably decreased from 763 n*M* in 1999 to 115 n*M* in 2002. Total particulate S values up to 574 n*M* for the deeper (1,365 m) vent site on the northeast flank of the cone suggest that the locus of the sulfur discharge shifted downslope by 2002. By contrast, plumes originating from the northwest caldera site have much less gas with a pH shift of –0.09 units and no detectable H_2S, total dissolvable Fe up to 955 n*M*, total dissolvable Mn up to 150 n*M*, and Fe/Mn values of 6.4. These

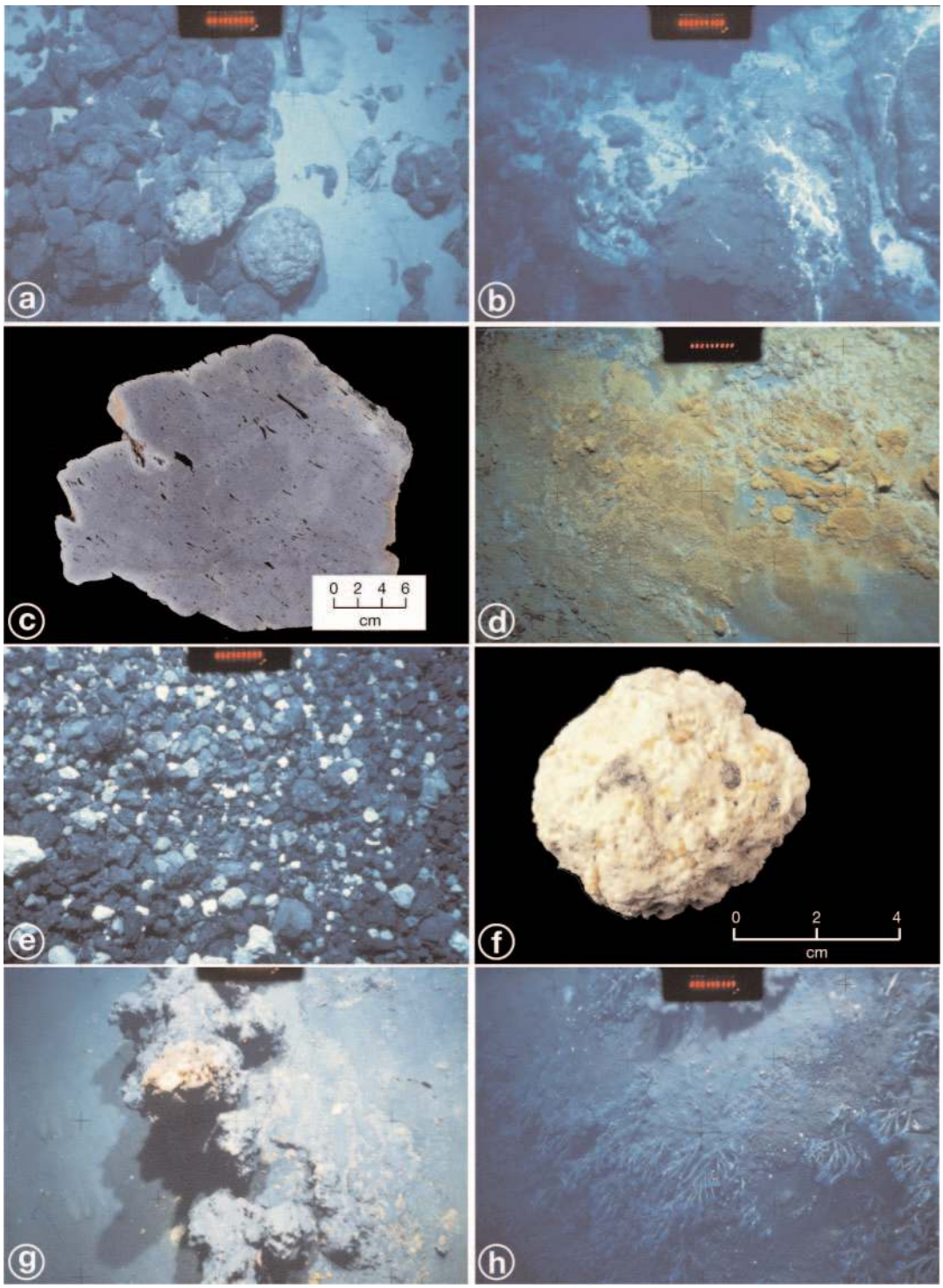

FIG. 3. a. Bread crust-type dacite lavas on ash-covered southeast flank of the cone (camera tow 54D-OFOS). Width of view ~2.3 m. b. More massive lava with interspersed ash and some hydrothermal alteration (white), northwest caldera site (51A-OFOS). Width of view ~2.8 m. c. Typical example of fresh, vesiculated, dacite lava from the cone site. d. Fe-stained ash and/or sediment on the flank of the volcanic cone (55A-OFOS). Width of view ~8.3 m. e. Talus seen along the southeast flank of the volcanic cone is dominated by relatively fresh dacite lava with pieces of highly altered rock (white) scattered throughout (54D-OFOS). Width of view ~4.7 m. f. Close-up of altered rock shown in (e). The sample is composed predominantly of silica (opal-C), natroalunite, native sulfur, and fine-grained pyrite, consistent with advanced argillic alteration (TAN01/07-135). g. View looking down on a ~2-m-high chimney spire, part way downslope, northwest caldera site. The white-yellow top of the spire is dominated by amorphous silica. Partially obscured (by ash), the yellowish material at the base of the chimney complex is Fe oxide staining (51B-OFOS). Width of view ~1.5 m. h. Long-neck barnacles, the dominant vent-related animal observed at the Brothers vents sites, are here seen on sediment-covered slope of the northwest caldera site (51A-OFOS). Width of view ~1.7 m. For location of camera tracks, see Figure 7.

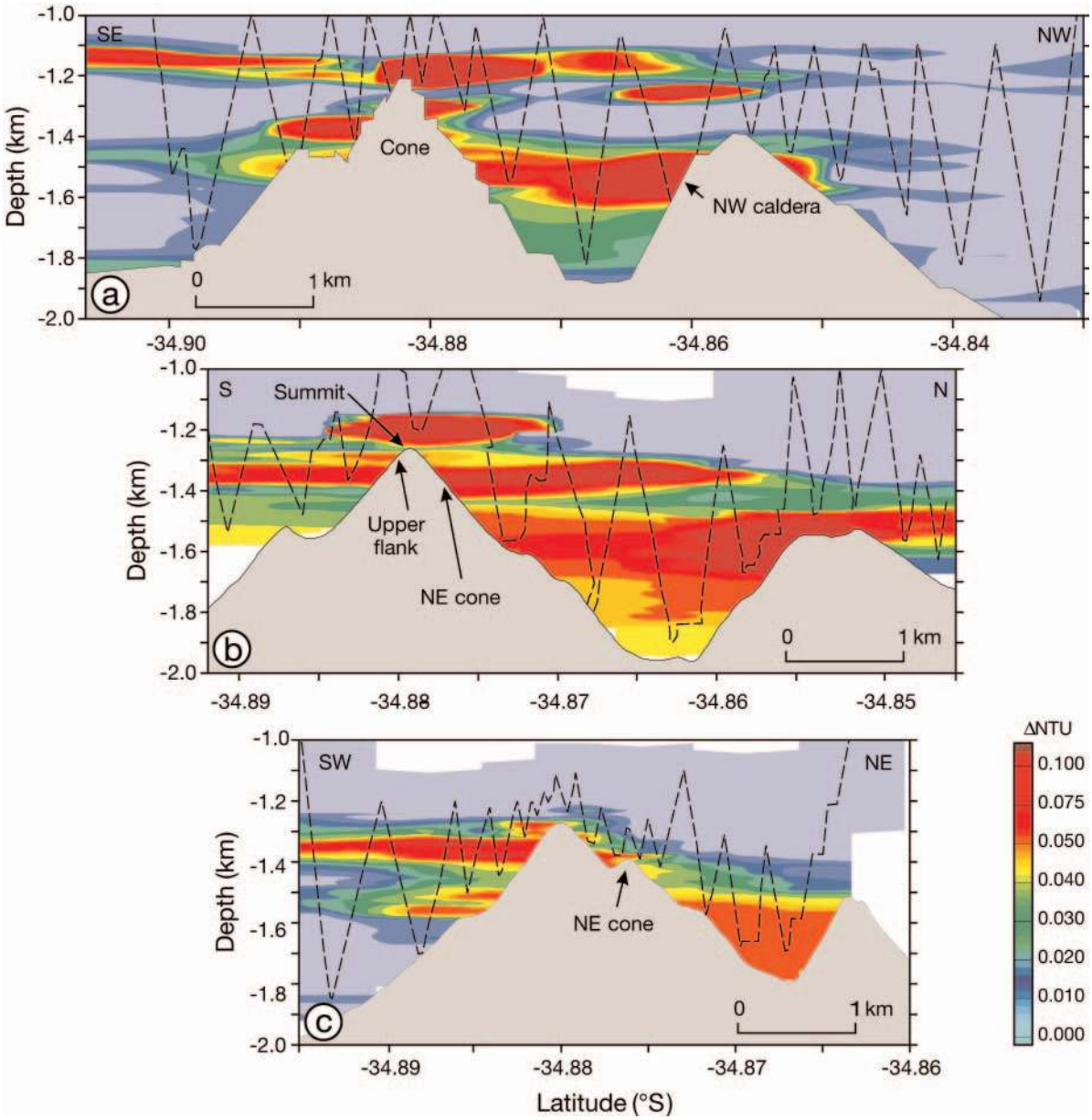

FIG. 4. a. Results of 1999 light-scattering measurements plotted as Δ-NTU (nephelometric turbidity units, a nondimensional optical standard) for plumes along a southeast to northwest traverse of the volcanic cone and northwest caldera sites (tow T6, modified after Baker et al., 2003; see Fig. 2). About ~750 vertical meters of hydrothermal plumes occur from the caldera floor to above the cone summit. b. Results of 2002 light-scattering measurements along a similar (S to N) track to that shown in (a) (tow T10; see Fig. 2). Hydrothermal discharge does not appear to have waned in the 3-year period between surveys with the caldera filled by plumes that locally overflow the caldera rim. This tow clearly shows three plumes originating from the main cone summit, upper flank, and the northeast (satellite) cone sites (see (a)), readily distinguished by depth and composition (see Table 1). c. Results of 2002 light-scattering measurements along a southwest-northeast traverse of the long axis of the volcanic cone (tow T12; see Fig. 2). Here, the main plume at the summit of the cone is not apparent and likely was advecting toward the northwest. The source of the deeper plume over the northeastern part of the cone can be seen originating over the summit of the northeast satellite cone. Note that the 1-km scale bars are related to distance along the tows for easier comparison between surveys and not distance as measured by latitude. Note also that the ΔNTU scale is not linear to accommodate the large range in values measured.

plumes have not changed their composition over the same 3-year interval, indicating steady-state conditions (Table 1).

In 1999, the cone plumes had maximum δ^3He values between 46 and 63 percent, and the northwest caldera plumes had δ^3He values up to 73 percent (δ^3He values represent the % increase in the value of ^{3}He/^{4}He relative to air; Table 1). In 2002, plumes from similar depths show increased values of δ^3He for the cone summit (to 83%) and northwest caldera plumes (to 90%), with the highest value from the vent site on the northeast flank of the cone (181%). The

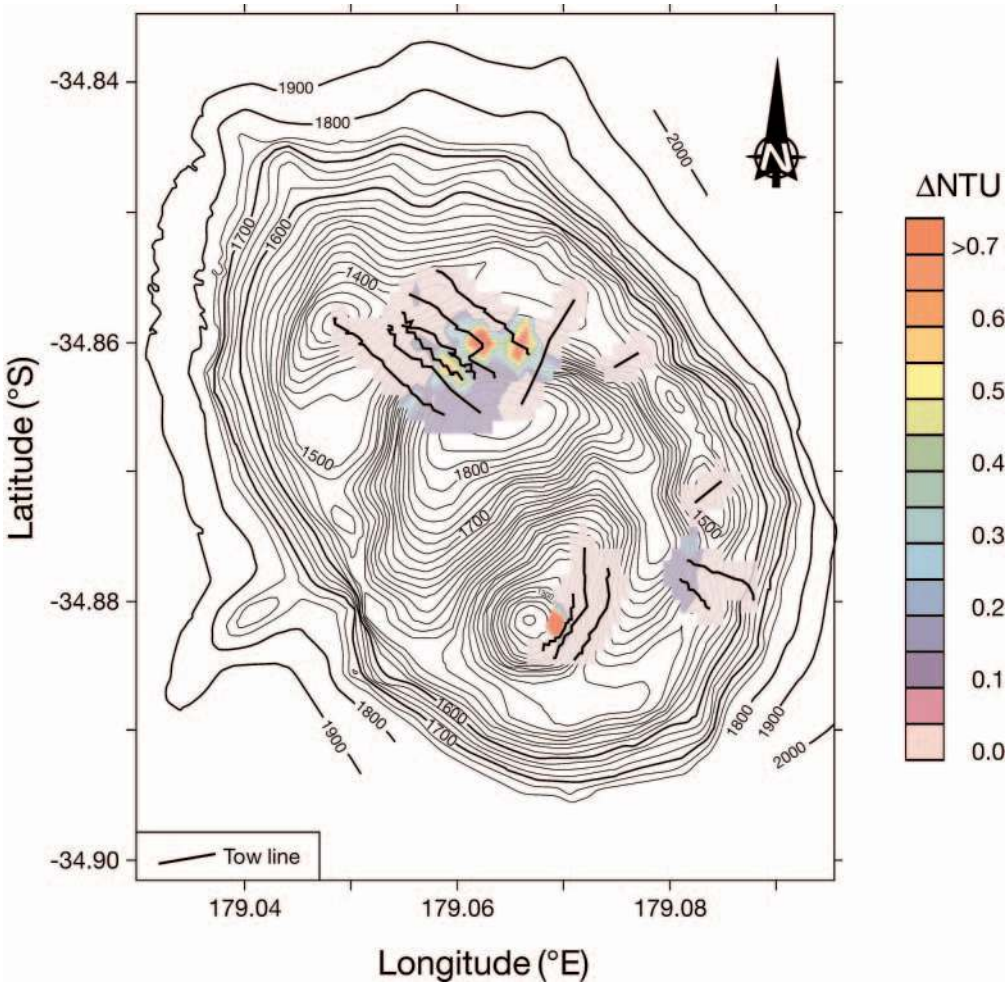

FIG. 5. Results of light-scattering measurements plotted as Δ-NTU from detailed surveys using MAPRs attached to camera sleds and TV grabs during the 1998 R/V *Sonne* 135 cruise. These sleds were towed within 5 to 10 m of the sea floor. The MAPR data highlight active vents within the northwest caldera site. No active vents sites were observed over the cone site although black smoke was seen near the summit. See Figures 2 and 4 to compare the locations of active sites with the main plumes mapped over Brothers.

plume over the upper flank of the cone showed a slight decrease in δ^3He (39%). In some cases, it was possible to estimate the ^{3}He/^{4}He value of the pure end-member He by fitting the slope of the [^{3}He] versus [^{4}He] trend. The end-member ^{3}He/^{4}He values estimated in this way indicate that the northwest caldera plumes have lower (more radiogenic) values than those from the cone site for samples from both 1999 and 2002 but that the absolute values increased at each site over this period (Table 1).

Particulates filtered from the plume samples were analyzed from both the cone and northwest caldera plumes, with the results for Fe, Cu, and S (as total particulate S, including elemental S) given in Table 1. Maximum concentrations of particulate Fe for the plume over the summit of the cone noticeably decreased from 1,213 n*M* in 1999 to 5 n*M* in 2002, in concert with the results for total dissolvable Fe from the same samples. Similarly, concentrations of particulate Cu decreased by an order of magnitude between samples collected in 1999 (3.4 n*M*) and those in 2002 (0.3 n*M*), coincident with a drop in total particulate S values over this time (Table 1). By contrast, particulate concentrations measured in northwest caldera plumes between 1999 and 2002 vary by <20 percent for Fe, and <5 percent for Cu and S values, consistent with steady-state conditions (Table 1). Particulates from both the northwest caldera plumes and those over the summit of the cone in 1999 have the highest concentrations of Fe, Cu, and Zn (Fig. 6). When combined with their relatively high Fe/Mn (Table 1) and Fe/Ti values, this is consistent with high-temperature, black smoker discharge (e.g., Feely et al., 1996; Baker et al., 2003). The plume over the northeast flank of the cone has slightly elevated particulate Cu values, but otherwise this plume and that over the upper flank of the cone appear to be dominated by lower temperature, probably diffuse venting, consistent with video images of these areas. The plume over the summit of the cone can be further differentiated from the other metal-rich plumes by its high concentrations (by up to two orders of magnitude) of particulate Al, although this is only apparent for the 1999 data (Massoth et al., 2003;

TABLE 1. Chemical Characteristics of Brothers Volcano Hydrothermal Plumes

Cruise/ site	Plume depth (m)	δ^3He[1] (%)	ΔpH[2]	CH_4[3] (n*M*)	H_2S[4] (n*M*)	TPS[5] (n*M*)	VS[5] (%)	PCu[5] (n*M*)	PFe[5] (n*M*)	TDFe[6] (n*M*)	TDMn[6] (n*M*)	Fe/Mn (mol/mol)	R/R_A[7]
NZAPLUME I (1999)													
Cone	1,195	63	–0.27		4250	763	(54)	3.4	1213	4720	260	18.2	6.4
	1,225	46	–0.10		2050	117	(42)	0.3	183	300	68	4.4	
NW	1,525	73	–0.06		-	441	(63)	4.5	769	955	150	6.4	5.9
NZAPLUME II (2002)													
Cone	1,195	83	–0.22	2.4	7000	115	(0)[8]	0.3	5	175	220	0.8	7.3
	1,245	39	–0.12	1.4						220	85	2.6	
	1,365	181	–0.44	4.0		574	(80)	0.6	41	85	255	0.3	7.4
NW	1,520	90	–0.09	1.8	-	466	(32)	4.7	873	875	140	6.4	6.9

Notes: - = below detection; blank space = not analyzed; abbreviations: mol = moles per liter; n*M* = nanomoles per liter; TDFe = total dissolvable Fe; TDMn = total dissolvable Mn; TPS = total particulate sulfur; VS = volatile sulfur (% of TPS lost under vacuum and considered to be dominantly native sulfur)

[1] δ^3He: Upon recovery of the CTD-rosette package, samples for helium analysis were immediately sealed into copper tubing using a hydraulic crimping device (Young and Lupton, 1983); helium concentrations and helium isotope ratios were determined using a 21-cm radius, dual collector mass spectrometer; the 1σ precision for the ^{3}He/^{4}He measurements is 0.2% in δ^3He; background δ^3He(%) values at 500- and 1,500-m depth are ~0.5% and ~13.0%, respectively; δ^3He values represent % increase in the value for ^{3}He/^{4}He above air ($\delta^3\text{He} = 100\ [(R/R_A) - 1]$)

[2] ΔpH refers to departure from regional depth trend determined by potentiometric combination electrode referenced to NBS standards at 25°C (1σ 0.005 pH units, detection limit <Δ0.02 pH units)

[3] CH_4 was determined using a combined automated purge and trap/gas chromatograph system (Ishibashi et al. (1997); analytical reproducibility is estimated at ~5%

[4] H_2S was determined in situ using the chemical analyzer SUAVE and the colorimetric detection of methylene blue with a detection limit of ~200 n*M* (Massoth and Milburn, 1997) during NZAPLUME I and from discrete samples aboard the ship during NZAPLUME II

[5] TPS, VS, particulate Fe (PFe), and Cu (PCu) were determined by thin-film X-ray fluorescence on filters (Feely et al., 1991; 1σ 11% S species, 2% Fe, 7% Cu)

[6] TDFe and TDMn were determined on unfiltered samples acidified to pH 1.6 using kinetic-catalytic colorimetric methods adopted for flow-through injection analysis (Massoth et al., 1998; 1σ ≤6% Mn, ≤8% Fe); TD refers to dissolved plus metal phases soluble in weak acid, such as freshly precipitated hydrothermal phases

[7] R/R_A: $R = {}^3\text{He}/{}^4\text{He}$ and $R_A = ({}^3\text{He}/{}^4\text{He})_{air}$

[8] The NZAPLUME II samples were not analyzed until a year after being collected and, although they were stored in a desiccator, may have lost some of their volatile sulfur; discrete water samples were collected in custom fabricated Teflon-coated PVC bottles closed by silastic springs; the values reported in Table 1 represent the samples with the highest concentrations for any one plume

Fig. 6). The relatively high S contents of the Brothers particulates (Baker et al., 2003) likely represents precipitation as sulfides from high-temperature, metal-rich plumes in the case of the northwest caldera site, but elemental S associated with magmatic ($CO_2 + SO_2 + H_2S$) outgassing in the case of the cone plumes (cf. Feely et al., 1999).

Hydrothermal alteration and mineralization

An extensive suite of hydrothermally altered rocks and mineralized samples, including stockworks, massive sulfides, and chimneys were recovered mainly from the northwest caldera site during the1998 R/V *Sonne* cruise (Stoffers et al., 1999a). Samples from the cone and southeast caldera sites come from the 1996 and 2001 R/V *Tangaroa* cruises. Camera and video tows were also done at all these sites, enabling geologic and hydrothermal alteration maps to be constructed.

Camera tows over the northwest caldera site (Fig. 7a) showed massive lava flows and ash and/or sediment cover (Fig. 3a-c), Fe-stained sediments (Fig. 3d), talus (Fig. 3e, f), active and extinct hydrothermal chimneys (Fig. 3g), and localized vent fauna (Fig. 3h). The largest contiguous zone of sulfide mineralization occurs along a narrow ledge at ~1,650 m, consistent with the active venting found by the MAPRs (Fig. 5) and is up to 50 m wide and strikes for ~600 m. Many 1- to 5-m-tall chimneys and spires occur in this zone, together with abundant sulfide talus and subcropping massive sulfides (Fig. 3g). The relatively narrow width of this zone is consistent with hydrothermal venting being controlled by caldera-wall ring faults. At least two smaller zones (up to 25 m across) hosting active black smoker chimneys and inactive spires occur higher up the caldera wall (Fig. 7a). MAPRs and video surveys have identified the western limit of this zone, but the eastern limit remains open (Fig. 7a).

Vigorous venting of black smoke is associated with chimneys at ~1,650 m depth, including three that are 1 to 2 m tall (Fig. 7a), although vent-specific macrofauna were not abundant. A few long-necked barnacles (Fig. 3h; see Buckeridge, 2000), a single galatheid crab, and minor occurrences of filamentous bacteria were the only living organisms observed in the area of active venting. The presence of clam shells, bacterial floc, and long-neck barnacles toward the deeper parts of the tows suggests that a vent fauna assemblage previously occurred at this location but is now very sparse (Fig. 7a). Together, these observations suggest that hydrothermal activity is presently waning and cannot support a large endemic population of vent fauna. Alternatively, the field has recently been rejuvenated and vent-specific organisms have not had time to recolonize the area.

A partially buried chimney field occurs near the sediment- and ash-covered rim of the caldera on a relatively flat escarpment. This is a more discontinuous zone of older eroded sulfide material and relict chimneys than the deeper zone, although it has a similar strike length of ~600 m (Fig. 7a). Shimmering, diffuse venting was noted near the caldera rim although no sulfide samples were recovered from this site.

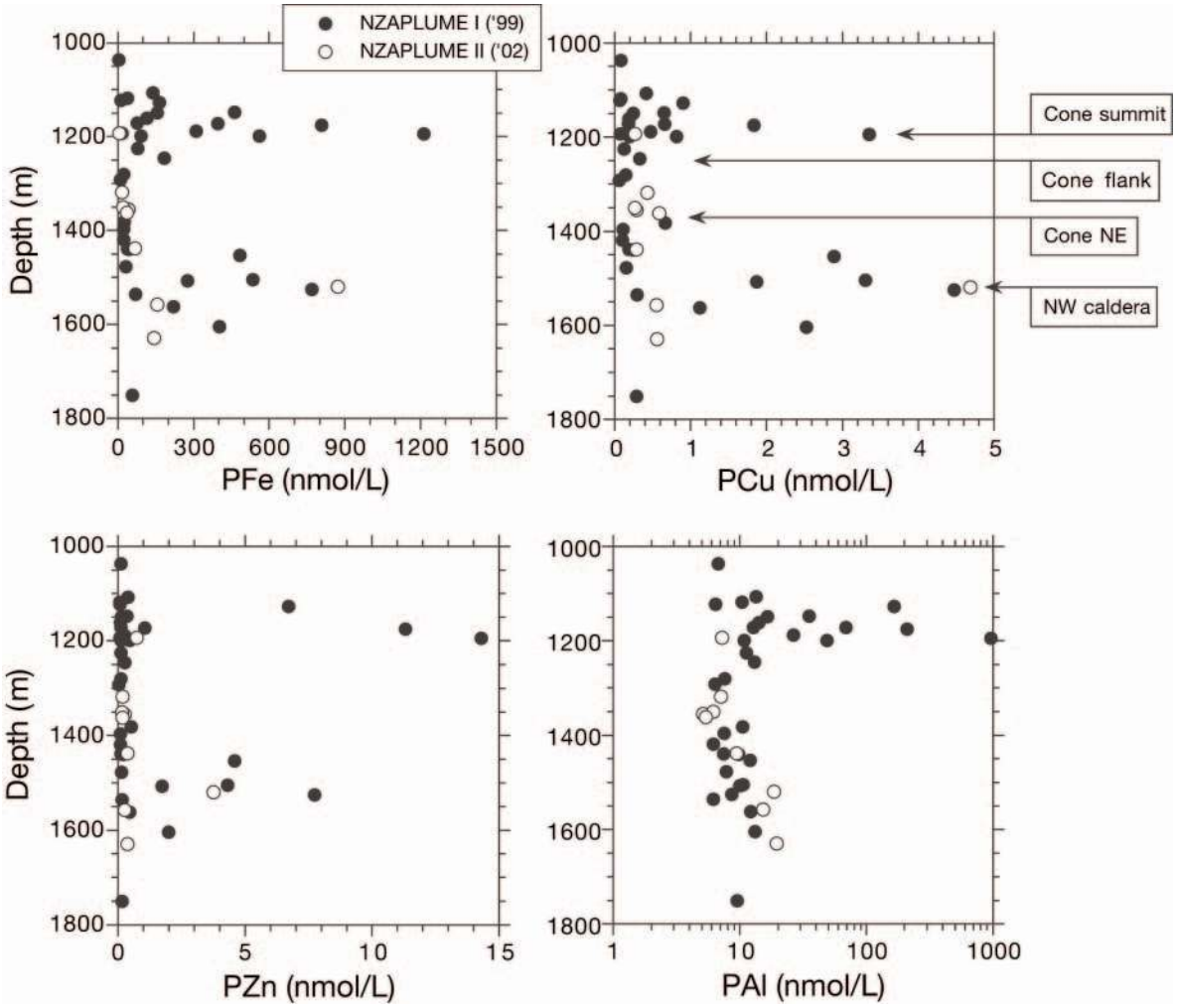

FIG. 6. Concentrations of particulate Fe, Cu, Zn, and Al (designated PFe, PCu, PZn, and PAl) in the hydrothermal plumes above Brothers volcano. Metal loads in the water column, including metals incorporated within the suspended matter, are recorded by volume, hence concentrations are expressed in nmol/L. The northwest caldera and 1999 cone summit plumes are easily distinguished with their relatively high concentrations of particulate Fe, Cu, and Zn and are indicative of high-temperature black smoker vents. Plumes originating from vents of the northeast cone site and to a lesser degree from the upper flanks of the main cone are less easily discerned in these plots, suggesting that they are dominated by diffuse venting. Particulate Al is only seen in the 1999 cone summit plume which showed a noticeable decrease in metals between 1999 and 2002 (see Table 1), suggestive of gas-rich, magmatic fluid discharge (see text).

A section of the southeast caldera wall where a single altered and partially mineralized dacite sample was recovered in 1996 (Wright et al., 1998) was photographed in 1998 by two camera tows (Fig. 7b). Gray, hydrothermally altered talus was observed at the base of the caldera wall during both tows, indicative of past hydrothermal activity. No sulfides were noted, although pieces of chimney were recovered in dredges during the 2001 TAN01/07 expedition.

Three camera tows were completed over the main cone where relatively fresh, glassy dacite talus dominates the slopes, especially near the summit (Fig. 7b). Scattered among the talus were ≤10-cm pieces of intensely altered rock, including fragments of native sulfur (Fig. 3e, f). A ~300-m-long zone of Fe oxide staining and alteration also was noted near the summit of the cone. Diffuse venting over a few hundred meters occurs near the summit of the cone and along a ridge to the northeast. A large near-bottom plume was noted here, although its source could not be located. Associated vent fauna is abundant and includes sulfide worms, limpets, shrimp (Webber, 2004), several large fields of stalked barnacles, and bacterial mats (Fig. 7b).

Dredging of the northwest caldera site recovered abundant glassy, vesiculated dacite lava with rims of Fe oxide staining (Fig. 3c). The lava locally is hydrothermally altered (Fig. 8a) with infilling of vesicles by native sulfur (cf. Fig. 8b). Other recovered material included volcaniclastic lapilli and breccias, both of which are commonly altered to chlorite and smectite (Fig. 8c, d). Relatively fresh, pumiceous ash was recovered during a single TV grab from the rim of the caldera. Six types of mineralized samples were recovered from the northwest caldera site: (1) pyritic stockwork breccias, (2) massive pyrite breccias, (3) pyrite-anhydrite breccias, (4) massive pyrite

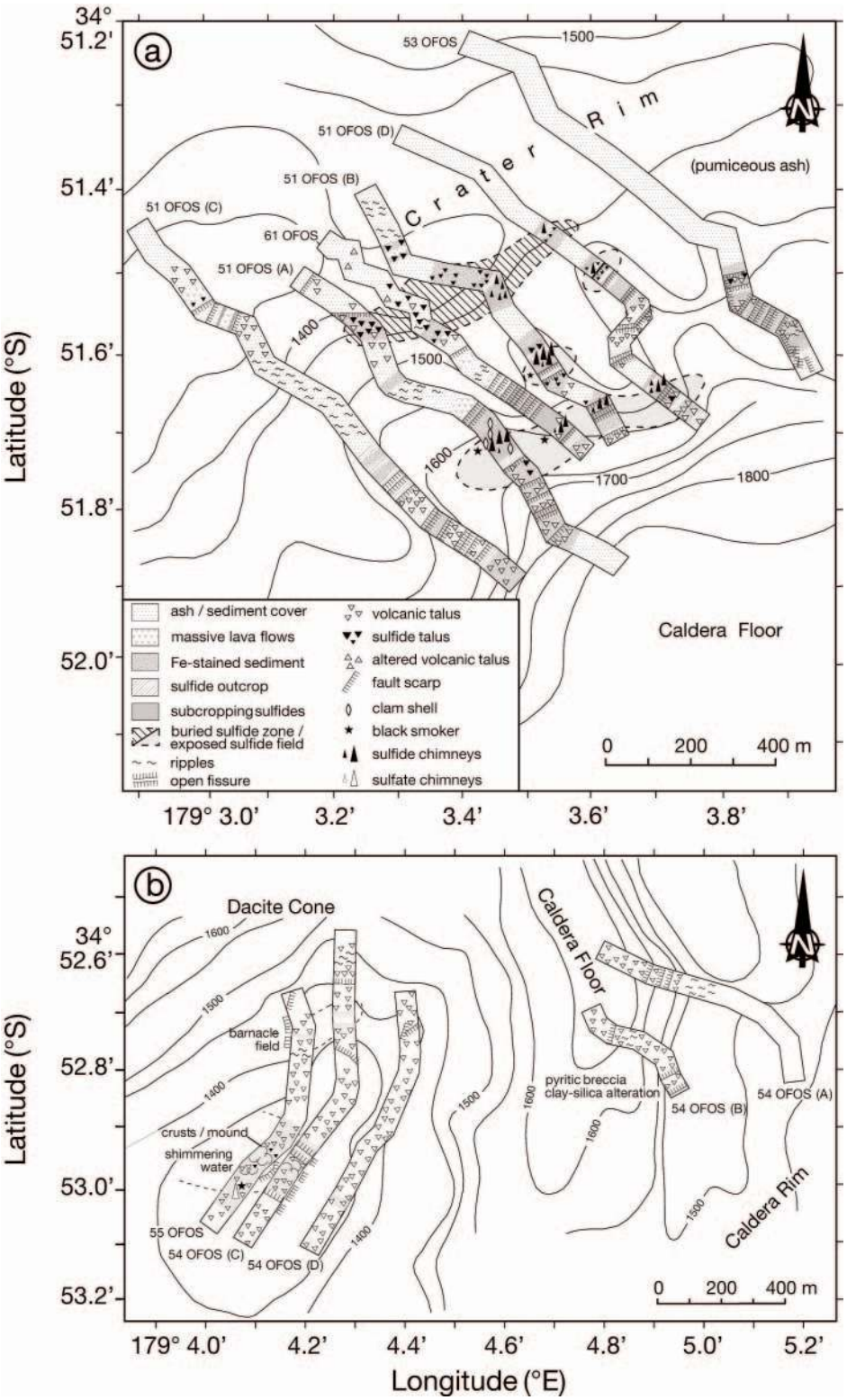

FIG. 7. a. Geology of the northwest caldera site constructed from towed video camera observations (contoured depth in meters). The caldera wall is relatively steep and is largely covered by ash and/or sediment although massive lava flows are seen locally (see Fig. 3). Two large zones containing relict chimneys and spires and subcropping massive sulfides were seen; one nearer the caldera floor and the other nearer the caldera rim. Actively venting chimneys were seen in the lower zone and part way up the caldera wall. b. Observations in towed camera surveys over the cone and southeast caldera sites. Only minor evidence was seen for past hydrothermal activity at the latter site. No actively venting chimneys were observed over the cone site, although several black smoker plumes were seen in 1999 as were abundant vent shrimp and pieces of hydrothermally altered rock (see Fig. 3). Diffuse venting and a large field of barnacles were seen down the northeast flank of the cone.

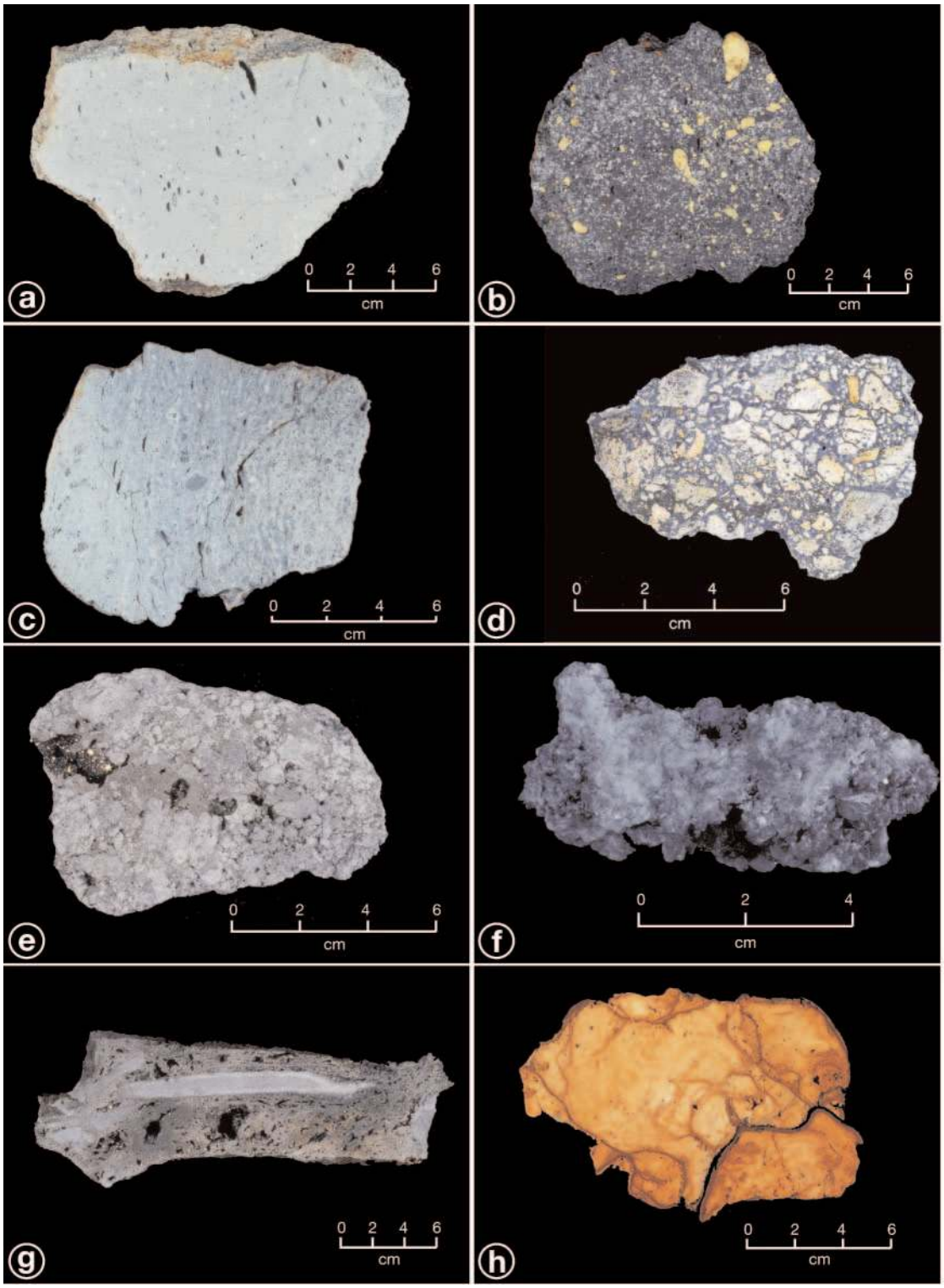

FIG. 8. a. Hydrothermally altered dacite (60DR-5; cf. Fig. 3c). b. Example of vesiculated lava (dacite) with native sulfur infilling of many of the vesicles (D99A-17). c. Hydrothermally altered pyroclastic rock from the northwest caldera site (68DR-9). d. Pyrite-silica breccia comprising large, angular clasts of silicified dacite with abundant disseminated pyrite in the matrix (68DR-1). e. Massive pyrite breccia considered to resemble the upper parts of typical stockwork zones beneath large massive sulfide deposits (52DR-8). f. Pyrite-anhydrite breccias consist of up to 70 to 80 percent crystalline anhydrite with minor disseminated pyrite (52DR-10). g. Massive pyrite crust with enclosed elongate ripup clasts of rock (sediment) + anhydrite ± finely disseminated pyrite (60DR-1). h. Example of an Fe oxide-silica crust commonly found in the peripheral parts of the deposits and in large areas near the caldera rim (56DR-11). All the samples come from the Brothers northwest caldera site except (b), which was recovered from Rumble V but is representative of material also found at Brothers.

crust, (5) Fe oxide-silica crusts, and (6) a massive sphalerite-rich chimney (Fig. 8e, h). Together, the mineralized samples suggest that an older sulfide deposit has been exposed by faulting along the caldera wall and the present black smoker venting at this site may represent a recent phase of activity.

Pyritic stockwork breccias: Two types of pyritic stockwork breccias were sampled: pyrite-silica breccia comprising large clasts of silicified dacite with abundant disseminated pyrite in the matrix (Fig. 8d; these rocks are typical of the upflow zones underlying other sea-floor massive sulfide deposits: e.g., Hannington et al., 1998), and massive pyrite-cemented breccias containing 25 to 50 percent pyrite by volume and clasts of intensely altered dacite.

Massive pyrite breccias: The massive pyrite breccias contain trace amounts of sphalerite and chalcopyrite where open cavities in the pyrite host euhedral crystals of anhydrite (Fig. 8e). These rocks, together with massive pyrite-cemented breccias, resemble the upper parts of typical stockwork zones where networks of pyrite vein grade upward into massive sulfide lenses.

Pyrite-anhydrite breccias: These breccias are commonly massive and consist of 70 to 80 percent crystalline anhydrite with minor disseminated pyrite (Fig. 8f), as well as large clasts of pyrite and anhydrite in a matrix of coarser grained anhydrite. They resemble pyrite-anhydrite breccias of active mid-ocean ridge sulfide deposits (e.g., Petersen et al., 2000) and also in many kuroko-type massive sulfide deposits on land (e.g., Kuroda, 1983; Shikazono et al., 1983). We interpret them as the erosional remnants of anhydrite mounds or chimneys that have collapsed and since been recemented by anhydrite.

Massive pyrite crust: Massive pyrite was recovered in one dredge near the deepest part of the caldera wall. It resembles massive colloform pyrite commonly found on the flanks of high-temperature vents on mid-ocean ridges (Hannington et al., 1998). Several large clasts of altered volcanic material, anhydrite, finely disseminated pyrite, and minor clay are contained in the crust and resemble ripup clasts that have been derived from older, eroded anhydrite chimneys or mounds and later incorporated in a growing pyrite crust (Fig. 8g).

Fe oxide-silica crusts: Abundant Fe oxides and amorphous silica occur as crusts in the peripheral parts of the deposit and in large areas near the caldera rim (Fig. 3d). These delicate crusts have formed from low-temperature discharge and along fractures in the more massive dacite flows. Most consist of brecciated fragments with relict chimney-like textures (Fig. 8h) and are likely to have formed by the repeated growth and collapse of small Fe silica chimneys at the cooler, outer margins of the deposit.

Sphalerite chimney: A massive sphalerite-rich chimney was recovered from the lower (~1,650 m) ledge at the northwest caldera site, near active chimneys. The chimney was intact and measured ~60 cm long and 20 cm in diameter. It is distinctly zoned with an inner core of mostly porous sphalerite and pyrite with minor chalcopyrite lining a central cavity at the base of the chimney and disseminated in the very center. An outer zone is dominated by amorphous silica, barite, pyrite, and marcasite where there are several examples of fossilized worm tubes. A galena-rich zone occurs toward the top of the chimney (Fig. 9). The exterior of the chimney is intensely silicified by amorphous silica. A cross section shows

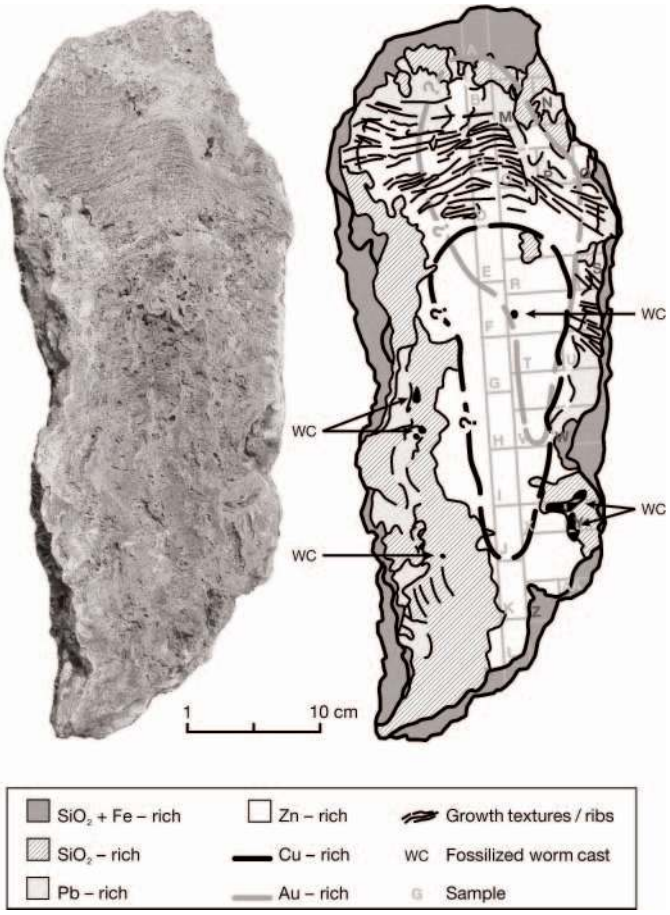

FIG. 9. Single intact chimney recovered from the lower slopes of the northwest caldera site. The interior of the chimney is chaotic with more pronounced banding (growth textures) indicative of lateral fluid flow near the top (i.e., a beehive-like chimney). Detailed geochemical analysis of samples from the interior to the outside margin of the chimney (see Table 2, App. 1) indicates distinct zones of SiO_2, Fe, Pb, and Zn enrichment, with zones of Au enrichment near the top of the chimney and Cu enrichment in its center.

ribbing and flange-like growth textures in a beehive-type structure near the top of the chimney, indicative of lateral fluid discharge (Fig. 9). Several relict pyrite-marcasite walls also are evident in the chimney interior indicating a complex growth history. Fluids have passed through the chimney via a complex array of interconnected channelways, with no discrete vent orifice present. The mineralogy and structure of the chimney closely resemble Zn-rich white smokers formed at 250° to 300°C at mid-ocean ridge sites (e.g., Hannington and Scott, 1988).

Mineralogy

Fifty-five samples from Brothers volcano were analyzed petrographically using both transmitted and reflected light microscopy. X-ray diffractometry was used to determine both the bulk mineralogy and clay fraction of these and other samples. Chemical analyses (n = 6) of silicate and sulfide minerals were obtained using the energy-dispersive X-ray attachment of a scanning electron microscope.

The degree of rock alteration ranges from complete (i.e., 100% of the primary minerals are replaced, apart from apatite

and zircon) to moderate (i.e., 50–60% of the primary minerals are still extant). Thirty-eight secondary minerals were identified in the altered and mineralized rocks, the most common being illitic clays including well-crystallized illite and interlayered illite-smectite, chlorite, corrensite, Na-Ca-Mg smectites including saponite, celadonite, kaolinite, opal-A, zeolites including Na clinoptilolite and stilbite, barite (ranging from pure barite to Sr-bearing barite), pyrite, marcasite, chalcopyrite, sphalerite (ranging from pure ZnS to Fe-bearing ZnS), leucoxene, hematite, and goethite (e.g., Fig. 10a). Less common are epidote, titanite, albite, quartz, lussatine (opal-C, length-fast disordered cristobalite; Graetsch, 1994), lussatite (opal-CT, length-slow cristobalite and/or tridymite; Graetsch, 1994), anhydrite, natroalunite, pyrrhotite, arsenopyrite, enargite, bornite, intermediate solid solution (iss), chalcocite, covellite, galena, anatase and/or rutile, birnessite, and native sulfur (e.g., Fig. 10b).

The secondary minerals occur either as replacement of original volcanic rock, direct hydrothermal precipitates, or sublimates from vapor (e.g., native sulfur). In a few cases, minerals such as jarosite ($KFe_3[SO_4]_2[OH]_6$) and tamarugite ($NaAl[SO_4]_2.6H_2O$) crystallized in humid conditions after the samples were recovered from the sea floor. Primary feldspars and ferromagnesian minerals are usually replaced by other silicate minerals and rarely by barite. Pyrite, goethite, anatase and/or rutile and hematite also replace titanomagnetite, glass, and ferromagnesian phases. The most common silicate minerals in the veins and vugs are opal-A, smectites, zeolites, quartz, and opal-C (Fig. 10c, d). Most of the sulfides, sulfates, and oxides and/or oxyhydroxides also are found in vugs and veins. Kaolinite commonly replaces earlier illitic clays and chlorite and, in one sample from the cone site, natroalunite.

The frequency and abundance of secondary minerals found in the three sites at Brothers volcano are summarized in Figure 11. These minerals are representative of a wide range of hydrothermal temperatures (ambient to ≥300°C), depths, and fluid compositions within the hydrothermal system. Our petrographic studies suggest that several hydrothermal regimes at the northwest caldera site have prevailed, as illustrated by sample SO135-52DR-10, an intensely altered volcanic rock. Here, the rock was initially altered to epidote + titanite + illite by neutral pH fluids that had equilibrated with the rock at ~230° ± 20°C (cf. Reyes, 1990). This sample was later leached by near acid-sulfate waters, further altering the rock to an assemblage of illite + anhydrite + pyrite at similar temperatures. Barite precipitated where seawater mixed with the hydrothermal fluids. Wispy, late-stage kaolinite replaced illite in some samples, indicative of an influx of <150°C acid waters. Opal-A, zeolites, and corrensite were sequentially deposited at lower temperatures, possibly reflecting increased mixing with seawater (e.g., sample SO135-59DR-05; Fig. 10e). Locally, opal-A and Fe sulfides cement fresh glass and hydrothermal rock fragments in lapilli sands (e.g., samples SO135 DR58-07, SO135 DR58-08, and SO135 DR58-10), suggesting rejuvenation of the hydrothermal regime following the eruptions that deposited the glass (Fig. 10f).

At the southeast caldera site, quartz, illitic clay, barite, and chalcopyrite are more abundant than in samples from the northwest caldera site. Bornite (Fig. 10g), intermediate solid solution, and natroalunite are also present, with the latter also found at the cone site (Fig. 10h); none of these minerals occur at the northwest caldera site. By contrast, Mn-Fe oxyhydroxides (including goethite and birnessite), epidote, titanite, chlorite, albite, and zeolites are absent from the southeast caldera site. Mineral assemblages seen here indicate that they originated near a magmatic-hydrothermal upflow zone.

The presence of native sulfur, tridymite, natroalunite, and kaolinite, and the abundance of lussatite in Brothers cone samples are similar to that of active craters within subaerial volcanoes. Unlike subaerial volcanic craters, however, natroalunite and kaolinite are not pervasive in the cone samples but instead are confined to 100-μm-wide fractures (e.g., TAN01/07-131-B2). These fractures are in turn cut by fractures filled by smectite, opal-A, pyrite, and lussatine (Fig. 10c, d), suggesting that upflowing fluids at the Brothers cone site varied between acid sulfate-type fluids and hydrothermal fluid and/or seawater mixtures.

Geochemistry of mineralized samples

Mineralized samples from the northwest caldera site (n = 61), including several from the large intact sphalerite chimney (Fig. 9), the breccia and/or stockwork (Fig. 8e-g), the hydrothermally altered rock with disseminated sulfides, and the Fe-Si crusts (Fig. 8h), were analyzed for their major, minor, trace, and rare earth elements (Table 2; see App.1 for complete results and analytical methods). These data, together with geochemical data obtained from mineralized samples collected in 1996 from the northwest caldera site, from Clark volcano, and Rumble II West volcano (Wright et al., 1998; de Ronde et al., 2003b; C.E.J de Ronde, unpub. data; Fig 1), are plotted in Figure 12.

Iron, Zn, Pb, Cu, Ba, and Si are the major elements in the mineralized samples. Iron concentrations show little variability owing to the abundance of pyrite in most samples. However, its abundance is low, on average, when compared to mid-ocean ridge deposits, consistent with source-rock elemental concentrations (Hannington et al., 2005). Relatively high concentrations of Zn (up to 38 wt %), Ba (up to 42 wt %), and Pb (up to 8 wt %), common in arc-related deposits, are positively correlated and likely reflect both the host-rock composition, including the input of subducted sediments (Stanton, 1994), and the temperature of formation. The generally lower concentrations of Cu compared to mid-ocean ridge sulfides (≤2.7 wt % in this study; one sample of 15.3 wt % reported by Wright et al., 1998) probably indicate relatively lower vent fluid temperatures at Brothers.

Significantly, high concentrations of the epithermal suite of elements, including Ag, Au, Tl, Ga, As, Sb, and Cd, occur in the samples (Table 2, App. 1). These elements may reflect low temperatures and/or boiling conditions and are typically associated with shallower (<500 m) sites. For example, the relatively high values of Tl (up to 270 ppm) have been reported previously only in pyritic crusts in very shallow-water boiling vent sites, such as the Calypso vents offshore New Zealand (Fig. 1), the Grimsey vent fields offshore Iceland, and the littoral vents of the California borderlands (Hannington et al., 1999).

The mineralized breccia and/or stockwork samples are distinguished from the chimney samples by their higher Cu concentrations, indicative of higher fluid temperatures (Table

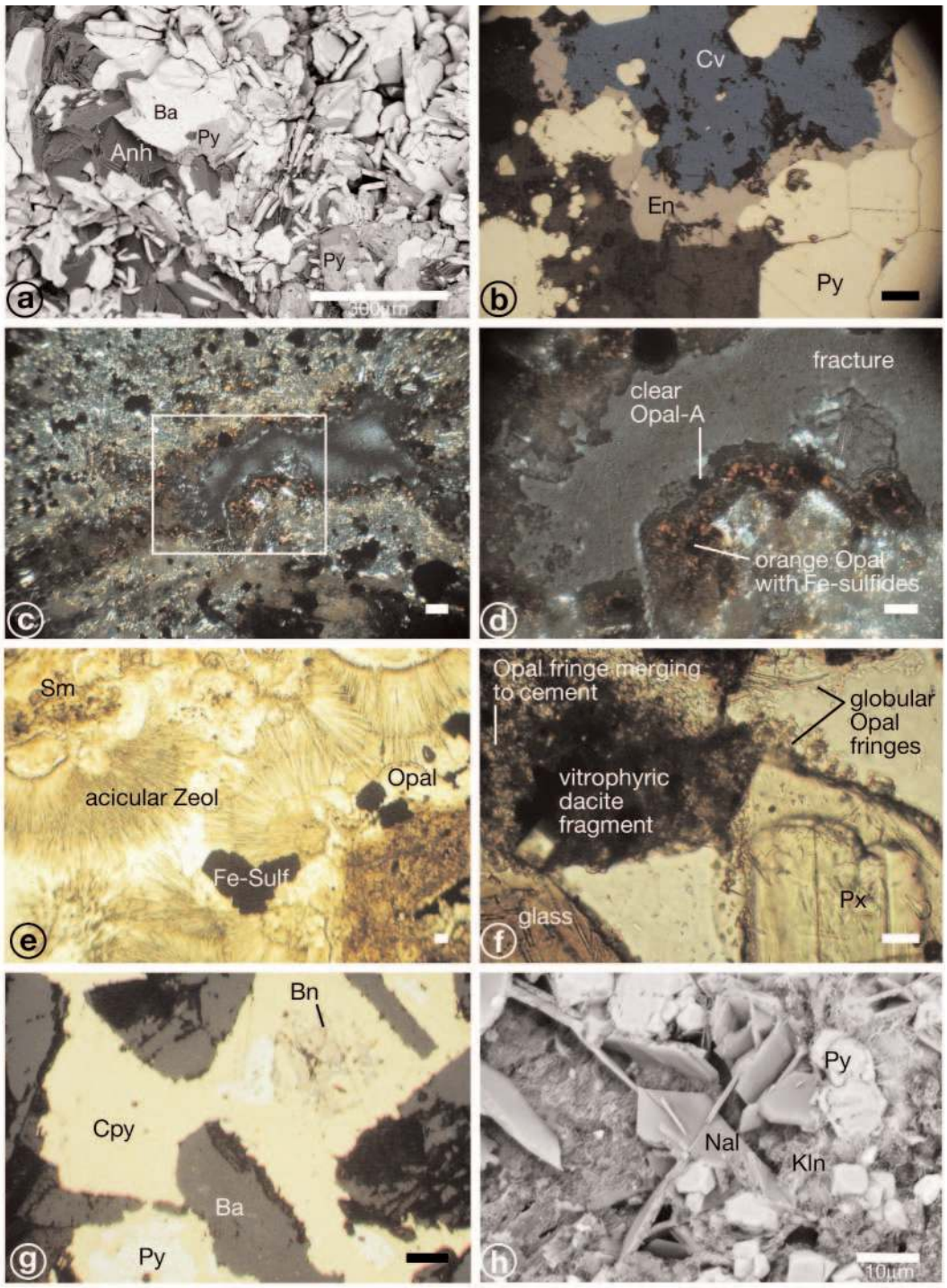

FIG. 10. a. SEM photograph of bladed (commonly rosette type) barite (Ba) intergrown with pyrite (Py) and anhydrite(Anh) from the southeast caldera site (sample TAN07/01-140). b. Photograph taken under reflected light of pyrite with enargite (En) partly altered to covellite (Cv; SO135-52DR-8D). c. Transmitted polarized light photomicrograph showing dacite matrix glass from the cone site completely recrystallized to kaolinite, smectite, opal-A, lussatite (opal-C), tridymite, and sulfides. d. Close-up of the area outlined in (c) showing a fracture lined by orange opal containing microcrystallline pyrite and later clear opal (TAN07/01-131-B2). e. Transmitted light photomicrograph of breccia sample from northwest caldera site showing opal-A, acicular zeolite (Zeol), Fe-rich sulfides (Fe-sulf), and smectite (Sm; 59DR-5). f. Photomicrograph of volcanic sandstone from the northwest caldera site showing loosely cemented fragments that commonly have a narrow rim of opal that later cements the sample (58DR-8). g. Sample from inferred upflow zone at the southeast caldera site. Early-stage bornite (Bn) and pyrite are mantled by chalcopyrite (Cpy) intergrown with barite (TAN07/01-140b). h. Bladed natroalunite (Nal) intergrown with kaolinite (Kln) and pyrite. This habit of natroalunite is commonly seen in magmatic hydrothermal systems (TAN07/01-131). Scale bar in each photomicrograph is 20 μm, unless otherwise indicated. For additional photomicrographs of ore minerals from Brothers, see de Ronde et al. (2003b).

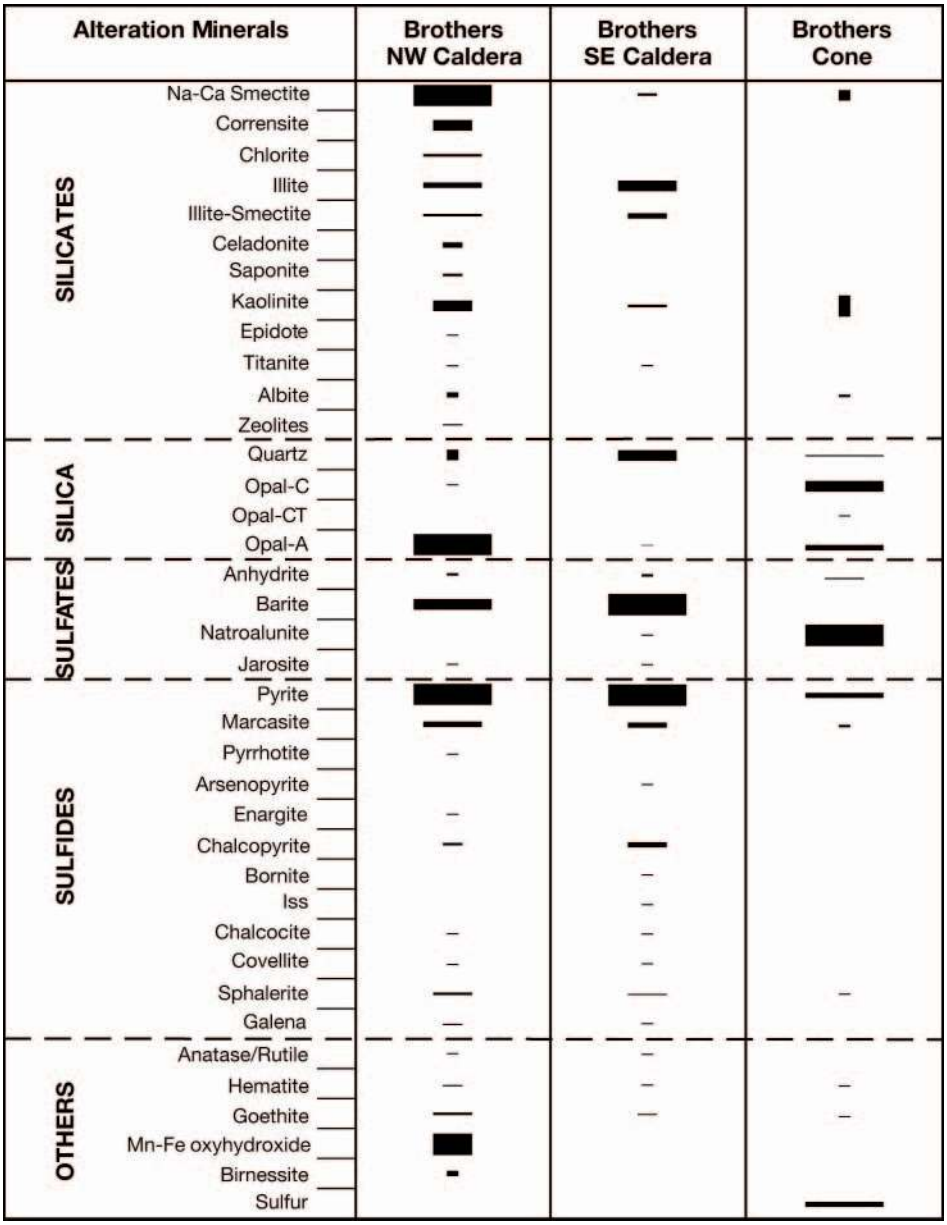

FIG. 11. Relative frequency and abundance of minerals found replacing rock and deposited in vugs and fractures in the northwest caldera, southeast caldera, and cone sites at Brothers. The number of different minerals found in the northwest caldera site is partly due to the greater number of samples collected and analyzed from this site, compared to the other two sites. Prehnite was also found in the volcanic sandstones of the northwest caldera site. The length and thickness of the bar denotes increasing frequency and abundance, respectively. Iss = intermediate solid solution.

2, Fig. 12). Conversely, Pb concentrations are highest in the chimney and Fe-Si crusts and/or sediment samples and likely indicate relatively low temperature fluids (cf. Hannington et al., 2005). The tight cluster of data for chimney samples in Figure 12 corresponds to analyses from the chimney shown in Figure 9 and is distinct from other inferred chimney samples from Brothers and Rumble II West (e.g., see Ba and Cu vs. Zn, Fig. 12).

Sulfur and Oxygen Isotopes

Sulfur isotope compositions were determined for sulfide (chalcopyrite, pyrite, sphalerite), sulfate (anhydrite, barite, natroalunite), and native sulfur separates from the northwest caldera, southeast caldera, and cone samples (n = 49). In addition, native sulfur was analyzed from Rumble V (n = 3). Oxygen isotope compositions (n = 9) were determined for all the sulfates (Table 3).

Sulfide δ^{34}S values for Brothers samples fall into two categories. Those from the intact sphalerite-rich chimney are between 0.2 and 2.1 per mil, similar to δ^{34}S values of –0.5 to 3.0 per mil for sulfides from previously recovered chimney fragments of the northwest caldera site and from Rumble II West volcano (de Ronde et al., 2003b). By contrast, sulfides from breccia and stockwork samples from Brothers northwest

TABLE 2. Geochemical Composition of Selected Sulfides from the Brothers Northwest Caldera Site

Sample type[1]	Fe (wt %)	Au (ppb)	As (ppm)	Sb (ppm)	Ag (ppm)	Ba (ppm)	Cd (ppm)	Cu (ppm)	Pb (ppm)	Zn (ppm)
Single intact chimney										
Low	0.7	17	215	23	38	6650	8	230	220	72100
High	15.0	1430	4390	579	1180	108000	700	3580	85200	380000
Average[2]	4.1	467	1080	189	340	40081	276	1081	25207	169541
± 1σ	4.4	479	1051	121	305	23044	194	949	28535	91996
n	27	17	27	27	27	27	27	27	27	27
Breccia/stockwork										
Low	4.2	58	6	0.4	0.4	170	0.2	26	9	12
High	42.9	1850	1630	169	2.8	11600	1.8	26500	180	420
Average	24	532	605	22	1.3	3488	1.1	2905	75	127
± 1σ	14	596	587	52	0.8	4102	0.7	7901	53	138
n	11	9	10	10	11	11	6	11	11	10
Hydrothermally altered rock with disseminated sulfides										
Low	3.8	4	13	0.7	0.1	640	0.3	25	11	12
High	8.9	190	143	16.2	5.0	8240	32	370	490	14400
Average	6.0	77	63	4.1	1.3	2494	6.5	107	109	2049
± 1σ	1.9	74	44	5.0	1.7	2471	12.5	118	151	4672
n	9	7	9	9	8	9	6	8	9	9
Fe-Si crusts/sediments										
Low	1.0	5	21	0.5	0.2	34	0.2	11	18	15
High	30.5	97	2620	88.4	1.4	2410	2.6	180	3720	1350
Average	11.0	37	646	15	0.6	831	1.0	65	789	308
± 1σ	11.3	33	825	25	0.5	773	0.8	67	1147	389
n	14	6	14	13	13	14	10	13	14	14

[1] Single intact chimney shown in Figure 9; examples of other rock types shown in Figure 8; for full data set, see Appendix 1
[2] Average calculated from those samples that had concentrations above the detection limit

caldera site, chimney fragments from the southeast caldera site, and intensely altered samples from the cone site (e.g., Fig. 3f) have mostly negative $\delta^{34}S$ values, between –4.7 and 0.3 per mil (Table 3, Fig. 13a). Native sulfur $\delta^{34}S$ values from the cone site are even more negative, between –8.3 and –3.9 per mil (Fig. 13b), similar to $\delta^{34}S_{sulfur}$ values for the Rumble V volcano, which are between –5.6 and –4.8 per mil (Table 2).

Sulfate $\delta^{34}S$ values for Brothers anhydrite and barite range between 20.5 and 23.8 per mil, similar to those reported previously (de Ronde et al., 2003b; Fig. 13a). Due to minimal fractionation between sulfate minerals and aqueous sulfate, the measured isotopic composition of sulfate minerals approximates the isotopic composition of the parent fluid (Seal et al., 2002, and references therein). Thus the results given in Table 3 indicate that barite and anhydrite were formed by mixing of Ba- and Ca-rich hydrothermal fluids with seawater (~21‰; Rees et al., 1978). The shift to slightly higher than seawater values could be ascribed to local thermochemical reduction of seawater during interaction with ferrous silicates and/or organic matter in the shallower part of the hydrothermal system (Shanks et al., 1995; Seal et al., 2000). Natroalunite $\delta^{34}S$ values are noticeably lower than the seawater value, ranging between 14.7 and 17.9 per mil.

The rate of isotopic exchange between dissolved sulfate and sulfide is relatively quick and isotopic equilibrium between the species is fairly easily attained as both the chemical and isotopic reactions involve simultaneous oxidation of sulfide-sulfur atoms and reduction of sulfate-sulfur. The most favorable conditions for isotopic exchange in typical hydrothermal systems are temperatures above ~200°C, near-neutral to slightly acidic conditions (i.e., pH $\approx$ 4–7), and $\Sigma S = 10^{-2}$ m (Ohmoto and Lasaga, 1982). We can therefore calculate temperatures of formation from the sulfur isotope compositions of coexisting mineral pairs. Values of $\Delta^{34}S_{barite\text{-}pyrite}$ range between 19.3 and 23.2 for mineralized northwest caldera samples (de Ronde et al., 2003b) and between 21.9 and 24.9 for southeast caldera samples (Table 3). Combining the fractionation factors for SO_4 minerals and aqueous sulfate (Ohmoto and Lasaga, 1982) with those of pyrite (Ohmoto and Rye, 1979) and solving for temperature, gives formation temperatures of 245° to 295°C for the northwest caldera site and 225° to 260°C for the southeast caldera site. The calculated temperatures for the northwest caldera samples are consistent with barite-hosted fluid inclusion homogenization temperatures which are mostly between ~240° and 290°C, with a prominent mode at 260° to 270°C (de Ronde et al., 2003b). Similarly, $\Delta^{34}S_{natroalunite\text{-}pyrite}$ pairs from cone mineralized samples range between 18.8 and 21.8 (Table 3), giving temperatures of 260° to 305°C.

Oxygen $\delta^{18}O$ values for sulfates range between 6.0 and 8.6 per mil with the exception of one barite sample having a value of 3.9 per mil (Table 3). The distinction between natroalunite and the other sulfates can be seen in a plot of $\delta^{34}S$ versus $\delta^{18}O$ values for the same samples (Fig. 13c). The apparent positive correlation between sulfate $\delta^{34}S$ and $\delta^{18}O$ values is consistent with isotopic equilibrium between S species and seawater over a temperature range (Robinson, 1977). Applying average fluid inclusion homogenization temperatures and $\delta^{18}O$ values

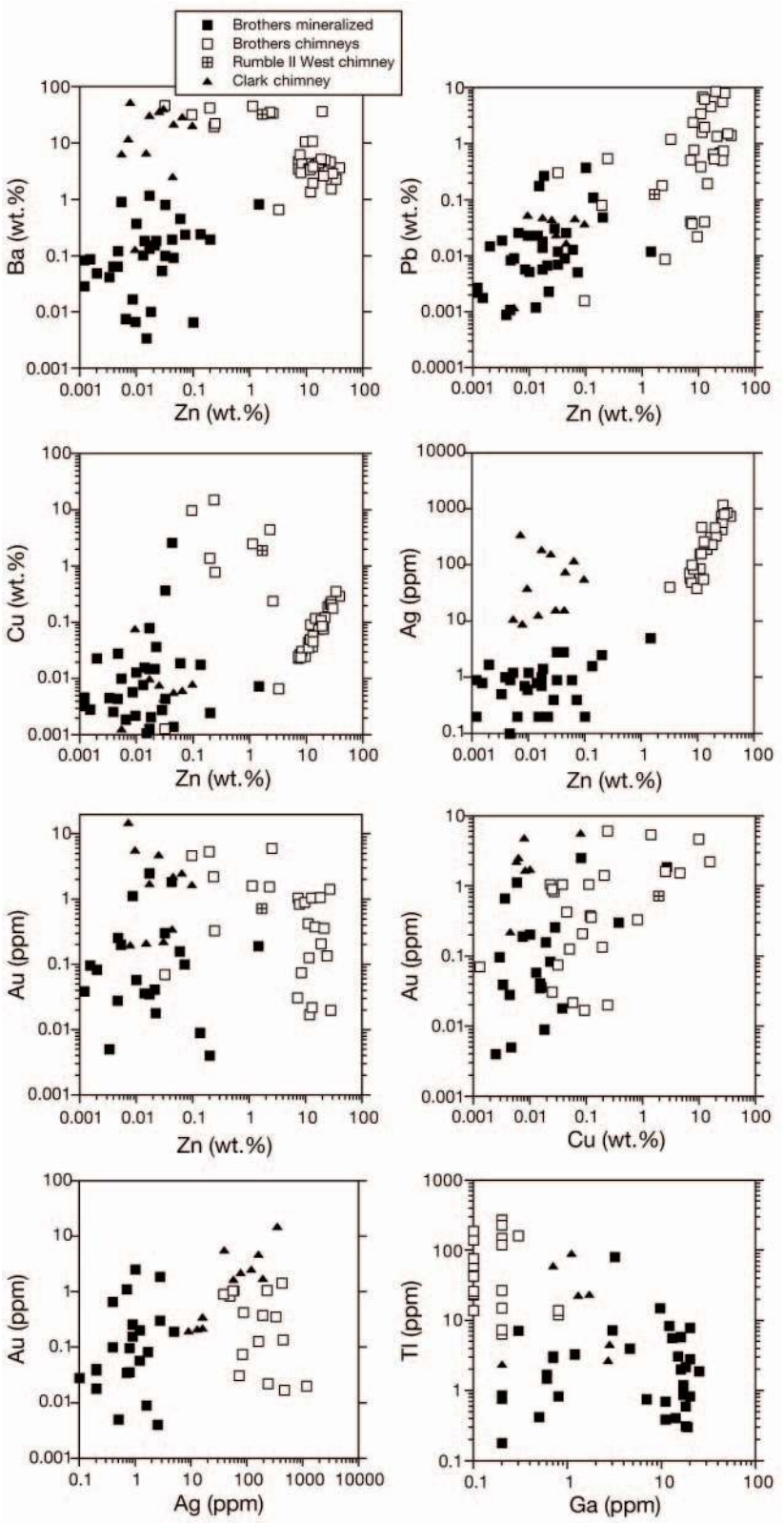

FIG. 12. Log/log plots of the concentrations of selected elements in mineralized samples recovered from Brothers (see Table 2). For comparison, results are also plotted for similar samples from Rumble II West and Clark volcanoes (Wright et al., 1998; de Ronde et al., 2003b; C.E.J. de Ronde, unpub. data). The open squares designating chimney samples from the Brothers northwest caldera site include the tightly clustered group from the chimney shown in Figure 9 (e.g., Cu vs. Zn) and fragments from other chimneys (Wright et al., 1998). Note that samples analyzed from the Brothers chimney are from the other half of the chimney shown in Figure 9.

TABLE 3. Sulfide and Sulfate $\delta^{34}S$ and $\delta^{18}O$ Data for Brothers Volcano

Location/ Sample no.	Mineral analyzed	$\delta^{34}S$[1] (‰)	$\delta^{18}O$[2] (‰)
Brothers			
Northwest caldera—chimney			
57DR-1b	Sphalerite	1.7	
57DR-1d	Pyrite	0.2	
57DR-1d	Sphalerite	1.5	
57DR-1f	Pyrite	1.4	
57DR-1i	Pyrite	2.1	
57DR-1o	Sphalerite	0.9	
57DR-1p	Sphalerite	1.2	
57DR-1s	Sphalerite	1.3	
57DR-1 (exterior)	Chalcopyrite	1.3	
57DR-1 (exterior)	Anhydrite	21.7	6.0
Northwest caldera—breccia/stockwork			
52DR-8a	Pyrite	–1.8	
52DR-8d	Anhydrite	23.3	8.3
52DR-8d	Pyrite	–1.2	
52DR-10	Anhydrite	22.2	7.7
52DR-10	Pyrite	–3.2	
60DR-1 (fines)	Pyrite	–1.9	
60DR-1 (coarse)	Pyrite	–2.9	
60DR-2	Pyrite	–2.7	
60DR-5[3]	Pyrite	–5.6	
68DR-1	Pyrite	–2.8	
68DR-2	Pyrite	–3.9	
68DR-3	Pyrite	–3.0	
68DR-8[3]	Pyrite	0.0	
68DR-8[3]	Sphalerite	–1.8	
68DR-10[3]	Sphalerite	–2.0	
Southeast caldera			
07/01-140a-1[4]	Pyrite	–0.4	
07/01-140b	Barite	23.8	6.8
07/01-140b[4]	Pyrite	–1.1	
07/01-140c-1[4]	Pyrite	0.3	
07/01-140c-2[4]	Pyrite	–3.3	
07/01-140c-3	Barite	20.5	3.9
07/01-140c-3[4]	Pyrite	–1.4	
07/01-140c-3[4]	Sphalerite	–2.9	
Cone			
004	Sulfur[5]	–8.3	
07/01-131a	Pyrite	–4.7	
07/01-131a	Sulfur	–5.6	
07/01-131b-1	Natroalunite	17.9	7.5
07/01-131b-1	Sulfur	–6.7	
07/01-131b-1	Pyrite	–3.9	
07/01-135	Natroalunite	16.9	8.0
07/01-135	Sulfur	–5.1	
07/01-136	Natroalunite	15.5	6.9
07/01-136	Sulfur	–3.9	
07/01-136	Sphalerite	–4.6	
07/01-136b	Pyrite	–3.9	
07/01-141a-2	Sulfur	–4.0	
07/01-141a-1	Natroalunite	14.7	7.2
07/01-141a-1	Pyrite	–4.1	
07/01-141b	Sulfur	–5.3	
Rumble V			
Summit vents			
D99A-17-1	Sulfur	–5.5	
D99A-17-2	Sulfur	–4.8	
D99A-14	Sulfur	–5.6	

Notes: All the DR samples are prefaced by "SO-135" (R/V *Sonne* cruise 135) and the 07/01 samples by "TAN" (R/V *Tangaroa* cruise); the D99A samples are from the 1999 NZAPLUME I cruise; for site locations, see Figure 1

[1] $\delta^{34}S$ values are normalized using IAEA-S-1 = 0.0 ± 0.2‰ and are reported relative to V-CDT; they have a precision and accuracy of ± 0.2‰

[2] $\delta^{18}O$ values are normalized using IAEA-SO-5 = 11.7 ± 0.2‰ and are reported relative to V-SMOW; they have a precision and accuracy of ± 0.3‰

[3] Hydrothermally altered lava

[4] Average for two separate analyses

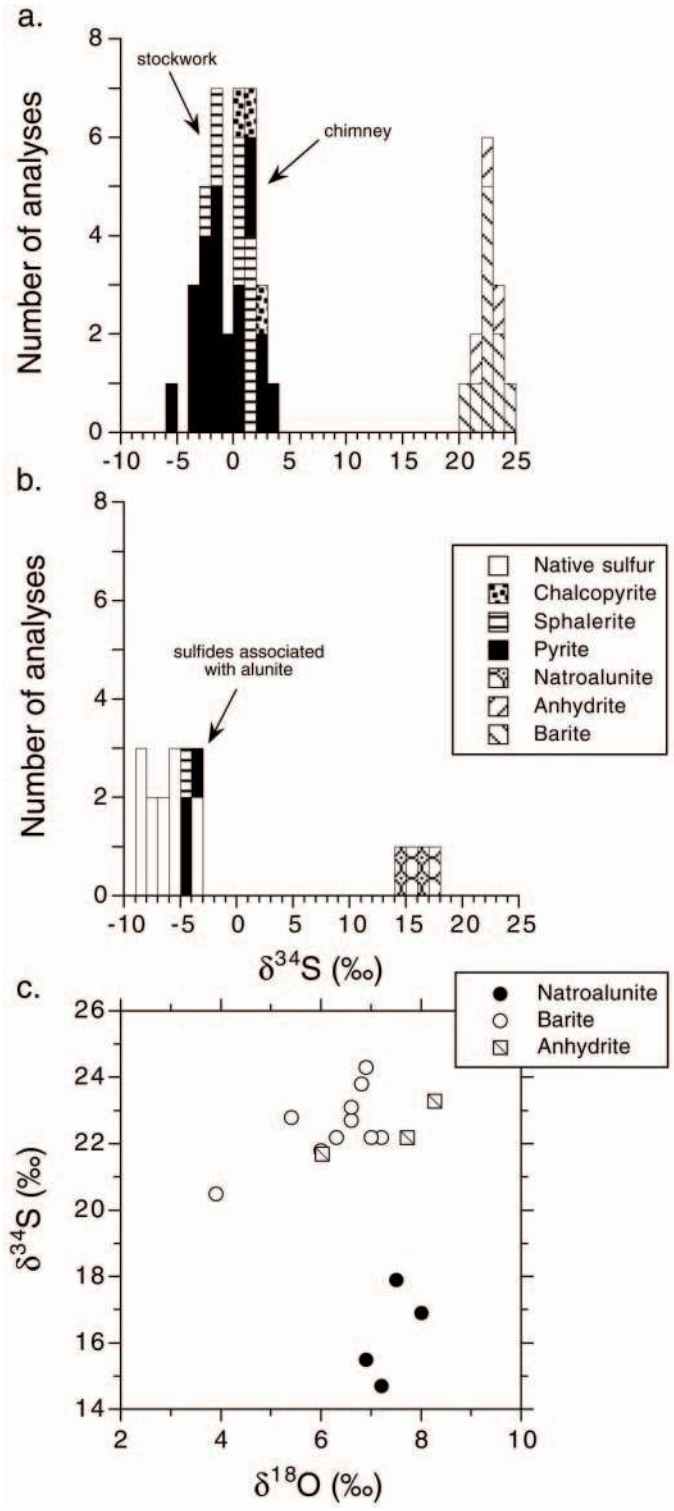

FIG. 13. Combined Brothers $\delta^{34}S$ data from this study (Table 3) and that of de Ronde et al. (2003) for the northwest caldera (a) and cone (b) sites. At the northwest caldera site, most of the sulfide $\delta^{34}S$ values <0 per mil are from stockwork samples, whereas those with values >0 per mil are either from a single chimney (see Fig. 9) or chimney fragments (de Ronde et al., 2003). At the cone site, $\delta^{34}S$ values of sulfide and native sulfur <0 per mil are considered indicative of a magmatic fluid component. c. Barite and anhydrite have typical seawater-dominant $\delta^{34}S$ values. $\delta^{34}S$ values of natroalunite, when combined with $\delta^{18}O$ values, indicate precipitation from a hydrothermal fluid.

from northwest caldera barite (de Ronde et al., 2003b) to the barite-H_2O fractionation curve of Seal et al. (2000), modified after Kusakabe and Robinson (1977), we calculate the $\delta^{18}O_{H_2O}$ value for water responsible for the precipitation of this barite to be between 1.5 and 2.3 per mil. Applying the same fractionation curve to barite $\delta^{18}O$ values from the southeast caldera site (Table 2) and the $\Delta^{34}S_{barite\text{-}pyrite}$ temperatures calculated above, $\delta^{8}O_{H_2O}$ values lie between –0.5 and 1.1 per mil. The range is similar to the measured $\delta^{18}O_{H_2O}$ values of vent fluids from other active sites (e.g., Shanks et al., 1995), although without corresponding δD_{H_2O} values it is difficult to determine a magmatic component in the water (de Ronde, 1995).

Fluid Inclusion Gases

Fluid inclusion gases analyzed by gas chromatography provide additional information on vent fluid chemistry at the Brothers hydrothermal sites. This technique enables gases to be analyzed from both sulfides and sulfates (Bray et al., 1991, see Table 4 for details). In a previous study, de Ronde et al. (2003b) analyzed sulfide and sulfate mineral composites from northwest caldera samples and one barite sample from the

TABLE 4. Gas Analyses of Fluid Inclusions within Sulfides and Sulfates from the Brothers Hydrothermal System (data for Minami Ensei and Nurukawa are show for comparison)

		Mole % (unless otherwise stated)										
Location/ sample	Mineral[1]	N_2^+	CH_4	CO_2	H_2O	COS[2] (ppm)	C_2H_4 (ppm)	$C_2H_6^+$ (ppm)	C_3H_4 (ppm)	C_3H_6 (ppm)	CO_2/CH_4	CO_2/N_2
Brothers (Kermadec arc)												
Northwest caldera												
Massive pyrite breccia												
60DR-1	Pyrite	0.020	0.007	0.123	99.839	99	11.1		2.2		18	6.2
60DR-2	Pyrite	0.015	0.027	0.135	99.812	43	52.5	7.6	6.2	3.4	5.0	9.0
Chimney												
57DR-1A/C	Galena	0.009	0.005	0.807	99.176	12	1.7	3.1		1.9	161	90
57DR-1A/E	Sphalerite	0.009	0.003	0.046	99.933	51	1.1	11.9	0.3	16.2	15	5.1
Southeast caldera												
Massive sulfides												
07/01-140c-1	Pyrite	0.014	0.125	2.383	97.465	0.02	1.3	112.6		53.3	19	170
07/01-140c-2	Pyrite	0.027	0.031	0.521	99.418		8.8		14.6		17	19
Minami Ensei knoll (Okinawa back arc)												
Taimatsu chimney												
575a-1	Sphalerite	0.040	0.024	0.627	99.274	310					26	16
575a-2	Sulfides	0.047	0.031	0.689	99.220	130	5.1				22	15
575c	Anhydrite	0.017	0.006	0.077	99.899	5	0.2		0.1	0.1	13	4.5
575e	Anhydrite	0.181	0.022	0.124	99.673						5.6	0.7
Yunoi chimney												
617d	Cemented sulfides	0.043	0.071	0.657	99.222	62	1.9	3.4	0.9		9.3	15
617a-1	Barite	0.023	0.054	0.544	99.379		3.2				10	24
617a-2	Barite	0.092	1.219	0.010	98.678		0.6			2.7	0.01	0.11
617c	Anhydrite	0.028	0.022	0.441	99.508						20	16
617e	Anhydrite	0.017	0.030	0.401	99.551	15	1.1			2.0	13	24
Four Brothers chimney												
649a	Anhydrite	0.015	0.011	0.348	99.626						32	23
649c	Anhydrite	0.016	0.047	0.076	99.860		17.2				1.6	4.8
Nurukawa koroko deposit (Tertiary back arc)												
Stockwork veins												
89-8-1-3	Quartz	0.005	0.006	0.045	99.943		1.0	9.2			7.5	9.0
3-2b	Quartz	0.004	0.007	0.055	99.933		0.6	5.9			7.9	14
8-4b	Quartz	0.004	0.010	0.073	99.912		0.4	13.9			7.3	18
89-8-7	Quartz	0.005	0.009	0.069	99.916		1.1	8.6			7.7	14

Notes: A ~0.8-g sample is crushed in a heated (~105°C) stainless steel crusher on-line to an HP5890 gas chromatograph; analyses run under isothermal (80°C) conditions; the crusher is pumped up to 7,000 p.s.i. and released, resulting in the appropriate crushing pressure, then released quickly to zero pressure; N_2^+ values are a combination of N_2-CO-Ar-O_2 where N_2 is the dominant gas; similarly, the $C_2H_6^+$ value is a combined C_2H_2/C_2H_6 peak where C_2H_6 is the dominant gas (see Bray et al., 1991, for details); detection limits for H_2O, CO_2, CH_4, and N_2 are on the order of 30 ppm molar and ~1 ppm molar for most hydrocarbons; all the DR sample numbers are prefaced by "SO135" (R/V *Sonne* cruise) whereas the 07/01 samples are prefaced by "TAN" (R/V *Tangaroa* cruise); sample numbers for the Minami Ensei knoll sites refer to the submersible *Shinkai 2000* dive numbers (i.e., dive 575 on 4/10/1991, dive 617 on 4/6/1992, dive 618 on 6/6/1992, dive 649 on 10/10/1992); Nurukawa samples 89-8-1-3, 3-2b, 8-4b, and 89-8-7 relate to samples SSO-1, CSO-1, CSO-2 and CSO-3 of Sasaki et al. (1995), respectively

[1] Dominant mineral in the sample; sulfides refers to a mixed sulfide sample

[2] Ppm are in molar units; blank space, below detection; samples 575a-1 and 575c contained 31.8 and 1 ppm C_4H_{10}, respectively

Rumble II West volcano. They compared their results with similar data for barite from the Myojinsho and Myojin Knoll vents sites of the Izu-Bonin arc and quartz stockwork veins from the Nurukawa kuroko-type (massive sulfide) deposit of Japan (Sasaki et al., 1995). Fluid inclusions from these deposits contain significantly higher concentrations of CO_2 and lesser amounts of CH_4 than the Kermadec samples. The relatively higher concentrations of CH_4 in the Kermadec samples were considered enigmatic by de Ronde et al. (2003b).

To better characterize the Brothers vent fluid compositions, we have analyzed supplementary samples of different mineralization types from other Brothers vents, including sulfide separates extracted from the massive pyrite breccia (Fig. 8g) and chimney (Fig. 9) from the northwest caldera site and chimney fragments recovered from the southeast caldera site. In addition, sulfide and sulfate separates were analyzed from several active chimneys from the Minami Ensei Knoll vent site, Okinawa trough (Aoki et al., 1993; Chiba et al., 1993; Table 4), with the further aim of comparing gas chemistry signatures of the Kermadec arc with other sites where vent fluid compositions have been well characterized, like the Izu-Bonin back arc. Subsamples of four of the six quartz vein samples from the Nurukawa kuroko deposit analyzed by Sasaki et al. (1995) were also reanalyzed in this study.

The combined gas data from this study and that of de Ronde et al. (2003b) are plotted in Figure 14. The majority of the new analyses indicate gas concentrations similar to those of de Ronde et al. (2003b), with the exception of the highest CO_2 values of 0.81 and 2.38 mol percent in pyrite from the southeast caldera chimney fragments and in galena from the outer zone of the chimney, respectively (Table 4). Fluid inclusion gases from the Minami Ensei samples generally fall within the range of the Brothers data with two barite samples having higher N_2 concentrations (up to 0.18 mol %).

The new gas data from the Nurukawa stockwork quartz veins plot within the range shown in Figure 14, in contrast to the data of Sasaki et al. (1995) which span a larger range, with CO_2 up to five times higher than ours and N_2 up to an order

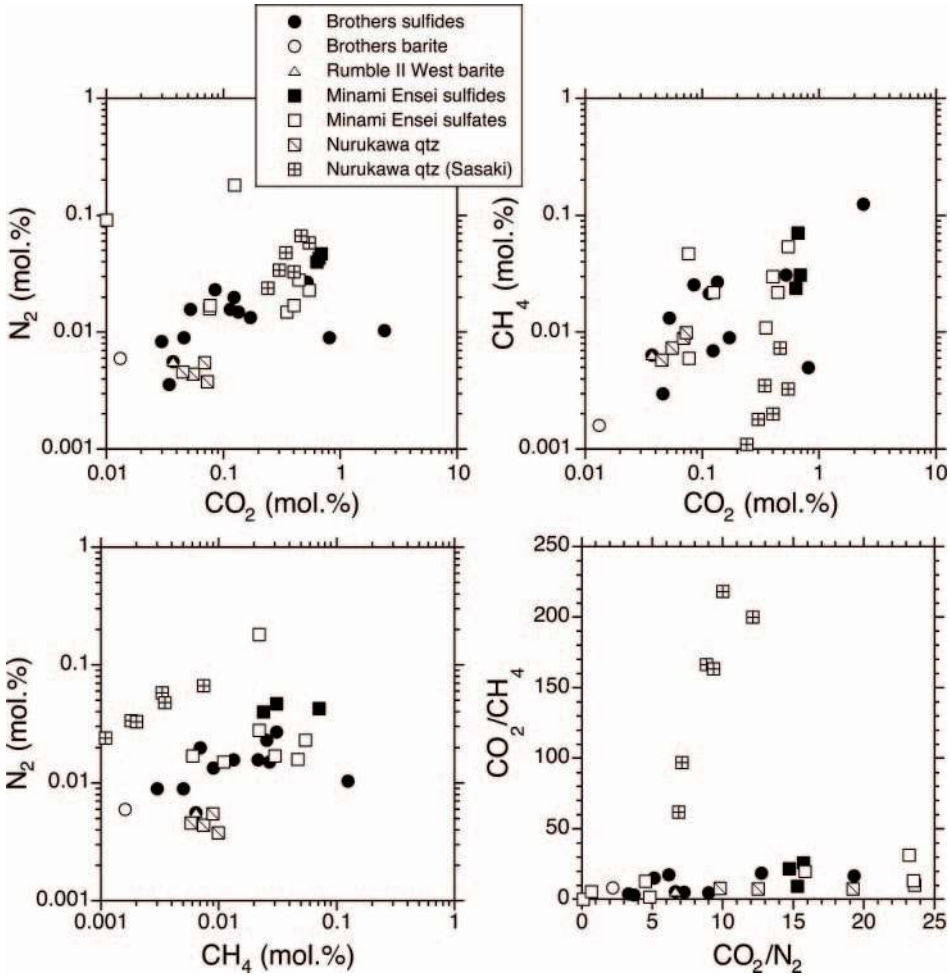

FIG. 14. Summary of gases contents from fluid inclusions in sulfide and sulfate minerals from the Brothers northwest and southeast caldera sites and Rumble II West, Kermadec arc. Also shown for comparison are results for the Minami Ensei vent site, Okinawa back arc, and the Nurukawa kuroko deposit, northern Honshu, Japan (Table 4; Sasaki et al., 1995; de Ronde et al., 2003b). Samples from all four localities give similar results and are largely indistinguishable in these plots. The Nurukawa data of Sasaki et al. (1995) show noticeably higher concentrations of CO_2 and N_2 than subsamples from the same samples analyzed in this study. Evidence for subsea-floor phase separation is noted by the slight positive correlations (excluding the Saskai et al., 1995 data) in the CO_2/CH_4 vs. CO_2/N_2 plot (see text).

of magnitude higher. Our measured CH_4 concentrations overlap those of Sasaki et al. (1995), although their values are up to 50 percent lower (Table 4, Fig. 14). We suggest that the data presented in de Ronde et al. (2003b) and in this study indicate similar gas compositions for all of the hydrothermal systems analyzed.

Microthermometric studies of Brothers fluid inclusions showed that, at the calculated temperatures of trapping, boiling was unlikely to have occurred at the sea floor (de Ronde et al., 2003b). However, slight positive trends in fluid inclusion gas plots (CO_2/CH_4 vs. CO_2/N_2), when combined with a range in fluid inclusion salinities from ~70 to 120 percent seawater values, suggest that subsea-floor phase separation probably occurred at the northwest caldera site prior to cooling by mixing with seawater and before venting on the sea floor. The additional gas data for this and the southeast caldera site, together with that from Minami Ensei and Nurukawa (Fig. 14), support the view that subsea-floor phase separation has affected vent fluid compositions at all these sites.

Dating of the Brothers Hydrothermal System

The chimney shown in Figure 9 was dated using ^{210}Pb, via ^{210}Pb/^{226}Ra disequilibrium, to provide an initial ^{226}Ra/Ba value. This enabled ages of other barite-rich samples to be determined from the decrease in ^{226}Ra/Ba due to radioactive decay of ^{226}Ra. The methods used to date mineralization are given in Appendix 2.

Brothers mineralization

Brothers chimney 57DR-1 was initially examined to determine if dating was possible from the disequilibrium between isotopes of the Th or U decay series (Ivanovich and Harmon, 1992). Although U concentrations range from 3.3 to 13.4 ppm, there was negligible ingrown ^{230}Th in the analyzed samples, indicating that this chimney was too young (<5,000 yr) for the ^{230}Th/^{234}U method. Beta counting the $PbCrO_4$ precipitates from four samples showed that ^{210}Pb and ^{226}Ra were not in equilibrium, probably as a result of hydrothermal overprinting (see App. 2). For example, during water/rock interaction Ba is leached twice as efficiently as Pb (Von Damm et al., 1985) with both elements then deposited in variable proportions within the rapidly (compared with the ^{210}Pb half-life of 22.3 yr) forming chimney. As there are no stable isotopes of Ra, we could not measure its concentration. Instead, as Ba is chemically very similar to Ra it is used as a proxy for Ra concentration. ^{226}Ra is transported and deposited with Ba in the hydrothermal fluid, and ^{210}Pb is transported with other Pb. The ^{226}Ra and ^{210}Pb in rock are assumed to be in secular equilibrium prior to extraction but, due to uneven distribution within the chimney, will not be in equilibrium for ~140 years (i.e., ~6 half lives of ^{210}Pb), allowing relatively young chimneys to be dated. In each chimney sample, the measured ^{210}Pb activity ($a_{^{210}Pb}$) is the sum of the activities of ^{210}Pb ingrown from ^{226}Ra and the decayed initial ^{210}Pb:

$$a_{^{210}Pb} = a_{^{226}Ra}\,(1 - e^{-\lambda t}) + K[Pb]\,e^{-\lambda t}, \quad (1)$$

where K = initial ^{210}Pb/[Pb], λ = ^{210}Pb decay constant = $ln2/^{210}$Pb half-life, and t = age.

Dividing the ^{210}Pb and ^{226}Ra activities of several samples by their Pb concentration and plotting the scaled values gives an isochron because all samples are virtually the same age. The gradient ($1 - e^{-\lambda t}$) of the ^{210}Pb/[Pb] versus ^{226}Ra/[Pb] plot (Fig. 15) is the fraction of ^{210}Pb ingrown toward equilibrium with ^{226}Ra, and from this the age of chimney 57DR-1 can be calculated.

Hence,

$$\begin{aligned}\text{Age} &= -ln\,(1 - e^{-\lambda t})/\lambda \\ &= -ln\,(1 - 0.57)22.3/0.693 \\ &= 27 \pm 6 \text{ yr.}\end{aligned} \quad (2)$$

In the absence of suitable ^{226}Ra/Ba values for the underlying rock, this relatively recent chimney material provides a good first-order approximation of the initial ^{226}Ra/Ba value at each location. The ^{226}Ra in chimneys is not supported by its relatively long half-life parent ^{230}Th, as Th is not extracted from rock during hydrothermal interaction. Thus, provided that Ba and ^{226}Ra were deposited together from a common source, and that the initial ^{226}Ra/Ba value is known, ages of ~500 to 15,000 years can be calculated from the decrease in ^{226}Ra/Ba due to radioactive decay.

Additional chimney fragments (n = 3) recovered in the dredges were then dated to better establish a history of hydrothermal activity at the northwest caldera site. Having successfully dated chimney 57DR-1 by the ^{210}Pb/^{226}Ra isochron method, the mean measured ^{226}Ra/Ba value was decay corrected to zero age (a relatively minor adjustment) and taken as the initial ratio for calculating the ages of mineralized samples found in the same general area. Other chimney fragments range in age from 890 ± 120 to 1,100 ± 120 years, while breccia samples range from <200 to 1,200 ± 500 years (Table 5).

Rumble II West mineralization

Chimney fragments from this volcano represent the only other sulfide mineralization recovered along the Kermadec

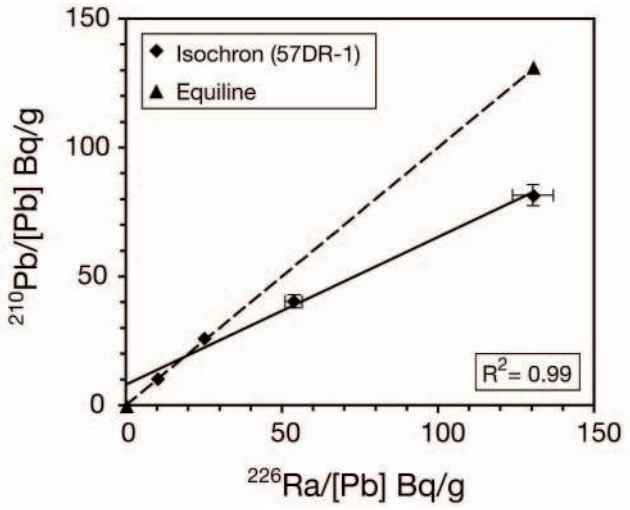

FIG. 15. Plot of ^{210}Pb/[Pb] vs. ^{226}Ra/[Pb] isochron for black smoker chimney 57DR-1 (see Fig. 9). As time elapses, the isochron pivots toward the equiline (i.e., the equilibrium position where ^{210}Pb = ^{226}Ra). The slope of the isochron ($1 - e^{\lambda t}$) is 0.57 and indicates an age of 27 ± 6 yr (see text for discussion). Errors limit this method to ages less than ~100 yr and where greater than the symbol, are ±1σ. Activities normalized to Pb concentrations which are given in Bq/g (Bq = 1 disintergration second^{-1}).

TABLE 5. Ages of Sea-Floor Mineralization Determined by $^{210}Pb/^{226}Ra$ and $^{226}Ra/Ba$ Values

Location/ sample[1]	Description	Ba (mg/kg)	$^{210}Pb/^{226}Ra$	^{226}Ra (Bq/kg)	^{230}Th (Bq/kg)	(^{226}Ra-^{230}Th)/Ba (Bq/kg)	Age (yr)
Brothers							
Northwest caldera							
57DR-1[2]	Whole chimney (5 samples)	40,300 ± 2,000	0.57 ± 0.07	910 ± 5	1.5 ± 0.5	22.6 ± 0.4	27 ± 6[3]
140b	Chimney fragment	394,000 ± 20,000		6,120 ± 10	nd	15.5 ± 0.8	890 ± 120
140c3	Chimney fragment	449,000 ± 22,000		6,980 ± 10	nd	15.6 ± 0.8	890 ± 120
X573/G	Chimney fragment	400,000 ± 20,000		5,700 ± 10	nd	14.3 ± 0.7	1,100 ± 120
52DR-8c	Pyrite breccia	490 ± 50		8.8 ± 1.0	2.3 ± 0.5	13.3 ± 2.6	1,200 ± 500
60DR-1	Mineralized breccia	2,900 ± 290		78 ± 0.5	0.9 ± 0.2	26.6 ± 2.7	<200
60DR-2	Mineralized breccia	620 ± 60		12 ± 1.1	1.9 ± 0.5	16.7 ± 2.5	720 ± 350
Rumble II West							
X656/A	Chimney fragment	90,000 ± 4,500		1,090 ± 20	nd	12.1 ± 0.7	1,500 ± 130[4]
Seawater		0.015[5]		0.0048	320		

Notes: Bq = radioactivity expressed in disintegrations per second; nd = not determined; errors given are 1σ; DR = dredge

[1] For sample descriptions and locations, see text; for sample X656/A, see de Ronde et al. (2003b)

[2] All the DR samples are prefaced by "SO-135" (R/V *Sonne* cruise 135)

[3] Age estimated using $^{210}Pb/^{226}Ra$

[4] Calculated using an assumed initial $^{226}Ra/Ba$ value; using an assumed initial $^{226}Ra/Ba$ value means that calculated errors for the estimated ages will become significantly smaller as the age of mineralization increases, and progressively exceeds the ^{226}Ra half-life

[5] Data from Li (1991); complete analytical data available on request to first author

arc that has been dated (Fig. 1). Using the initial $^{226}Ra/Ba$ value derived from the Brothers chimney in the age calculations, we derive a mineralization age at Rumble II West of 1,500 ± 130 years, similar to the oldest mineralization ages found at Brothers (Table 5).

Discussion

Multibeam mapping of the sea floor, in combination with towed camera and/or video surveys, allows the Brothers plume surveys to be placed in a geologic context. Moreover, chemical analysis of the plumes in conjunction with detailed studies of the altered rocks and mineralized samples recovered during dredging allows a detailed analysis of the interplay between magmatic and hydrothermal processes.

Two distinct hydrothermal systems are presently active at Brothers: the northwest caldera and cone sites. Plumes emanating from these two sites span the range of chemical compositions for submarine hydrothermal activity seen anywhere along the Kermadec arc (de Ronde et al., 2001; Massoth et al., 2003). The structural setting and sea-floor manifestations of the two active vent sites are different. For example, the northwest caldera site is perched on the slopes of the caldera where the local permeability is controlled by faulting, whereas venting at the cone site is located at the summits of the main and satellite cones where talus predominates. Both sites appear to be located on large-scale regional lineaments (Fig. 2a). Focused venting, as denoted by black smoker chimneys and numerous spires, is seen mainly at the northwest caldera site, although it must also have occurred over the cone summit in 1998 to 1999, while extensive diffuse venting was observed during camera tows down the flanks of the cone.

The age of the hydrothermal systems at these two sites is also different. The northwest caldera site has at least two main areas of massive sulfide formation with an older, largely inactive area situated near the caldera rim, whereas the presently active vent field (including numerous inactive spires) occurs lower on the wall (Fig. 7a). Dating results show that the chimney recovered from the lower slopes is only 27 years old, while other mineralized samples range in age up to ~1,200 years. When combined with petrographic studies, this shows that the northwest caldera site has had a protracted history and is much older than the cone vent site(s). No massive sulfides have been recovered from the cone site and no chimneys were seen during the camera tows. When combined with similarly old ages for sulfide fragments from Rumble II West, this shows that Kermadec hydrothermal systems have been extant for at least 1,200 to 1,500 years and possibly a lot longer (Table 5).

The Tonga-Kermadec arc system has a relatively simple tectonic setting, although sediment thickness on the subducting Pacific plate increases toward New Zealand from ~200 m at 30° S to ~500 m near 36° S (Carter et al., 1996; Fig. 1). Southern Kermadec arc lavas include contributions from three sources: (1) depleted Harve trough mantle, (2) fluid derived from altered MORB crust with a slight input of sedimentary Pb, and (3) Pacific sediment melt (Haase et al., 2002). Submarine volcanogenic massive sulfide deposits formed in oceanic settings can normally be differentiated from those influenced by proximity to continental rocks on a simple ternary diagram by plotting relative concentrations of Cu, Pb, and Zn (Fig. 16). For example, average compositions of deposits formed along mid-ocean ridges and intraoceanic arcs, such as the Izu-Bonin arc, plot in the oceanic crust field, distinct from those with continental affinities, such as kuroko deposits and deposits in nascent back arcs like the Okinawa trough (cf. Fouquet et al., 1993). However, sulfides recovered from Brothers and other volcanoes of the Kermadec arc plot largely within the continental crust field (Fig. 16), consistent with a continental subcrust or a continentally derived sediment component in the southern Kermadec

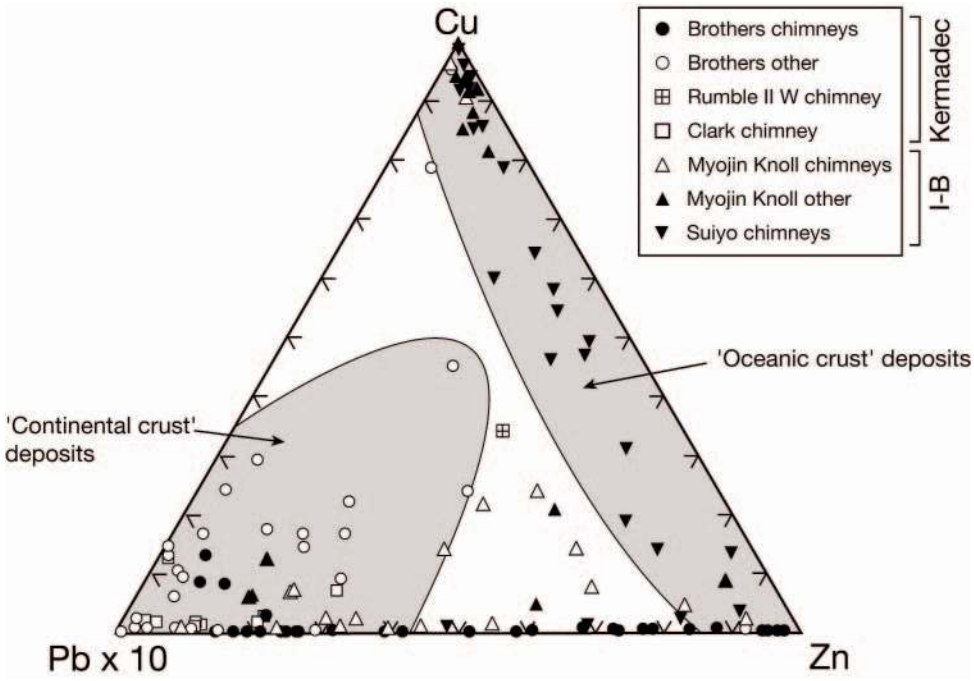

FIG. 16. Cu-Pb-Zn ternary diagram illustrating the bulk compositions of sulfide samples from Kermadec and Izu-Bonin (I-B) arc hydrothermal vent sites. Samples other than chimney samples (designated "other" in the legend) include brecciated massive sulfides, disseminated sulfides, and layered sulfides. The single Rumble II West data point and eight of the Brothers analyses are from Wright et al. (1998); the remainder are from this study (see App. 1). The Suiyo seamount data are from Watanabe et al. (1995) and the Myojin Knoll data are from Iizasa et al. (1997, 1999). All the sulfides from the Suiyo chimneys, some of the sulfides from the Myojin chimneys, and all the "other" Myojin sulfide data plot directly in the field of oceanic crust deposits of Fouquet et al. (1993). By contrast, many of the Brothers chimney sulfides and all the other Brothers sulfides, sulfides from Clark volcano (C.E.J. de Ronde, unpub. data), and the single Rumble II West chimney sample plot in or very near the field of deposits in continental crust, indicating a crustal or sediment contribution to the source rocks (cf. Fouquet at al., 1993). Other factors, such as the temperature of formation, may also influence the bulk compositions of the sulfides.

lavas. In addition, these relationships also partly reflect the temperature of formation of the samples.

Evidence for magmatic contributions

Magmatic fluids, including both gas and liquid components, are a primary source of metals in ore deposits formed at volcanic arcs (e.g., Sawkins and Kowalik, 1981; Sawkins, 1984; Hedenquist and Lowernstern, 1994; Stanton, 1994). Several lines of evidence indicate a magmatic component in vent fluids discharging from the Brothers hydrothermal system, especially at the cone site.

Plumes from the cone site show large negative shifts in ΔpH of which ~70 percent is ascribed to CO_2 discharge with lesser amounts of SO_2 and H_2S. Conservative estimates of end-member concentrations of CO_2 in the vent fluid are ~25 m*M* for the northwest caldera site and >100 m*M* for the cone site (Massoth et al., 2003), the latter considerably higher than typical mid-ocean ridge vent fluids of ≤22 m*M* (Von Damm, 1995) and requiring a degassing magma source (e.g., Butterfield et al., 1990). This compares with fluid inclusion CO_2 concentrations of 0.03 to 2.38 mol percent (avg 0.35 mol %) for Brothers mineralized samples (de Ronde et al., 2003b; Table 4). Hydrogen sulfide concentrations in the cone plumes are very high relative to those at mid-ocean ridges (Massoth et al., 2003), with the end-member concentration conservatively estimated (from a 2,000× plume dilution) at 14 m*M* and thus significantly enriched over typical mid-ocean ridge vent fluids (Von Damm, 1995). Concentrations of magmatic ^3He (Lupton, 1983) in the Brothers plumes are some of the highest measured for the Kermadec arc (de Ronde et al., 2001), with the δ^3He value of 181 percent for one of the cone plumes, the single highest recorded value.

Elemental sulfur is common at Brothers, especially at the cone site. In plumes above this site, where H_2S concentrations are highest, 40 to 80 percent of the particulate sulfur is present as elemental sulfur (Table 1). Fragments of sulfur up to 5 cm have been recovered by dredges from the cone site (de Ronde et al., 2001), and there is commonly an infilling of vugs and vesicles in cone lavas with sulfur (Fig. 8b). When sulfur gases mix together or with seawater, elemental sulfur and acid can be produced via oxidation and hydrolysis reactions (e.g., Lyon, 1974; Giggenbach, 1996):

$$2H_2S + SO_2 \rightarrow 2H_2O + 3S^0, \quad (3)$$

and

$$3SO_2 + 2H_2O \rightarrow 2H_2SO_4 + S^0. \quad (4)$$

Magmatic sulfur volcanoes and other surficial sulfur deposits are commonplace at degassing subaerial volcanoes, such as White Island (Giggenbach, 1996). Witness of an analogous underwater sulfur eruption at the northwest Rota-1 volcano on the Mariana arc, shows yellow-colored plumes

containing molten globules of elemental sulfur that are conclusively magmatic in origin. (see http://oceanexplorer.noaa.gov/explorations/04fire/logs/april01/media/brimstone01_video.html).

Acid in itself is not diagnostic of magmatic fluids. However, acid and sulfate can be generated in large quantities in volcanoes discharging high concentrations of magmatic volatiles (Giggenbach, 1996; Massoth et al., 2003):

$$4SO_2 + 4H_2O \rightarrow 3H_2SO_4 + H_2S, \quad (5)$$

$$H_2SO_4 \rightarrow HSO_4^- + H^+, \quad (6)$$

and

$$H_2S + 2H_2O \rightarrow SO_4^{2-} + 2H^+. \quad (7)$$

These reactions and reactions (3) and (4) were likely involved in the formation of the advanced argillic mineral assemblage of silica polymorphs + natroalunite + native sulfur + pyrite ± kaolinite found at the cone site (Figs. 3f, 11), which is common to subaerial magmatic hydrothermal systems (e.g., Arribas, 1995). In subaerial magmatic hydrothermal systems, alunite forms at high temperatures in low pH (<3.0) fluids where it has a distinct bladed morphology (Arribas, 1995, and references therein). Similar bladed natroalunite is seen in the cone mineralization (Fig. 10h). Its hydrothermal origin is confirmed by calculated $\Delta^{34}S_{sulfate\text{-}sulfide}$ formation temperatures of 260° to 305°C. The natroalunite is also isotopically distinct from both barite and anhydrite (Fig. 13c), which are precipitated largely from seawater. Bladed natroalunite has been reported from several other sea-floor sites where a magmatic origin is proposed (e.g., Hine Hina of the Valu Fa Ridge: Herzig et al., 1998; Conical seamount of the Tabar-Lihir-Tanga-Feni arc: Petersen et al., 2002). High Al concentrations in plumes above the cone summit (Fig. 6) are likely due to natroalunite particulates. Similarly high Al concentrations were found in the northwest Rota-1 plumes where scanning electron microscope studies confirm the presence of natroalunite (Lebon et al., 2004).

The occurrence of chalcocite, bornite, intermediate solid solution, chalcopyrite, and pyrite in sulfide samples recovered from the southeast caldera site, and enargite-bearing veins in a rhyodacitic sample from the northwest caldera site are evidence of high-sulfidation conditions. The latter sample was probably partly exhumed from a deeper level within the hydrothermal system that had already partly waned. These assemblages, together with the advanced argillic alteration, indicate magmatic fluids that are relatively oxidized and then acidified when mixed with seawater (e.g., Giggenbach, 1997).

Sulfur isotope compositions of Brothers sulfides are also consistent with contributions from a magmatic source (Fig. 13a, b). Values of $\delta^{34}S$ that are >0 per mil all come from the sphalerite-rich chimney (Fig. 9) or fragments of massive sulfides (de Ronde et al., 2003b) from the northwest caldera site and are consistent with mixing of hydrothermal fluid with seawater, either close to the sea floor or in the walls of the chimneys (e.g., Janecky and Shanks, 1988). Values of $\delta^{34}S$ that are <0 per mil come from either stockwork samples at the northwest caldera site, from massive sulfide fragments recovered from the southeast caldera site, or from the natroalunite-bearing rocks of the cone site. At temperatures >400°C, sulfur gases, and SO_2 in particular, dominate the redox equilibrium of arc volcano magmatic gases (Giggenbach, 1987). Where SO_2 is reduced to H_2S, sulfides forming from these fluids will have $\delta^{34}S$ values close to 0 per mil. However, once the volcanic gases cool below 400° to 350°C (probably via mixing of H_2S-rich solutions with SO_4-rich ones at, or near, the depositional sites; Ohmoto and Lasaga, 1982), SO_2 will disproportionate according to reactions (4) and (5) above, generating reduced and oxidized species. This is accompanied by a kinetic isotope effect which causes the sulfide to become enriched in ^{32}S and the sulfate in ^{34}S, with the sulfides precipitated from the fluid having $\delta^{34}S$ values <0 per mil, whereas the $\delta^{34}S$ values of the sulfates will be >0 per mil (Ohmoto and Rye, 1979; Ohmoto and Lasaga, 1982). This is consistent with sulfur isotope compositions reported here for Brothers, with concomitant negative $\delta^{34}S$ values of (1) stockwork sulfides from the northwest caldera site, (2) chimney sulfides from the southeast caldera site, and (3) sulfides and elemental sulfur associated with advanced argillic alteration from the cone site and the positive $\delta^{34}S$ values of coexisting natroalunite (Table 3, Fig. 13). A similar interpretation has been made for $\delta^{34}S$ compositions from the mineralized Hine Hina vent field (Herzig et al., 1998), Conical seamount (Petersen et al., 2002), and vent fluids from the DESMOS caldera of the Manus back-arc basin, Papua New Guinea (Gamo et al., 1997). Together with $\delta^{34}S$ data from the Brothers hydrothermal sites, these results confirm significant magmatic contributions to these systems and are consistent with disproportionation of exsolved SO_2 from a magma (Fig. 17).

Iron concentrations in the Brothers plumes are some of the highest values recorded for submarine hydrothermal systems, with the 1999 cone summit plume value of 4,720 n*M* being 6 to 27 times higher than that of typical mid-ocean ridge plumes (de Ronde et al., 2001; Massoth et al., 2003). More significant are Fe/Mn values in the plume (~18) which are much higher than values of 2 to 3 common in mid-ocean ridge plumes. The combination of high Fe concentrations and high Fe/Mn values suggests three possible magmatic processes (Massoth et al., 2003): (1) chemical weathering of wall rock by magmatic CO_2, (2) dissolution of wall rock by highly acidic fluids resulting from the discharge of SO_2 and H_2S, and/or (3) direct exsolution of an Fe-bearing brine phase. If processes (1) and (2) were dominant, plume Fe/Mn values would approach those for Kermadec arc rocks, which they do not (Massoth et al., 2003). However, brines trapped in fluid inclusions related to dacitic magmas have Fe/Mn values that are similar to the Brothers plumes, although at significantly higher concentrations (up to 4M Fe: Ulrich et al., 2001, as reported in Massoth et al., 2003). Even if the magmatic fluid contained only 1M Fe, with an estimated vent fluid composition of 9.4 mM (2,000× dilution) calculated from the enriched 1999 cone summit plume, an additional dilution of ~100× would still account for the high Fe concentrations in the plume (Massoth et al., 2003).

Evidence for pulsed magmatic activity

By nature of their tectonic environment, discrete magmatic events are commonplace along spreading ridges and other submarine plate boundaries. They are characterized by release of large volumes of hydrothermal fluid ("megaplumes"

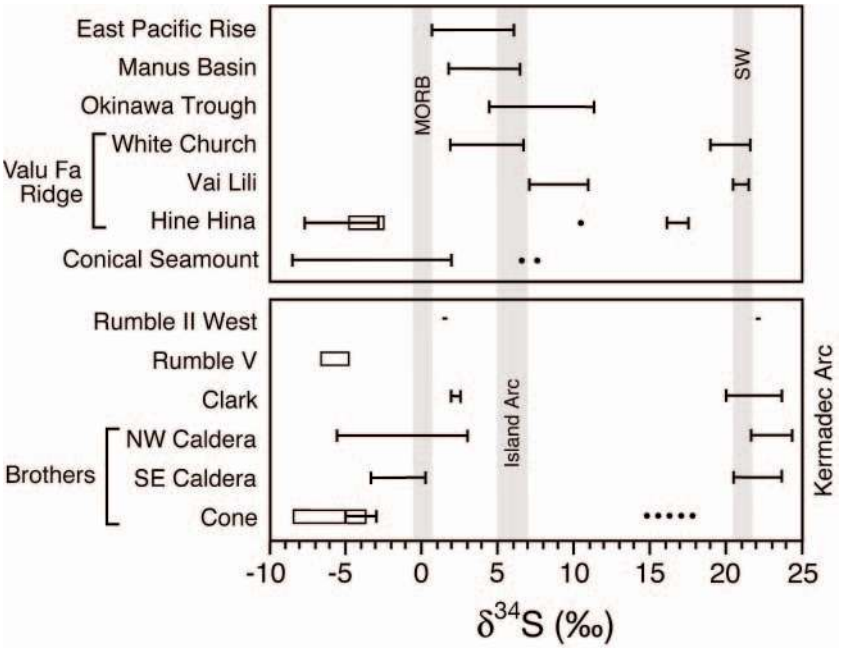

FIG. 17. Compilation of sulfur isotope data for sulfides and sulfates from different vent sites along the Kermadec arc, including Brothers, Rumble II West, and Rumble V (de Ronde et al. (2003b; this work) and Clark (C.E.J. de Ronde, unpub. data). Shown for comparison are typical $\delta^{34}S$ values for vent sites from various tectonic settings (Urabe and Kusakabe, 1990; Herzig et al., 1993, and references therein; Petersen et al., 2002). Horizontal bars relate to sulfides with $\delta^{34}S$ values <15 per mil and sulfates with $\delta^{34}S$ values >15 per mil. Small black dots represent natroalunite, and open boxes are native sulfur. Areas shaded in gray are the fields for rock sulfur from mid-ocean ridge basalt (MORB) and island arc, and seawater (SW) sulfate (references given in Herzig et al., 1993).

of Baker et al., 1987) and temporal changes in vent fluid chemistry (e.g., 9° N of the East Pacific Rise: Von Damm, 2000; Endeavour segment of the Juan de Fuca Ridge: Lilley et al., 2003). Magmatic influences on these events, as for subaerial volcanoes, can cause large increases in the concentrations of the magmatic gases CO_2, SO_2, H_2, and He and shifts in pressure, temperature, and redox conditions in the high-temperature reaction zone. This in turn influences phase separation, causing large changes in the concentrations of Cl and ore-forming metals within the hydrothermal fluids (e.g., Giggenbach, 1996; Christenson, 2000; Von Damm, 2000; Lilley et al., 2003). Radiogenic isotope studies of arc lavas suggest that degassing occurs continuously along volcanic arcs for periods up to several decades just prior to eruption and longer if degassing is discontinuous (Turner et al., 2004). Considering several of the Kermadec volcanoes have been volcanically active in the recent past, magmatic contributions to their submarine hydrothermal systems are likely to be commonplace.

Plume data for the cone site shows a dramatic change in composition between 1999 and 2002, while that for the northwest caldera site remained largely unchanged (Table 1). The main plume above the cone summit, in particular, showed significant increases in δ^3He (30%) and H_2S (65%), with a similar shift in ΔpH. By contrast, spectacular drops were noted in particulate Fe concentrations (242×), total dissolvable Fe (26×), Fe/Mn values (from 18.2 to 0.8), and to a lesser degree, particulate Cu (10×) and total particulate S (6.6×; Table 1). Helium R/R_A values for the 1999 northwest caldera plumes were slightly more radiogenic (5.9) than those from the cone site (6.4). Furthermore, R/R_A values at both sites were shifted higher by about 1 unit in the 2002 plumes (Table 1) with values for the combined vent sites increasing from 6.1 ± 0.5 in 1999 to 7.2 ± 0.1 in 2002 (Fig. 18), showing an overall increase in nonradiogenic (mantle) He in the system. This

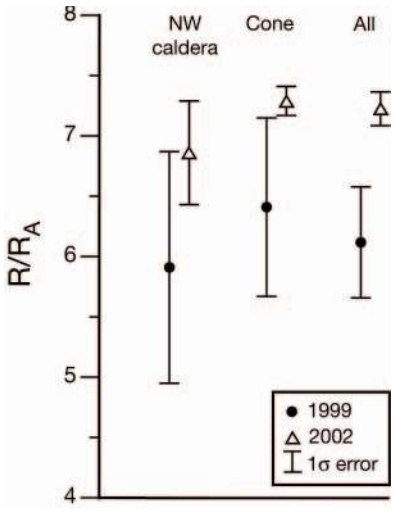

Fig. 18. Plot of end-member R/R_A values for Brothers hydrothermal plumes between 1999 and 2002, where $R = {}^3He/{}^4He$ and $R_A = ({}^3He/{}^4He)_{air}$. These values were estimated from linear regression fits to the $[{}^3He]$ vs. $[{}^4He]$ concentration data. There is a measurable shift to less radiogenic R/R_A values over this time interval for plumes from both northwest caldera and cone sites, consistent with increasing magmatic input into the hydrothermal system.

is consistent with an increased magmatic input over the 3-yr period and suggests a deep magmatic He source. These results also show that He isotope ratios are not affected by high-level processes, such as phase separation.

Discharge of Fe-rich magmatic fluids, coincident with intrusion of new magma into the hydrothermal reservoir and dissolution of the chilled magma, has been documented for the subaerial Copahue volcano in Argentina (Varekamp et al., 2001). Here, extremely acidic (pH <1) sulfate-chloride brines occur as hot springs which showed an increase in Mg, Na, Al, and Fe concentrations beginning at, or just before, the time of eruption (Varekamp, 2004). Prior to eruption, the hot springs were saturated with silica phases, anhydrite, hematite, and a suite of Cu minerals indicative of a deep-seated ore-forming system, with saturation of an additional suite of minerals, including alunite and jarosite during and after the eruption, similar to that at the Brothers cone.

Together, these results suggest that the cone hydrothermal system has been perturbed by a pulse of magmatic activity that in 1998 to 1999 initially expelled the Fe-rich fluids of the summit plume and which exsolved large concentrations of gases, later facilitating phase separation. This would have caused the subsequent deposition of metals in the subsea floor in 2002, consistent with fluid inclusion gas (de Ronde et al., 2003a; Fig. 14) and sulfide geochemical data (Fig. 12).

Evolution of the Brothers hydrothermal system

A range of depositional temperatures at the Brothers hydrothermal system, from near-ambient seawater values to ~300°C, are indicated by the major gangue, sulfide, and oxides and/or oxyhydroxide minerals in the mineralized and hydrothermally altered samples. The different alteration assemblages also were influenced by the interaction between seawater, magmatic fluid, the degree of hydrothermal water-rock interaction, and changing reduction-oxidation potential and temperature. These parameters appear to have varied over time and space throughout the evolution of the hydrothermal system, as illustrated schematically in Figure 19.

Where hydrothermal fluids have equilibrated with the rock, they can be described as evolved with an alteration assemblage of neutral pH type. By contrast, juvenile cation-leaching acidic waters represent only partial equilibration between water and rock (Giggenbach, 1997). Episodic volcanism, coincident with the evolution of the hydrothermal system, is indicated by opal-A and Fe sulfides cementing fresh glass at the northwest caldera site. Periodic influx of magmatic-hydrothermal fluids also may have initiated cycles of hydrothermal activity (Fig. 19). For example, evidence for past magmatic fluid influx at both the northwest and southeast caldera sites is indicated by early deposition of sulfides such as enargite and bornite and sulfate phases such as natroalunite (Fig. 11), while the cone site is presently discharging magmatic, gas-rich fluids. With a decrease in magmatic input and an increase in hydrothermal water-rock interaction, the

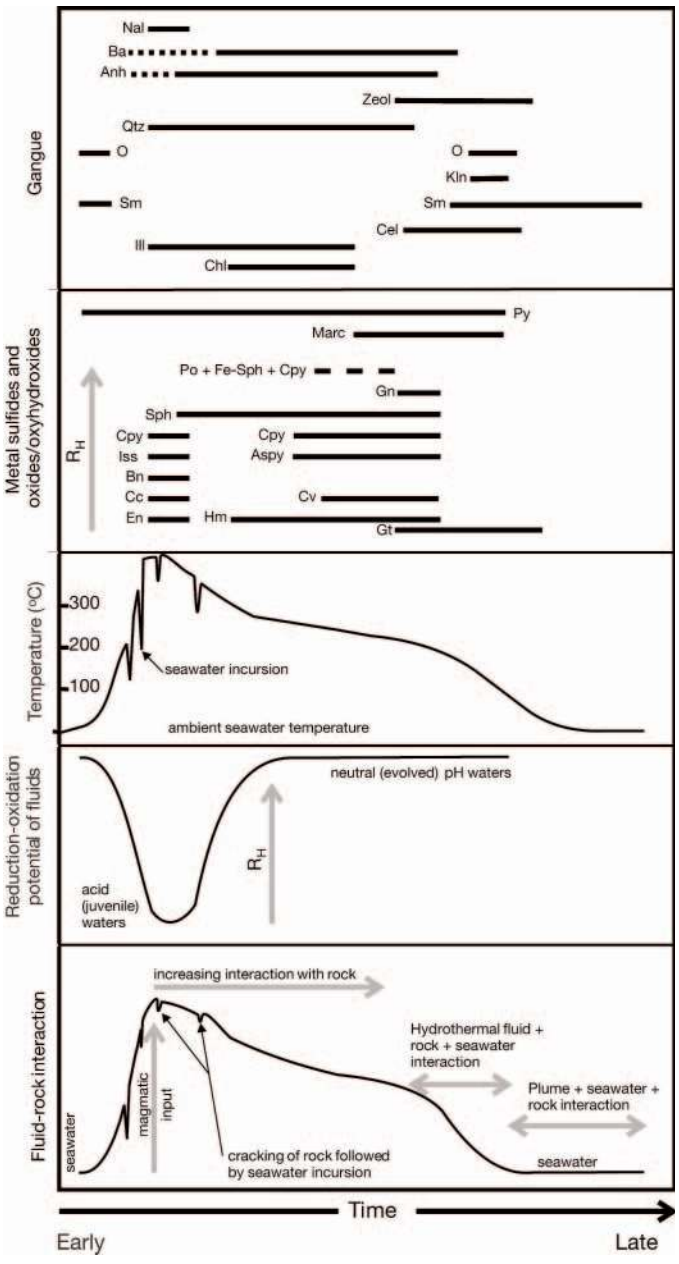

FIG. 19. Schematic diagram summarizing the major factors affecting deposition of metal sulfides, oxides and/or oxyhydroxides, silicates, amorphous silica, and sulfate gangue minerals as the various parts of the Brothers submarine magmatic-hydrothermal system evolve with time. A major factor affecting gangue (top panel) and metal sulfide and oxide and/or oxyhydroxide (2nd panel) mineral deposition, over time, is changing temperature (3rd panel) as the system heats up after an initial magmatic pulse and is periodically cooled by the incursion of seawater through thermally induced cracks in the rock. Chalcopyrite closely associated with bornite, chalcocite, enargite, and intermediate solid solutions in the Cu-Fe-S system are often characteristic of high-temperature magmatic conditions. Variations occur in the reduction-oxidation potential ($R_H = \log a_{H_2}/_{H_2O}$) of the end-member fluids, with magmatic fluids relatively oxidized and acidic compared to seawater and hydrothermal fluids (4th panel). Neutral (evolved) pH waters develop from long-term interaction of a large volume of rock with magmatic fluids and seawater. We can thus summarize the formation of hydrothermal fluids affected by the interaction between seawater, magmatic fluids, and rock (bottom panel). Abbreviations: Anh = anhydrite; Aspy = arsenopyrite; Ba = barite; Bo = bornite; Cc = chalcocite; Cel = celadonite; Chl = chlorite; Cpy = chalcopyrite; Cv = covellite; En = enargite; Fe-Sph = Fe-rich sphalerite; Gn = galena; Gt = goethite, Hm = hematite; I = illite; Iss = intermediate solid solution; Kln = kaolinite; Marc = marcasite; Nal = natroalunite; O = opal; Po = pyrrhotite; Py = pyrite; Qtz = quartz; S = native sulfur; Sph = sphalerite; Sm = smectite; Zeol = zeolite. Figure modified after Reyes et al. (2004).

hydrothermal fluids become more evolved and alteration mineral assemblages change accordingly with temperature, depth, and distance from the main magmatic influx zone. An increase in seawater entrainment further cools the hydrothermal system, which is shown by the assemblage zeolites + opal-A + smectite (including Na-Ca smectite, corrensite, and saponite) + celadonite + pyrite and/or marcasite + hematite + goethite (Fig. 19). Iron-Mn oxyhydroxides (including goethite and birnessite), smectite, and opal-A are deposited at the lowest temperatures.

The geologic context for the evolution of the hydrothermal system is illustrated in Figure 20. Faults provide direct

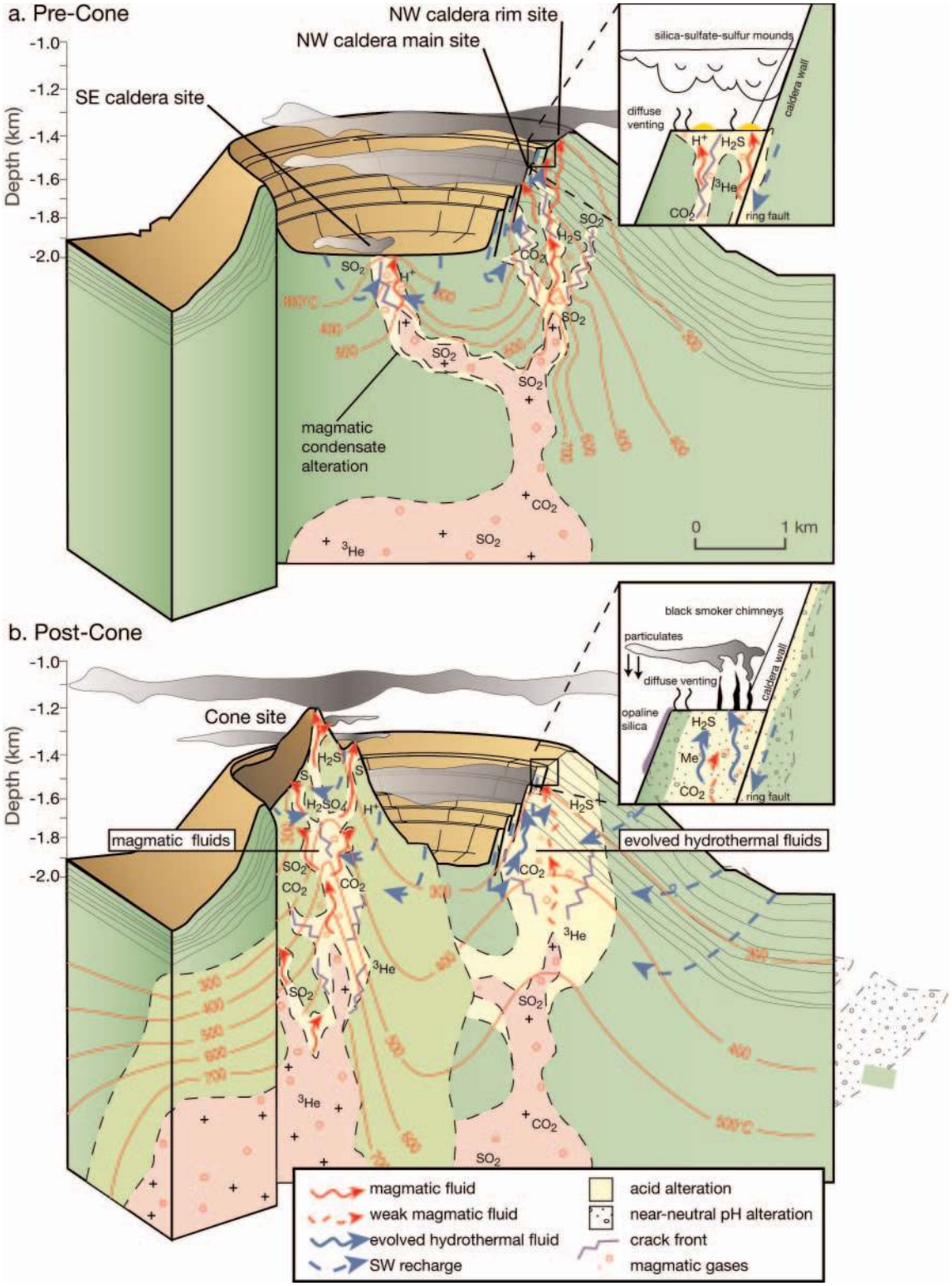

pathways from crystallizing magma and other parts of the magmatic-hydrothermal system to the sea floor. Unlike subaerial magmatic-hydrothermal systems (e.g., Giggenbach et al, 1990; Reyes at al, 2003), it is proposed that a crack zone instead of a vapor conduit extends upward from the crystallizing magma to the sea floor. This is formed when cold seawater penetrates the hydrothermal system from the caldera ring faults and initially comes into contact with buoyant hot fluids. This crack zone may be represented near the sea floor by samples from the cone site. Here, 100-μm cracks focused acid sulfate waters that condensed from magmatic fluids with these early veinlets subsequently cut by fractures containing smectite and opal-A, indicative of dilution and quenching of the hydrothermal fluids by seawater. Sulfide-rich chimneys, represented by samples from the southeast caldera site, were probably deposited within the main upflow zone of a magmatic-hydrothermal system, once the crack zone had been partly sealed by secondary mineral deposition due to mixing with seawater.

Near the periphery of the magmatic-hydrothermal fluid upflow zone, subsea-floor rocks are completely overprinted by acidic waters, forming an assemblage of illitic clays + anhydrite + quartz + pyrite + arsenopyrite + sphalerite + galena. Rocks in these zones, however, can be further overprinted by seawater-dominated fluids (as is presently occurring at the northwest caldera site), represented by low-temperature smectites. Deposits of opaline silica, Fe-Mn oxyhydroxides and corrensite occur on the sea floor at the margins of these zones (Fig. 20).

Mineral paragenesis studies, isotopic compositions, dating and sulfide geochemical data, when combined with plume data, show that the Brothers hydrothermal system has experienced several episodes of magmatic activity over its lifetime and in each case, has impacted on the mineralization style at any one site. The northwest caldera vent site is a partly exhumed, waning, but steady-state hydrothermal system that is today dominated by evolved seawater but which has seen episodic injections of magmatic fluids. The southeast caldera site represents the main upflow of a relatively well established active magmatic-hydrothermal system on the sea floor where sulfide-rich chimneys are extant. The cone site is a nascent magmatic-hydrothermal system where crack zones localize upwelling acid waters from depth.

Acknowledgments

We thank B.J. Barry for determining Ba concentrations by ion beam analysis using the KN van de Graaf accelerator at the GNS Rafter Laboratory and measuring the radionuclide activities by gamma spectrometry. M.R. Clark supplied the TAN07/01 samples. Thanks are due to officers and crew of R/V *Sonne* and R/V *Tangaroa* for at-sea operations. Reviews by R.A. Binns and P.G. Spry, and comments made on an earlier draft by I.J. Graham, improved this paper. M. Park and J. Vodanovich helped construct several of the figures. This paper was initiated during the session "The Changing Vision of Marine Minerals" sponsored by the Society of Economic Geologists at the 2002 Geological Society of America Annual Meeting. Funding for this work was provided by the New Zealand Foundation for Research Science and Technology (FRST) contracts C05X0207 and C01X0203, the German Bundesministerium fuer Forschung und Technologie (BMFT Project #03G0135A), the U.S. NOAA VENTS program, and the Geological Survey of Canada. C. de R. would like to dedicate this paper to the late Marinus de Ronde in recognition of his never-ending encouragement to seek answers to some of the world's mysteries.

March 18, August 10, 2005

REFERENCES

Aoki, M., Matsumoto, T., Kimura, M., and Fujioka, K., 1993, Hydrothermal activity and topographic features in the western part of the Minami-Ensei knoll, northern Okinawa trough: JAMSTEC Symposium on Deep Sea Research, p. 309–320 (in Japanese with English abstract and figure captions).

Arribas, A., Jr., 1995, Characteristics of high-sulfidation epithermal deposits, and their relation to magmatic fluid: Mineralogical Association of Canada Short Course Series, v. 23, p. 419–454.

Baker, E.T., Massoth, G.J., and Feely, R.A., 1987, Cataclysmic hydrothermal venting on the Juan de Fuca Ridge: Nature, v. 329, p. 149–151.

Baker, E.T., and Milburn, H.B., 1997, MAPR: A new instrument for hydrothermal plume mapping: RIDGE Events, Newsletter of the Ridge 2000 program (http://ridge2000.bio.psu.edu/science/contact.html), v. 8, p. 23–25.

Baker, E.T., Feely, R.A., de Ronde, C.E.J., Massoth, G.J., and Wright, I.C., 2003, Submarine hydrothermal venting on the southern Kermadec volcanic arc front (offshore New Zealand): Location and extent of particle plume signatures: Geological Society of London Special Publication, v. 219, p. 141–161.

Bray, C.J., Spooner, E.T.C., and Thomas, A.V., 1991, Fluid inclusion volatile analysis by heated crushing, on-line gas chromatography: Applications to Archean fluids: Journal of Geochemical Exploration, v. 42, p. 167–193.

FIG. 20. Schematic cartoon depicting the evolution of the Brothers hydrothermal system(s). The cross section is approximately along line T6 in Figures 2 and 4a. A. Brothers caldera after collapse of the initial volcanic edifice. Heat from the original magma chamber drives the hydrothermal system at the northwest caldera site with magmatic fluids initially dominant. Recharge of the hydrothermal system is largely via caldera ring faults. The (extinct) vent field near the caldera rim was the first expression of hydrothermal activity at Brothers with the active (younger) vent field located nearer the caldera floor. The time interval between formation of these two sites is unknown. Cyclic volcanic activity is thought to be responsible for periodic rejuvenation of the hydrothermal system (see Fig. 19), causing disinterment of parts of the existing hydrothermal system and renewed magmatic input at depth. Dating of mineralized samples shows that hydrothermal activity has been ongoing for at least 1,200 years in this area with present-day plume chemistry suggesting that this site is now dominated by hydrothermal fluids of predominantly seawater origin. Formation of the southeast caldera vent site at the base of the caldera wall may have predated the emplacement of the cone, and there is evidence for magmatic fluids having been expelled from chimneys here. B. Emplacement of the dacite cone within the caldera, near its southern wall. Mineral assemblages at the cone site indicate that vent fluids here contain a significant magmatic component with temperatures up to ~300°C. Plume measurements during the 2002 NZAPLUME II survey suggest an increase in magmatic activity at this site since 1998 to 1999. The age of cone emplacement is unknown. Abbreviation: Me = metals.

Brownlow, A.H., 1979, Geochemistry: Englewood Cliffs, NJ, Prentice-Hall, 498 p.

Buckeridge, J.S., 2000, *Neolepas osheai* sp. nov., a new deep-sea vent barnacle (Cirripedia: Pedunculata) from Brothers caldera, south-west Pacific ocean: New Zealand Journal of Marine and Freshwater Research, v. 34, p. 409–418.

Carter, L., Carter, R.M., McCave, I.N., and Gamble, J., 1996, Regional sediment recycling in the abyssal southwest Pacific Ocean: Geology, v. 24, p. 735–738.

Chiba, H., Nakashima, K., Gamo, T., Ishibashi, J., Tsunogai, U., and Sakai, H., 1993, Hydrothermal activity at the Minami-Ensei knoll, Okinawa trough: Chemical characteristics of hydrothermal solutions: JAMSTEC Symposium on Deep Sea Research, p. 271–282 (in Japanese with English abstract and figure captions).

Christenson, B.W., 2000, Geochemistry of fluids associated with the 1995–1996 eruption of Mt. Ruapehu, New Zealand: Signatures and processes in the magmatic-hydrothermal system: Journal of Volcanology and Geothermal Research, v. 97, p. 1–30.

de Ronde, C.E.J., 1995, Fluid chemistry and isotopic characteristics of seafloor hydrothermal systems and associated VMS deposits: Potential for magmatic contributions: Mineralogical Association of Canada Short Course Series, v. 23, p. 479–509.

de Ronde, C.E.J., Baker, E.T., Massoth, G.J., Lupton, J.E., Wright, I.C., Feely, R.A., and Greene, R.G., 2001, Intra-oceanic subduction-related hydrothermal venting, Kermadec volcanic arc, New Zealand: Earth and Planetary Science Letters, v. 193, p. 359–369.

de Ronde, C.E.J., Massoth, G.J., Baker, E.T., Ishibashi, J., Walker, S.L., Lupton, J.E., and the Shipboard Scientific Party, 2002, Hydrothermal venting associated with the Kermadec intra-oceanic arc—contrasting arc segments for hydrothermal activity: Initial results of the NZAPLUME II cruise [abs.]: InterRidge Theoretical Institute (IRTI) Conference, Sept. 9–11, 2002, Pavia, Italy, Abstracts, p. 38.

de Ronde, C.E.J., Massoth, G.J., Baker, E.T., and Lupton, J.E., 2003a, Submarine hydrothermal venting related to volcanic arcs: Society of Economic Geologists Special Publication 10, p. 91–110.

de Ronde, C.E.J., Faure, K., Bray, C.J., Chappel, D.A., and Wright, I.C., 2003b, Hydrothermal fluids associated with seafloor mineralization at two southern Kermadec arc volcanoes, offshore New Zealand: Mineralium Deposita, v. 38, p. 217–233.

de Ronde, C.E.J. Massoth, G.J., Baker, E.T., Lupton, J.E., Arculus, R.J., Wright, I.C., Stoffers, P., Ishibashi, J., Walker, S.L., Greene, R.R., Faure, K., and Takai, K., 2004, Systematic survey of the Kermadec-Tonga intraoceanic arc between 1999 and 2004: A significant source of diverse submarine hydrothermal emissions [abs.]: EOS Supplement, Transactions of the American Geophysical Union, v. 85, no. 47, p. F1909.

Delteil, J., Ruellan, E., Wright, I.C., and Matsumoto, T., 2002, Structure and structural development of the Havre trough (SW Pacific): Journal of Geophysical Research, v. 107 (B7), 10.1029/2001JB000494, p. 2143–2161.

Feely, R.A., Massoth, G.J., and Lebon, G.T., 1991, Sampling of marine particulate matter and analysis by X-ray fluorescence spectrometry: American Geophysical Union Monographs, v. 63, p. 251–257.

Feely, R.A., Baker, E.T., Marumo, K., Urabe, T., Ishibashi, J., Gendron, J.F., Lebon, G.T., and Okamura, K., 1996, Hydrothermal plume particles and dissolved phosphate over the super-fast-spreading southern East Pacific Rise: Geochimica et Cosmochimica Acta, v. 60, p. 2297–2323.

Feely, R.A., Baker, E.T., Lebon, G.T., Gendron, J.F., Resing, J.A., and Cowen, J.P., 1999, Evidence for iron and sulfur enrichments in hydrothermal plumes at Axial volcano following the January-February 1998 eruption: Geophysical Research Letters, v. 26, p. 3649–3652.

Fouquet, Y., von Stackelberg, U., Charlou, J.-L., Erzinger, J., Herzig, P.M., Mühe, R., and Wiedicke, M., 1993, Metallogenesis in back-arc environments: the Lau basin example: Economic Geology, v. 88, p. 2154–2181.

Gamble, J.A., and Wright, I.C., 1995, The southern Havre trough: Geological structure and magma petrogenesis of an active backarc rift complex, *in* Taylor, ed., Backarc basins: Tectonics and magmatism: New York, Plenum Press, p. 29–62.

Gamble, J.A., Woodhead, J.D., Wright, I.C., and Smith, I.E.M., 1996, Basalt and sediment geochemistry and magma petrogenesis in a transect from oceanic island arc to rifted continental margin arc: the Kermadec-Hikurangi margin, SW Pacific: Journal of Petrology, v. 37, p. 1523–1546.

Gamo, T., Okamura, K., Charlou, J.-L., Urabe, T., Auzende, J.-M., Ishibashi, J., Shitashima, K., Chiba, H., and the Shipboard Scientific Party of the ManusFlux Cruise, 1997, Acidic and sulfate-rich hydrothermal fluids from the Manus back-arc basin, Papua New Guinea: Geology, v. 25, p. 139–142.

Giggenbach, W.F., 1987, Redox processes governing the chemistry of fumarolic gas discharges from White Island, New Zealand: Applied Geochemistry, v. 2, p. 143–161.

——1992, The composition of gases in geothermal and volcanic systems as a function of tectonic setting: International Symposium on Water-Rock Interaction, WRI-7, Park City, Utah, Proceedings, v. 8, p. 873–878.

——1996, Chemical composition of volcanic gases, *in* Tilling, R.I., and Scarpa, R., eds., Monitoring and mitigation of volcano hazards: Berlin, Springer-Verlag, p. 221–256.

——1997, The origin and evolution of fluids in magmatic-hydrothermal systems, *in* Barnes, H.L., ed., Geochemistry of hydrothermal ore deposits: 3rd ed.: New York, Wiley-Interscience, p. 737–796.

Giggenbach, W.F., Garcia, N., Londono, A., Rodriquez L., Rojas, N., and Calvache, M.I., 1990, The chemistry of fumarolic vapor and thermal-spring discharges from the Nevado del Ruiz volcanic-magmatic-hydrothermal system, Colombia: Journal of Volcanology and Geothermal Research, v. 42, p. 13–39.

Giggenbach, W.F., Shinohara, H., Kusakabe, M. and Ohba, T., 2003, Formation of acid volcanic brines through interaction of magmatic gases, seawater, and rock within the White Island volcanic-hydrothermal system, New Zealand: Society of Economic Geologists Special Publication 10, p. 19–40.

Graetsch, H., 1994, Structural characteristics of opaline and microcrystalline silica minerals: Reviews in Mineralogy, v. 29, p. 209–232.

Hannington, M.D., and Scott, S.D., 1988, Mineralogy and geochemistry of a hydrothermal silica-sulfide-sulfate spire in the caldera of Axial Seamount, Juan de Fuca Ridge: Canadian Mineralogist, v. 26, p. 603–625.

Hannington, M.D., Galley, A.G., Herzig, P.M., and Petersen, S., 1998, A comparison of the TAG Mound and stockwork complex with Cyprus-type massive sulfide deposits: Proceedings Ocean Drilling Program, Scientific Results Volume Leg 158, p. 389–415.

Hannington, M.D., Poulsen, K.H., Thompson, J.F.H., and Sillitoe, R.H., 1999, Volcanogenic gold in the massive sulfide environment: Reviews in Economic Geology, v. 8, p. 319–350.

Hannington, M.D., de Ronde, C.E.J., and Petersen, S., 2005, Modern seafloor tectonics and submarine hydrothermal systems: Economic Geology 100th Anniversary Volume, p. 111–141.

Haase, K.M., Worthington, T.J., Stoffers, P., Garbe-Schönberg, D., and Wright, I.C., 2002, Mantle dynamics, element re-cycling, and magma genesis beneath the Kermadec arc-Harve trough: Geochemistry Geophysics Geosystems, v. 3, no. 11, 1071, doi: 10.1029/2002GC000335.

Hedenquist, J.W., and Lowenstern, J.B., 1994, The role of magmas in the formation of hydrothermal ore deposits: Nature, v. 370, p. 519–527.

Hedenquist, J.W., Simmons, S.F., Giggenbach, W.F., and Eldridge, C.S., 1993, White Island, New Zealand, volcanic-hydrothermal system represents the geochemical environment of high-sulfidation Cu and Au ore deposition: Geology, v. 21, p. 731–734.

Herzig, P.M., Hannington, M.D., Fouquet, Y., Von Stackelberg, U., and Petersen, S., 1993, Gold-rich polymetallic sulfides from the Lau back arc and implications from the geochemistry of gold in sea-floor hydrothermal systems of the southwest Pacific: Economic Geology, v. 88, p. 2182–2209.

Herzig, P.M., Hannington, M.D., and Arribas, A., Jr., 1998, Sulfur isotopic composition of hydrothermal precipitates from the Lau back-arc: Implications for magmatic contributions to seafloor hydrothermal systems: Mineralium Deposita, v. 33, p. 226–237.

Iizasa, K., Naka, J., Yusa, M., and Fiske, R.S., 1997, Sulfide chimneys and massive sulfides at Myojin Knoll caldera, Izu-Ogasawara arc: JAMSTEC Journal of Deep Sea Research, v. 13, p. 443–456 (in Japanese with English abstract).

Iizasa, K., Fiske, R.S., Ishizuka, O., Yuasa, M., Hashimoto, J., Ishibashi, J., Naka, J., Horii, Y., Fujiwara, Y., Imai, A., Koyama, S., 1999, A kuroko-type polymetallic sulfide deposit in a submarine silicic caldera: Science, v. 283, p. 975–977.

Ishibashi, J., Wakita, H., Okamura,K., Nakayama, E., Feely, R.A., Baker, E.T., Marumo, K., and Maruyama, A., 1997, Hydrothermal methane and manganese variation in the plume over the superfast-spreading southern East Pacific Rise: Geochimica et Cosmochimica Acta, v. 61, p. 485–500.

Ivanovich, M., and Harmon, R.S., 1992, Uranium-series disequilibrium: Applications to earth, marine, and environmental sciences, 2nd ed.: Oxford, Clarendon Press, 910 p.

Janecky, D.R., and Shanks, W.C., III, 1988, Computational modeling of chemical and isotopic reaction processes in seafloor hydrothermal systems: Chimneys, massive sulfides, and subadjacent alterations zones: Canadian Mineralogist, v. 26, p. 805–825.

Kuroda, H., 1983, Geologic characteristics and formation environment of the Furutobe and Matsuki Kuroko deposits: ECONOMIC GEOLOGY MONOGRAPH 5, p. 149–166.

Kusakabe, M., and Robinson, B.W., 1977, Oxygen and sulfur isotope equilbria in the BaSO-HSO-H_2O system from 110 to 350°C and applications: Geochimica et Cosmochimica Acta, v. 41, p. 1033–1044.

Lebon, G., Resing, J., Baker, E., Embley, R., and Lupton, J., 2004, Chemical characteristics of plumes above and around NW Rota submarine volcano: Before and during the March 2004 eruption [abs.]: EOS Supplement, Transactions of the American Geophysical Union, v. 85, no. 47, p. F1884.

Li, Y-H., 1991, Distribution patterns of the elements in the ocean: A synthesis: Geochimica et Cosmochimica Acta, v. 55, p. 3223–3240.

Lilley, M.D., Butterfield, D.A., Lupton, J.E., and Olson, E.J., 2003, Magmatic events can produce rapid changes in hydrothermal vent chemistry: Nature, v. 422, p. 878–881.

Lupton, J.E., 1983, Terrestrial inert gases: Isotope tracer studies and clues to primordial components in the mantle: Annual Reviews in Earth and Planetary Science, v. 11, p. 371–414.

Lyon, G.L., 1974, Geothermal gases, *in* Kaplan, I.R., ed., Natural gases in marine sediments: New York, Plenum Press, p. 141–150.

Massoth, G.J., and Milburn, H.B., 1997, SUAVE (Submersible System Used to Assess Vented Emissions): A diverse tool to probe the submarine hydrothermal environment [ext. abs.]: Marine Analytical Chemistry for Monitoring and Oceanographic Research International Workshop, Brest, France, November 17–19, 1997. Available at http://www.pmel.noaa.gov/vents/geochem/suave/about_suave.html

Massoth, G.J., Baker, E.T., Feely, R.A., Lupton, J.E., Collier, R.W., Gendron, J.F., Roe, K.K., Maenner, S.M., and Resing, J.A., 1998, Manganese and iron in hydrothermal plumes resulting from the 1996 Gorda Ridge event: Deep-Sea Research II, v. 45, p. 2683–2712.

Massoth, G.J., de Ronde, C.E.J., Lupton, J.E., Feely, R.A., Baker, E.T., Lebon, G.T., and Maenner, S.M., 2003, Chemically rich and diverse submarine hydrothermal plumes of the southern Kermadec volcanic arc (New Zealand): Geological Society of London Special Publication, v. 219, p. 119–139.

Massoth, G.J., Baker, E.T., Lupton, J.E., de Ronde, C.E.J., Walker, S.L., Ishibashi, J., Worthington, T.J., Arculus, R.J., Resing, J.A., Greene, R.R., Lebon, G.T., Nakamura, K., and Stoffers, P., 2004, A systematic reconnaissance of submarine hydrothermal venting along the south Tonga (Tofua) intraoceanic arc [abs.]: EOS Supplement, Transactions of the American Geophysical Union, v. 85, no. 47, p. F1946.

Moore, W.S., and Stakes, D., 1990, Ages of barite-sulfide chimneys from the Mariana trough: Earth and Planetary Science Letters, v. 100, p. 265–274.

Ohmoto, H., and Lasaga, A.C., 1982, Kinetics of reactions between aqueous sulfates and sulfides in hydrothermal systems: Geochemica et Cosmochimica Acta, v. 46, p. 1727–1745.

Ohmoto, H., and Rye, R.O., 1979, Isotopes of sulfur and carbon *in* Barnes, H.L. ed., Geochemistry of hydrothermal ore deposits, 2nd ed.: New York, Wiley-Interscience, p. 509–567.

Petersen, S., Herzig, P.M., and Hannington, M.D., 2000, Third dimension of a presently forming VMS deposit: TAG hydrothermal mound, Mid-Atlantic Ridge, 26°N: Mineralium Deposita, v. 35, p. 233–259.

Petersen, S., Herzig, P.M., Hannington, M.D., Jonasson, I.R., and Arribas, A., Jr., 2002, Submarine gold mineralization near Lihir Island, New Ireland fore-arc, Papua New Guinea. ECONOMIC GEOLOGY, v. 97, 1795–1813.

Rapien, M.H., Bodnar, R.J., Simmons, S.F., Szabo, C.S., Wood, C.P., and Sutton, S.R., 2003, Melt inclusion study of the embryonic porphyry copper system at White Island, New Zealand: Society of Economic Geologists Special Publication 10, p. 41–59.

Rees, C.E., Jenkins, W.J., and Monster, J., 1978, The sulfur isotope geochemistry of ocean water sulfate: Geochimica et Cosomochimica Acta, v. 42, p. 377–382.

Resing, J.A., Feely, R.A., Massoth, G.J., and Baker, E.T., 1999, The water-column chemical signature after the 1998 eruption of Axial volcano: Geophysical Research Letters, v. 26, p. 3645–3648.

Resing, J.A., Lupton, J.L., Feely, R.A., and Lilley, M.D., 2004, CO_2 and ^3He in hydrothermal plumes: Implications for mid-ocean ridge CO_2 flux: Earth and Planetary Science Letters, v. 226, p. 449–464.

Reyes, A.G., 1990, Petrology of Philippine geothermal systems and the application of alteration minerals in their assessment: Journal of Volcanological and Geothermal Research, v. 43, p. 279–309.

Reyes, A.G., Grapes, R., and Clemente, V.C., 2003, Fluid-rock interaction at the magmatic-hydrothermal interface of the Mount Cagua geothermal system, Philippines: Society of Economic Geologists Special Publication 10, p. 197–222.

Reyes, A.G., de Ronde, C.E.J., and Soong, C.W.R., 2004, A submarine magmatic-hydrothermal system at Brothers volcano, Kermadec: New Zealand Geothermal Workshop, 26th, 7–8 December, 2004, Taupo, New Zealand, University of Auckland, Proceedings p. 46–52.

Robinson, B.W., 1977, Isotopic equilbria in hydrothermal barites: New Zealand Department of Scientific and Industrial Research Bulletin, v. 218, p. 51–56.

Ruellan, E., Delteil, J., Wright, I., and Matsumoto, T., 2003, From rifting to active spreading in the Lau bain-Havre tough backarc system (SW Pacific): Locking/unlocking induced by seamount chain subduction: Geochemistry Geophysics and Geosystems, v. 4, 8909, doi: 10.1029/2001GC000261.

Sawkins, F.J., 1984, Metal deposits in relation to plate tectonics, 2nd ed.: Berlin, Springer-Verlag, 461 p.

Sawkins, F.J., and Kowalik, J., 1981, The source of ore metals at Buchans: Magmatic versus leaching models: Geological Association of Canada Special Paper, v. 22, p. 255–267.

Seal, R.E., II, Alpers, C.N., and Rye, R.O., 2000, Stable isotopes systematics of sulfate minerals: Reviews in Mineralogy and Geochemistry, v. 40, p. 541–602.

Sasaki, M., Iizasa, K., and Sawaki T., 1995, Characteristics of gases in fluid inclusions from the Nurukawa Kuroko deposit and submarine sulfide deposits of the Izu-Ogasawara arc, Japan: Resource Geology, v. 45, p. 1–10.

Shanks, W.C., III, Böhlke, J.K., and Seal, R.R., II, 1995, Stable isotopes in mid-ocean ridge hydrothermal systems: Interactions between fluids, minerals and organisms: Geophysical Monograph, v. 91, p. 194–221.

Shikazono, N., Holland, H.D., and Quirk, R.F., 1983, Anhydrite in Kuroko deposits, mode of occurrence and depositional mechanism: ECONOMIC GEOLOGY MONOGRAPH 5, p. 329–344.

Smith, I.E.M., Brothers, R.N., Muiruri, F.G., and Browne, P.R.L., 1988, The geochemistry of rock and water samples from Curtis Island volcano, Kermadec Group, southwest Pacific: Journal of Volcanology and Geothermal Research, v. 34, p. 233–240.

Stanton, R.L., 1994, Ore elements in arc lavas: Oxford Monographs on Geology and Geophysics, v. 29, 391 p.

Stoffers, P., Wright, I.C., and the Shipboard Scientific Party, 1999a, Cruise report Sonne 135, Havre Trough-Taupo Volcanic Zone: Tectonic, magmatic and hydrothermal processes, Suva-Fiji-Wellington, New Zealand, Sept. 9–Oct. 15, 1998: Berichte-Reports, Institut für Geowissenschaften, Universität Kiel, Nr. 1, 77 p.

Stoffers, P., Wright, I.C., de Ronde, C.E.J., Hannington, M.J., Villinger, H., Herzig, P., and the Shipboard Party, 1999b, Little studied arc-backarc system in the spotlight: EOS, Transactions of the American Geophysical Union, v. 80, p. 353 and 359.

Turner, S., Black, S., and Berlo, K., 2004, ^{210}Pb-^{226}Ra and ^{228}Ra-^{232}Th systematics in young arc lavas: Implications for magma degassing and ascent rates: Earth and Planetary Science Letters, v. 227, p. 1–16.

Urabe, T., and Kusakabe, M., 1990, Barite-silica chimneys from the Simisu rift, Izu-Bonin arc: Possible analog to hematitic chert associated with Kuroko deposits: Earth and Planetary Science Letters, v. 100, p. 283–290.

Varekamp, J.C., 2004, Copahue volcano: A modern terrestrial analog for the opportunity landing site?: EOS, Transactions of the American Geophysical Union, v. 85, p. 401 and 407.

Varekamp, J.C., Ouimette, A., Herman, S., Delpino, D., and Bermudez, A., 2001, The 1990–2000 eruptions of Copahue, Argentina: A "bee-hive volcano" in turmoil: Geology, v. 29, p. 1059–1062.

Von Damm, K.L., 2000, Chemistry of hydrothermal vent fluids from 9°-10° N, East Pacific Rise: "Time zero", the immediate posteruptive period: Journal of Geophysical Research, v. 105, p. 11,203–11,222.

Von Damm, K.L., Edmond, J.M., Grant, B., and Measures, C.I., 1985, Chemistry of submarine hydrothermal solutions at 21°N, East Pacific Rise: Geochimica et Cosomochimica Acta, v. 49, p. 2197–2220.

Watanabe, K., Shibata, A., Kajimura, T., 1995, Comparison of the bulk chemical composition between hydrothermal sulfides from Suiyo Seamount and sea-floor hydrothermal sulfides from the other areas: JAMSTEC Journal of Deep Sea Research, v. 11, p. 351–361 (in Japanese with English abstract).

Webber, W.R., 2004, A new species of Alvinocaris (Crustacea: Decapoda: Alvinocarididae) and new records of alvinocaridids from hydrothermal vents north of New Zealand: Zootaxa, v. 444, p. 1–26.

Worthington, T.J., 1999, Geology and petrology of Raoul volcano: Magma genesis and fractionation processes beneath the Tonga-Kermadec arc: Unpublished Ph.D. thesis, New Zealand, University of Auckland, 436 p.

Wright, I.C., 1997, Morphology and evolution of the remnant Colville and active Kermadec arc ridges south of 33° 30' S: Marine Geophysical Researches, v. 19, p. 177–193.

Wright, I.C., and Gamble, J.A., 1999, Southern Kermadec submarine caldera arc volcanoes (SW Pacific): Caldera formation by effusive and pyroclastic eruption: Marine Geology, v. 161, p. 207–227.

Wright, I.C., Parson, L.M., and Gamble, J.A., 1996, Evolution and interaction of migrating cross-arc volcanism and back-arc rifting: An example from the southern Havre trough (35° 20'-37° S): Journal of Geophysical Research, v. 101, p. 22,071–22,086.

Wright, I.C., de Ronde, C.E.J., Faure, F., and Gamble, J.A., 1998, Discovery of hydrothermal sulfide mineralization from southern Kermadec arc volcanoes (SW Pacific): Earth and Planetary Science Letters, v. 164, p. 335–343.

Wright, I.C., Gamble, J.A., and Shane, P.A., 2003, Submarine, silicic volcanism of the Healy caldera, southern Kermadec arc (SW Pacific): I. Volcanology and eruption mechanisms: Bulletin of Volcanology, v. 65, p. 15–29.

Young, C., and Lupton, J.E., 1983, An ultratight fluid sampling system using cold-welded copper tubing: EOS, Transactions of the American Geophysical Union, v. 64, p. 735.

APPENDIX 1

Geochemistry Results for Brothers Mineralized Samples

Sample no. Unit Detection limit	SiO_2 (wt %) 0.01	Ca (wt %) 0.01	Total S (wt %) 0.01	Fe (wt %) 0.01	Au (ppb) 2	Hg (ppm) 1	As (ppm) 0.5	Sb (ppm) 0.1	Ag (ppm) 0.1	Ba (ppm) 2	Bi (ppm) 0.5
A. Brothers volcano											
Chimney											
57DR-1A	86.0	0.05	2.98	3.99			412	23	41	6650	
57DR-1B	43.0	0.06	15.90	1.44		30	499	279	740	36500	
57DR-1C	32.9	0.04	19.60	1.14		29	566	331	750	36900	
57DR-1D	24.0	0.04	28.90	14.43	135	32	4390	205	440	32800	
57DR-1E	28.2	0.04	25.00	10.85	1430	42	2660	215	430	46700	
57DR-1F	53.4	0.04	13.70	7.21	1050	7	1670	69	58	47200	
57DR-1G	37.2	0.04	23.00	14.99	835	10	3210	52	50	62300	
57DR-1H	36.0	0.04	18.20	9.03	905	9	1910	70	38	106000	
57DR-1I	22.1	0.04	24.20	12.04	1050	12	2650	149	56	108000	
57DR-1J	63.7	0.04	9.70	2.49	429	5	574	143	87	43700	
57DR-1K	76.6	0.04	6.58	2.44	31	7	532	47	73	34700	
57DR-1L	71.9	0.04	7.56	2.62	75	5	507	98	84	43400	
57DR-1M	32.9	0.04	17.00	0.96	20	39	588	579	1180	20100	
57DR-1N	65.6	0.05	8.15	2.93	17	21	481	150	470	13700	
57DR-1O	54.4	0.04	14.00	0.91		26	318	265	580	15600	
57DR-1P	43.2	0.04	16.20	0.99		39	503	329	850	22800	
57DR-1Q	34.5	0.06	17.30	1.29		38	829	262	800	29100	
57DR-1R	66.2	0.04	9.70	1.83	375	12	358	128	190	41400	
57DR-1S	60.1	0.04	10.80	1.48		14	463	163	310	44900	
57DR-1T	52.8	0.03	14.10	2.61	357	14	752	280	330	50000	
57DR-1U	68.0	0.04	7.93	2.15		9	615	93	160	35400	
57DR-1V	39.0	0.04	19.80	8.47	1060	12	1860	296	230	52000	
57DR-1W	75.8	0.04	5.82	1.71		9	502	73	100	30300	
57DR-1X	74.2	0.04	6.74	0.66	127	8	215	144	160	34100	
57DR-1Y	51.7	0.04	12.30	0.72		20	1020	298	460	26100	
57DR-1Z	66.0	0.05	8.68	0.85	22	10	227	179	240	38600	
57DR-1AA	62.8	0.06	7.95	1.69		18	848	192	260	19600	
Breccia/stockwork											
52DR-8a	8.7	0.06	43.10	38.38					0.9	290	4.0
52DR-8d	41.4	0.06	24.60	22.06	250		120	2.0	1.0	11600	3.1
52DR-10	2.9	8.93	38.40	27.03	1120	4	1630	169.0	0.7	170	5.0
59DR-5	71.0	1.33	4.59	4.22	58		163	5.2	1.2	3740	
59DR-7	59.5	0.89	5.71	5.21	203		208	6.6	1.2	9040	
60DR-1 sand	8.9	0.09	41.90	36.27	83		163	11.0	1.7	490	0.4
60DR-1 sulfide	0.5	0.06	50.30	42.93	303	8	1150	5.4	2.8	8020	0.5
60DR-2	5.0	0.04	44.90	39.43	258	1	455	2.1	0.9	1220	7.1
68DR-2	45.9	0.06	21.00	18.42	1850	2	1340	15.6	2.8	1970	3.6
68DR-3	44.1	0.06	23.70	21.08	663		818	4.5	0.4	1180	2.8
68DR-11	62.0	0.89	1.92	5.78			5.5	0.4	1.0	650	
Hydrothermally altered rock with disseminated sulfides											
52DR-11	62.6	0.45	0.82	6.79	18		17	1.1	0.2	1820	0.6
52DR-13	48.0	0.20	8.03	7.21	158		143	6.5	0.9	4590	
52DR-16	67.5	0.82	2.74	4.85	190	4	109	16.2	5.0	8240	
52DR-17	60.0	0.87	0.97	8.89	100		87	3.7	0.4	2390	
56DR-1	63.3	2.58	0.02	5.32			13	0.7		1010	
60DR-4	63.0	0.33	9.26	8.33	39		67	1.3	0.2	830	0.7
60DR-6	58.1	0.31	2.37	5.34	28		42	0.8	0.1	640	0.3
68DR-8	66.3	2.49	0.46	3.79			24	1.3	0.9	990	
68DR-10	65.4	2.54	0.78	3.88	4		65	5.3	2.5	1940	
Fe-Si crusts/sediments											
52DR-14	49.2	0.19	0.07	28.08			1060	88.4	0.2	65	
56DR-6	66.5	0.13	0.11	15.06			1590	11.2	0.2	34	
56DR-7	94.6	0.04	0.04	1.61			140	6.2		930	
56DR-11	72.7	0.14	0.12	10.36			1050		0.2	75	0.3
57DR-2	94.2	0.03	0.05	1.04			75	5.5	0.4	540	
57DR-3	93.5	0.04	0.13	1.84			131	2.7	0.2	1330	
60DR-7	75.0	0.07	4.63	3.96	97		70	0.7	0.8	860	1.7
62GTV-1	32.0	0.50	0.18	30.53			1710	47.6	1.4	100	
62GTV-2	61.4	2.73	0.54	5.54	36		92	2.4	0.8	1820	0.8
63GTV-1	44.3	1.67	0.18	16.11	9		205	2.6	1.6	2410	0.4
63GTV-2	63.0	2.82	0.76	3.50	41		26	0.5	0.2	1540	0.5
63GTV-3	62.6	2.63	1.03	3.28	35		21	1.1	0.7	1440	0.5
68DR-5	89.0	0.06	0.11	4.35	5		260	15.0	0.5	420	
69DR-1	32.6	0.26	0.09	31.72			2620	16.1	0.6	67	

APPENDIX 1. *(Cont.)*

Sample no. / Unit / Detection limit	Cd (ppm) 0.2	Cu (ppm) 10	Co (ppm) 5	Ga (ppm) 0.1	In (ppm) 0.05	Mo (ppm) 0.2	Pb (ppm) 2	Sn (ppm) 0.5	Sr (ppm) 5	Te (ppm) 0.5
A. Brothers volcano										
Chimney										
57DR-1A	8	67		0.1		7.6	12100		280	
57DR-1B	350	2080		0.2		8.8	56800	2.5	1490	0.3
57DR-1C	700	2920		0.8		17.0	14200	1.3	1270	0.7
57DR-1D	610	1910		0.2		41.0	6970	0.8	1330	0.3
57DR-1E	590	2090		0.2		55.0	5040	0.6	1720	0.3
57DR-1F	150	230		0.1		54.0	410	0.7	3820	
57DR-1G	130	270		0.2		81.0	380	0.8	4250	
57DR-1H	180	250		0.2		54.0	220	1.2	6330	
57DR-1I	310	370		0.3		82.0	410	1.8	6880	
57DR-1J	220	450	7	0.1		24.0	3900		3400	
57DR-1K	73	250		0.1		21.0	5130	0.7	1490	
57DR-1L	140	310		0.1		12.0	7770	0.5	1800	
57DR-1M	320	2390		0.1		8.6	84100	0.9	990	0.4
57DR-1N	84	920		0.1		13.0	69300	0.6	660	
57DR-1O	570	2120		0.2		28.0	7470	1.7	710	0.3
57DR-1P	610	3580		0.2		23.0	15200	1.3	1030	0.5
57DR-1Q	290	1810		0.8		16.0	80300	0.8	1990	0.4
57DR-1R	240	1180		0.2		19.0	1950	0.6	1730	
57DR-1S	170	750				15.0	46100		1460	
57DR-1T	390	1230		0.1		18.0	13600	0.5	1700	0.3
57DR-1U	96	360		0.1		15.0	34700	1.5	1370	
57DR-1V	430	1100	6	0.1		36.0	6530		2680	0.2
57DR-1W	57	240	6			13.0	24400	0.8	1300	
57DR-1X	180	500				22.0	16000		1590	
57DR-1Y	230	770				32.0	85200		1350	
57DR-1Z	190	580				7.5	20000	1.5	2840	
57DR-1AA	140	460		0.2	0.16	6.6	62400	0.6	1260	
Breccia/stockwork										
52DR-8a	0.4	47	220	4.6		150.0	22	0.9	64	28.0
52DR-8d	1.2	810	210	11.0	0.13	97.0	180	0.9	450	30.0
52DR-10	1.6	59	750	3.2	0.09	560.0	58	4.6	490	93.0
59DR-5		130	8	13.0		13.0	52	1.0	160	0.3
59DR-7		100	12	15.0	0.09	10.0	91	1.8	140	
60DR-1 sand		230	160	6.9		10.0	150		860	0.4
60DR-1 sulfide	1.5	3740	1100	1.2	0.43	29.0	70		680	
60DR-2	0.2	280	120	3.0	0.22	74.0	83		26	95.0
68DR-2	1.8	26500	10	20.0	4.80	98.0	90	3.1		29.0
68DR-3		36	15	9.7	0.15	55.0	21	1.3	10	16.0
68DR-11		26	11	18.0	0.05	3.0	9	1.6	85	1.7
Hydrothermally altered rock with disseminated sulfides										
52DR-11		370	11	20.0	0.43	11.0	23	1.5	54	0.8
52DR-13	2.1	190	12	25.0	0.58	13.0	130	2.2	1000	44.0
52DR-16	32.0	74	9	16.0	5.60	37.0	120	2.2	200	
52DR-17	2.8		7	14.0	0.09	3.6	51	1.5	150	
56DR-1	0.4	79	9	18.0	0.08	21.0	12	3.6	230	
60DR-4		33	16	20.0	0.06	9.0	27	2.5	13	2.8
60DR-6		44	12	19.0		5.1	11	1.8	13	3.8
68DR-8	0.3	44	6	18.0		2.2	120	1.5	250	
68DR-10	1.3	25	12	18.0	0.07	3.1	490	1.9	250	
Fe-Si crusts/sediments										
52DR-14	2.6			0.8		17.0	3720		65	0.4
56DR-6	0.2	11		0.5		48.0	1780	0.6	31	
56DR-7	0.7	14		0.2		3.1	260	1.4	10	
56DR-11		19		0.2		40.0	260	0.9	42	
57DR-2	0.4	28		0.2		2.2	310	2.0	68	
57DR-3		13		0.3		2.9	140	0.7	21	
60DR-7		29	20	11.0		29.0	18	1.3	250	12.0
62GTV-1	1.7	21		0.6		46.0	2680		210	
62GTV-2	0.7	160	8	17.0	0.28	12.0	230	2.0	280	1.8
63GTV-1	1.5	180	13	12.0	0.10	160.0	1100	0.9	260	1.4
63GTV-2	1.6	150	10	16.0	0.10	11.0	68	1.8	260	1.3
63GTV-3	0.6	150	12	17.0	0.11	8.0	58	1.9	260	1.4
68DR-5		46		0.6		7.8	190	4.5	45	
69DR-1	0.2	22		0.7		86.0	230		67	

APPENDIX 1. *(Cont.)*

Sample no. Unit Detection limit	Th (ppm) 0.02	Tl (ppm) 0.0	U (ppm) 0.02	V (ppm) 5	Zn (ppm) 5	Ce (ppm) 0.1	Dy (ppm) 0.02	Er (ppm) 0.02	Eu (ppm) 0.02	Gd (ppm) 0.02
A. Brothers volcano										
Chimney										
57DR-1A		23.0	7.9	10	32200		0.02		0.23	0.03
57DR-1B		6.6	4.2		264000	0.2			0.08	
57DR-1C	0.04	12.0	4.3		380000	1.1	0.13	0.07	0.11	0.16
57DR-1D		270.0	3.5		238000	0.4			0.10	
57DR-1E		150.0	6.3		266000				0.25	
57DR-1F		140.0	15.0		72600	0.1	0.02		0.82	0.02
57DR-1G		230.0	11.0		76800	0.2			0.87	0.02
57DR-1H	0.13	120.0	9.4		95400	0.3	0.06	0.03	0.99	0.05
57DR-1I		160.0	5.4		128000	0.5			0.73	0.02
57DR-1J		57.0	12.0		109000	0.5			0.52	0.03
57DR-1K		61.0	14.0		72100	0.1			0.33	0.02
57DR-1L		43.0	7.9		83300	0.2			0.37	
57DR-1M		14.0	3.1		277000	0.2			0.02	
57DR-1N		24.0	6.9	6	117000				0.14	0.02
57DR-1O		6.4	6.0		274000	0.2			0.03	
57DR-1P		7.4	4.1		331000	0.2			0.03	
57DR-1Q	0.33	14.0	3.1	6	293000	2.7	0.17	0.06	0.13	0.20
57DR-1R		27.0	10.0	5	145000	0.3			0.38	0.02
57DR-1S		8.3	4.8	5	165000	0.2			0.12	0.03
57DR-1T		77.0	8.4	6	213000	0.2			0.63	0.03
57DR-1U		26.0	6.4	7	110000	0.1			0.22	
57DR-1V		190.0	7.2		182000	0.2			0.45	
57DR-1W		22.0	6.3	7	79200	0.2			0.27	
57DR-1X		26.0	8.4		115000	0.5			0.40	
57DR-1Y		21.0	3.7	6	201000	0.2			0.14	
57DR-1Z		13.0	4.5		129000	0.4			0.36	
57DR-1AA		15.0	4.7	15	129000	0.3	0.05	0.03	0.23	0.08
Breccia/stockwork										
52DR-8a	0.76	4.0	1.4	26	12	25.0	1.40	0.92	3.20	2.40
52DR-8d	0.88	0.7	1.7	41	170	15.0	2.50	1.60	1.40	2.50
52DR-10	0.30	80.0	1.2	13	85	4.0	0.88	0.50	0.75	1.10
59DR-5	2.00	5.6	3.0	91	100	25.0	4.50	2.90	2.00	4.50
59DR-7	2.60	3.1	2.2	110	54	32.0	5.90	3.80	2.50	6.10
60DR-1 sand	1.00	0.8	4.0	46	20	75.0	1.50	0.98	3.90	1.60
60DR-1 sulfide	0.05	3.3	1.3		320	5.2	0.18	0.04	2.60	0.93
60DR-2	0.62	7.3	1.7	32	47	19.0	1.60	1.00	0.56	1.40
68DR-2	0.98	7.9	1.0	83	420	28.0	2.10	1.20	1.80	2.60
68DR-3	0.92	15.0	1.7	70		64.0	4.40	1.80	2.90	7.20
68DR-11	2.40	0.3	1.5	120	39	39.0	5.40	3.40	1.40	5.60
Hydrothermally altered rock with disseminated sulfides										
52DR-11	2.80	2.8	1.6	83	220	37.0	6.40	4.00	1.30	6.60
52DR-13	2.70	1.9	6.9	150	590	39.0	4.40	2.80	2.40	4.30
52DR-16	2.60	5.8	7.6	82	14400	32.0	6.00	3.70	2.00	6.00
52DR-17	2.40	0.4	1.7	71	720	31.0	5.60	3.50	1.50	5.70
56DR-1	2.80	2.2	1.8	92	130	35.0	6.50	4.10	1.60	6.60
60DR-4	1.60	0.8	1.8	110	12	35.0	3.80	2.10	1.90	4.90
60DR-6	1.80	0.3	2.8	130	46	27.0	4.10	2.50	1.30	4.40
68DR-8	2.90	0.6	2.1	87	320	38.0	6.70	4.20	1.70	6.90
68DR-10	3.20	2.2	1.5	92	2000	39.0	6.90	4.40	1.70	6.80
Fe-Si crusts/sediments										
52DR-14	0.03	0.8	13.0	14	1000	2.1	0.28	0.15	0.12	0.39
56DR-6	0.03	0.4	10.0	6	150	0.8	0.13	0.07	0.03	0.16
56DR-7		0.8	11.0	5	450		0.02		0.06	0.03
56DR-11		0.2	9.4	17	64	0.2	0.04	0.02		0.04
57DR-2		0.9	8.1	5	280		0.02			0.04
57DR-3	0.05	7.1	4.8		170	0.3	0.03	0.02	0.07	0.04
60DR-7	1.00	0.4	1.8	51	15	25.0	2.30	1.30	0.78	2.70
62GTV-1	0.02	1.7	12.0	22	180	1.6	0.29	0.16	0.04	0.30
62GTV-2	2.70	1.2	2.3	110	140	31.0	5.60	3.50	1.40	5.50
63GTV-1	1.60	8.4	6.9	99	1350	20.0	3.80	2.30	0.63	3.60
63GTV-2	2.60	2.0	2.0	93	210	30.0	5.30	3.40	1.50	5.00
63GTV-3	2.60	0.9	1.8	86	170	33.0	5.60	3.70	1.60	5.70
68DR-5	0.02	1.5	8.7		33	0.8	0.08	0.04		0.11
69DR-1	0.04	3.1	11.0	16	96	4.0	1.10	0.75	0.29	1.20

APPENDIX 1. *(Cont.)*

Sample no. Unit Detection limit	Ho (ppm) 0.02	La (ppm) 0.1	Lu (ppm) 0.02	Nd (ppm) 0.1	Pr (ppm) 0.02	Sm (ppm) 0.02	Tb (ppm) 0.02	Tm (ppm) 0.02	Y (ppm) 0.05	Yb (ppm) 0.05
A. Brothers volcano										
Chimney										
57DR-1A				0.2	0.02	0.04			0.10	
57DR-1B				0.2	0.03	0.05			0.04	
57DR-1C	0.03	0.3		0.8	0.16	0.18	0.03		0.68	0.04
57DR-1D		0.2		0.3	0.05				0.16	0.02
57DR-1E				0.2	0.02	0.03			0.05	
57DR-1F				0.3	0.04	0.04			0.08	
57DR-1G				0.2	0.05				0.07	
57DR-1H	0.03		0.03	0.2	0.09	0.07	0.03	0.03	0.14	0.04
57DR-1I				0.3	0.09	0.03			0.11	
57DR-1J				0.5	0.11	0.02			0.09	
57DR-1K				0.3	0.05				0.05	
57DR-1L				0.3	0.08				0.02	
57DR-1M				0.2	0.03	0.02			0.02	
57DR-1N				0.2	0.02	0.04			0.06	
57DR-1O		0.1		0.2	0.03	0.02			0.08	
57DR-1P		0.1		0.3	0.03	0.03			0.02	
57DR-1Q	0.03	1.5		1.1	0.29	0.25	0.03		0.92	0.06
57DR-1R				0.3	0.05	0.03			0.09	
57DR-1S				0.2	0.03	0.03			0.04	
57DR-1T				0.2	0.04	0.03			0.07	
57DR-1U				0.2	0.03				0.08	
57DR-1V				0.3	0.04	0.04			0.04	
57DR-1W				0.3	0.05	0.02			0.04	
57DR-1X				0.3	0.07	0.02			0.04	
57DR-1Y				0.3	0.04	0.02			0.04	
57DR-1Z				0.3	0.07	0.02			0.03	
57DR-1AA		0.3		0.3	0.07	0.05			0.66	0.04
Breccia/stockwork										
52DR-8a	0.31	9.5	0.17	21.0	4.00	5.60	0.26	0.16	9.30	1.00
52DR-8d	0.54	5.3	0.29	11.0	2.30	2.70	0.44	0.26	16.00	1.90
52DR-10	0.19	1.6	0.08	4.2	0.69	1.50	0.16	0.08	6.30	0.48
59DR-5	0.99	10.0	0.47	16.0	3.70	4.40	0.75	0.44	30.00	2.90
59DR-7	1.30	13.0	0.59	22.0	4.70	5.50	0.98	0.61	38.00	3.80
60DR-1 sand	0.34	44.0	0.19	30.0	8.60	3.70	0.21	0.17	9.60	1.10
60DR-1 sulfide	0.02	2.8		2.7	0.66	0.97	0.06		0.72	0.04
60DR-2	0.34	10.0	0.16	10.0	2.40	2.10	0.24	0.16	10.00	1.00
68DR-2	0.42	13.0	0.19	16.0	3.80	3.30	0.38	0.18	12.00	1.20
68DR-3	0.74	29.0	0.25	39.0	9.00	9.20	0.89	0.25	21.00	1.60
68DR-11	1.20	17.0	0.54	24.0	5.40	5.60	0.89	0.54	36.00	3.60
Hydrothermally altered rock with disseminated sulfides										
52DR-11	1.40	15.0	0.71	24.0	5.20	5.70	1.10	0.66	44.00	4.40
52DR-13	0.98	17.0	0.52	22.0	5.10	4.10	0.74	0.47	30.00	3.20
52DR-16	1.30	12.0	0.66	22.0	4.70	5.30	1.00	0.60	40.00	4.10
52DR-17	1.20	13.0	0.60	20.0	4.40	5.00	0.95	0.57	38.00	3.80
56DR-1	1.50	15.0	0.72	23.0	4.90	5.80	1.10	0.66	44.00	4.50
60DR-4	0.77	15.0	0.31	21.0	4.80	5.40	0.75	0.33	24.00	2.00
60DR-6	0.84	12.0	0.37	16.0	3.60	4.30	0.69	0.37	26.00	2.30
68DR-8	1.40	17.0	0.68	25.0	5.40	6.20	1.10	0.64	46.00	4.30
68DR-10	1.50	16.0	0.72	24.0	5.40	6.10	1.20	0.68	45.00	4.70
Fe-Si crusts/sediments										
52DR-14	0.06	0.8	0.02	1.5	0.31	0.34	0.05	0.02	2.60	0.11
56DR-6	0.03	0.3		0.6	0.13	0.14	0.02		0.94	0.07
56DR-7				0.3	0.02	0.02			0.15	
56DR-11		0.1		0.2	0.03	0.05			0.26	0.02
57DR-2				0.2	0.02	0.02			0.18	0.02
57DR-3		0.1		0.3	0.05	0.04			0.17	0.02
60DR-7	0.47	12.0	0.22	14.0	3.30	3.20	0.40	0.20	15.00	1.30
62GTV-1	0.06	0.6	0.02	1.2	0.22	0.27	0.05	0.02	1.70	0.16
62GTV-2	1.20	14.0	0.60	20.0	4.40	4.90	0.93	0.56	37.00	3.90
63GTV-1	0.80	8.9	0.40	13.0	2.80	3.20	0.62	0.36	24.00	2.50
63GTV-2	1.10	13.0	0.57	18.0	4.10	4.80	0.90	0.53	34.00	3.50
63GTV-3	1.20	14.0	0.60	20.0	4.50	5.20	0.95	0.57	39.00	3.80
68DR-5	0.02	0.4		0.7	0.12	0.12			0.51	0.04
69DR-1	0.25	1.7	0.12	3.0	0.59	0.80	0.19	0.11	8.60	0.68

Notes: Analyzed by ICP-MS and ICP-ES at the Geological Survey of Canada laboratories; fusion followed by multiacid dissolution; Au, Hg, As and Sb analyzed by INAA by Activation Laboratories, Ancaster, Ontario; total sulfur analyzed by combustion at high temperature followed by infrared detection (LECO); blank space = below detection; sample 57DR-1O contained 21 (ppm) Ni; for location of samples 57DR-1A to 57DR-1AA, see Figure 9; all Brothers samples collected during the *Sonne*-135 cruise; abbreviations: ba = barite; DR = dredge; GTV = TV grab; ma = marcasite; min sep = mineral separation; ppb = parts per billion; ppm = parts per million; py = pyrite; wt % = weight percent

APPENDIX 2

Methods Used in the Dating of Mineralized Samples

Mineralized samples rich in barite were analyzed for Ba and Pb by X-ray fluorescence. Barium was also determined gravimetrically and by proton induced X-ray emission using a 2.5-MeV proton beam. The isotope ^{226}Ra and its decay products, ^{214}Pb, ^{214}Bi, and ^{210}Pb, were measured by gamma spectrometry using a low background, high-resolution Ge detector. The weighted average ^{214}Pb and ^{214}Bi counts were taken as a proxy for ^{226}Ra, as the latter, with its relatively low energy gamma emission, is subject to matrix correction errors and spectral interference by ^{235}U.

Several samples, including five from the chimney 57DR-1 (Fig. 9) and two hydrothermally altered rocks (01/07-131a, 01/07-135; see Fig. 3f), were powdered and leached with a mixture of hot HCl and HF to dissolve Fe, Cu, and SiO_2. Excess acid was evaporated and the residue fused with KF. Fluoride was then eliminated by fusion with H_2SO_4 and Na_2SO_4 and the solidified salt dispersed in hot water. The precipitate, $Ba(^{226}Ra)SO_4 + PbSO_4$, was separated by centrifuging and the supernatant solution retained for U and Th isotope analysis. Some of the Pb was extracted from the sulfate precipitate by leaching with hot dilute HCl, with the remainder recovered when $BaSO_4$ was decomposed by fusion with Na_2CO_3 to retrieve any occluded Th. Samples low in SiO_2 were leached with hot HCl and HNO_3 only, before fusing the residual $Ba(^{226}Ra)SO_4$ and $PbSO_4$ with Na_2CO_3 (a better decomposition procedure, developed since this study, has a preliminary fusion with $Na_2SO_4 + K_2SO_4 + H_2SO_4$). The cooled melt, including many matix elements, was dissolved in hot water and the $Ba(^{226}Ra)SO_4$ and $PbSO_4$ precipitate recovered by centrifuging. Any silicate is removed by adding HNO_3 + HF, evaporating to dryness, and then fusing again with $Na_2SO_4 + K_2SO_4 + H_2SO_4$. Uranium and Th were then coprecipitated with $Fe(OH)_3$, purified by ion exchange, and electrodeposited onto stainless-steel cathodes for ^{230}Th, ^{232}Th, ^{234}U, and ^{238}U analysis by alpha spectrometry. Barium was later recovered as barite, weighed, and gamma counted after one month to check that ^{226}Ra, ^{214}Pb, and ^{214}Bi were in secular equilibrium (i.e., their radioactivities were equal to each other, thus verifying that ^{222}Rn gas, the first decay product of ^{226}Ra, did not escape, and confirming the $^{226}Ra/Ba$ values measured in the original chimney samples). Lead was also separated, radiochemically purified by anion exchange, precipitated as $PbCrO_4$ and, after waiting one month for ingrowth of ^{210}Bi, analyzed by beta counted under an aluminum foil absorber that stopped the weak ^{210}Pb beta and alpha emissions from ingrowing ^{210}Po. The instrument used was a thin window gas-flow proportional counter with a guard and anticoincidence circuitry. Results are summarized in Table 5.